Nocturnal Wave-like Air Motion in Forests

A Dissertation
Presented to the Faculty of the Graduate School
of
Yale University
in Candidacy for the Degree of
Doctor of Philosophy

By Xinzhang Hu

Dissertation Director: Xuhui Lee

May, 2001

Table of Contents

List of Figures

This thesis is dedicated to my wife Yong Li

and my parents

Chaoming Hu and Songlan Duan.

Acknowledgements

I am indebted to my advisor, Prof. Xuhui Lee, for his constant support and encouragement. It was his early and influential observational work that inspired this dissertation, and his timely assistance guided me through every stage of this research.

I would like to thank a few others for their help and kindness. Prof. Ronald B. Smith took the time to engage me in thorough and enjoyable discussions on wave dynamics. The two-layered wave model was first developed while I took his class. As a teaching assistant in his classes, I had even more opportunities to learn from him.

I am grateful as well to Dr. Donald E. Aylor for his help and encouragement. His insight and suggestions greatly helped me in choosing my research topic. Under his guidance, my knowledge of transport processes in plant canopies was greatly broadened.

Dr. David E. Stevens kindly provided the two dimensional flow solver used in my research. He helped me implement an early version of the canopy model, and he has always been more than patient when being pestered with my endless questions.

The research for this dissertation was funded with the following fellowships and grants: Yale University Fellowship, G. Evelyn Hutchinson Fellowship, John F. Enders Research Grant.

Xinzhang Hu

New Haven, Connecticut

December, 2000

Preface

Since the early 1980's, with the concern of the potential environment changes caused by the anthropogenic CO_2, there have been increasing practices to quantify the long-term net ecosystem exchange of CO_2 between forests and the atmosphere. For example, Desjardins *et al.* (1982, 1985) and Alvo *et al.* (1984) measured the CO_2 flux over boreal forests with air-borne eddy covariance instruments. By measuring the CO_2 concentration profile and the CO_2 fluxes across the soil-atmosphere and the canopy-atmosphere interfaces, Wofsy *et al.* (1993) estimated the annual net ecosystem-atmosphere exchange of CO_2 in a temperate forest. Hollinger *et al.* (1994) tried to use measured CO_2 flux to examine whether the knowledge on leaf-level processes was sufficient to understand the ecosystem-level exchange. The long-term continuous measurement (Sellers *et al.*, 1995) provides opportunities to identify the role of a particular forest ecosystem in the global carbon cycle. The responses of forest systems to the climate variability in a range of temporal scales, such as seasonal variation (Susanna *et al.*, 1996), annual cycle (Black *et al.*, 1996), and interannual variation (Goulden *et al.*, 1996a), have been studied by integrating the hourly CO_2 data. These researches will be extremely useful in building realistic models to make more convincing projections on the global changes.

Most field measurements employ micrometeorological techniques to quantify the fluxes of CO_2 and other scalar entities across the canopy-atmosphere interface. There are several advantages of this approach. Firstly, compared with the “brute force” chamber method, it is possible to measure the fluxes without disturbing the natural environment of the sources. Secondly, it is an inherent average over a surface area that increases with the instrument height. Hourly tower-based measurements represent averages over a few hundred meters to about 1 kilometer in the upwind direction. Such high temporal and spatial resolution data sets are of great importance to improve the parameterization of the land-surface exchange in Atmosphere General Circulation Models and the calibration of satellite observations (Sellers *et al.*, 1997).

The prerequisite to the application of micrometeorological techniques is the thorough understanding of the atmospheric transportation processes in plant canopies. Over the last four decades, knowledge of the turbulence in the atmospheric boundary layer has been advanced tremendously. Nowadays, fast-response instruments are routinely used to measure the atmospheric turbulence and fluxes of chemical species. The experiment designs, such as the sampling frequency, instrument height, fetch, averaging time, and data processing, etc., are based on our current knowledge of the turbulence in the atmospheric boundary layer (Businger, 1986; Baldocchi *et al.*, 1988; Fowler and Duyzer, 1989; Dabbert *et al.*, 1993; Kaimal and Finnigan, 1994; Lenschow, 1995). For tower-based measurements in forests, in order to get good spatial representation, the instruments are usually mounted a few meters to about 20 meters above the treetops. The existence of a constant flux layer between the canopy top and the instrument height guarantees that the measured fluxes represent those from the underlying systems. Most of the considerations guiding the observation design are well established for unstable and neutral conditions when rigorous atmospheric turbulence dominates the exchange process. Under stable conditions, due to the intrinsic complexity of the nocturnal atmospheric boundary layer and the nighttime interactions between plant canopies and the air, similar guidelines have not been established. In fact, the setup of current tower-based flux measurement systems is often optimized for unstable or neutral conditions in the daytime. The data poorly represents the exchange processes under stable conditions at night. Under very stable conditions, the constant flux layer may be very shallow or does not exist at all, and turbulence frequently decouples from the surface (Marht, 1999; Wofsy *et al.*, 1993). Under such conditions, the measured CO_2 flux may not represent the efflux from the underlying forest systems and may cause uncertainty in the estimate of the long-term carbon sequestration.

Compared with the rigorous daytime turbulence exchange, the nocturnal exchange does not play a major role for most of the quantities of interest because the strong nocturnal radiative cooling at the canopy top would significantly suppress the turbulence diffusion. As a result, the nocturnal exchange over forests has not received enough attention in the past. However, there are compelling reasons to understand the nocturnal exchange processes over the forests. For example, the nighttime CO_2 released by respiratory activities is comparable in magnitude to the photosynthesis uptake by the forest in the daytime. The nighttime CO_2 fluxes measured by the eddy correlation technique are extremely variable and often seem unreasonably low on clear and calm nights (Black *et al.*, 1996; Goulden *et al.*, 1996b; Lee *et al.*, 1997; Yang *et al.*, 1997). The erratic behavior of the measured nighttime CO_2 flux implies the uncertainty in the estimation of the long-term carbon sequestration by forests.

In addition, the nocturnal exchange process is of interest for numerous applications. For instance, the nighttime buildup of carbon dioxide concentration within forests is one way to estimate the respiration rates of forest ecosystems (Woodwell and Dykeman, 1966; Whittaker, 1975). NO_2 and other biogeochemically important trace gases tend to accumulate in the canopy during the night (Kaplan *et al.*, 1988; Bakwin *et al.*, 1990). Certain fungal spores are released and transported at the forest floor at night (Schmidt and Wood, 1972). All of these applications demand a better understanding of the nocturnal exchange processes in forests.

When focusing our attention to the nighttime atmospheric exchange processes in forests, we find that the importance of the frequently observed wave-like air motions, loosely referred to as canopy waves after Lee (1997), has been neglected for a long time. Paw U *et al.* (1989) have demonstrated that wave-like motions were often observed in a variety of plant canopies, from short crops to tall forests. The field measurement in a boreal forest (Lee and Barr, 1998) has found wave events with various intensities in 40% of the nighttime observations. Along with other observational studies (Maitani *et al.*, 1984; Maitani, 1989; Fitzjarrald and Moore 1990), it is safe to say that the wave-like motion is a common type of air motion in forests.

Although waves are frequently found in the field observations for flux measurement, they have not received enough attention from the micrometeorology community. There were not many field experiments designed specifically for the study of canopy waves. Only a few simple models have been developed to explain the mechanism of canopy waves (Paw U *et al.*, 1989; Fitzjarrald and Moore 1990; Lee, 1997). The wave dynamics, wave-canopy interaction, and associated transportation processes have not been fully understood yet. The neglect is mainly due to the fact that nighttime fluxes of most micrometeorological quantities, such as momentum, heat and water vapor, are only very small fractions of their daytime values. Another reason is the wide-spread perception that pure linear gravity waves do not transport scalar quantities because the wave components of scalars are in quadrature with the vertical wind fluctuation, which generates zero mean vertical fluxes. In addition, most of the tower-based flux measurements are made at only one or at most a couple of heights. The coarse vertical resolution is just simply not enough to capture the salient wave activities.

Outside the micrometeorology community, the importance of the atmospheric waves are well appreciated by meso-scale and large-scale meteorologists. Numerous atmospheric phenomena are the direct or indirect results of waves of a wide range of scales. For example, waves associated with the jet stream form the mid-latitude frontal systems and generate synoptic scale weather. Mountain clouds and some orographical rain patterns are the manifestations of mountain waves (Smith, 1979). It is well established that waves can significantly affect the global atmospheric energy and momentum balance during their generation, propagation and dissipation. Carrying the same belief, we may expect that the influence of nighttime canopy waves that occur near treetops might considerably affect the development of the nocturnal stable boundary layer at heights well above the ground. By virtue of their simple temporal and spatial variations, some features of canopy waves are particularly suitable for mathematical and physical description. Furthermore, the wave model put forward by Lee (1997) indicates that canopy waves are shear instabilities of the Kelvin-Helmholtz type, sharing the same mechanism as that of the coherent structures in the daytime canopy turbulence (Raupach *et al.*, 1996). It might be a better way to study the shear generated coherent structures by studying the relatively simple canopy waves first. Most importantly, the resulting vertical turbulent mixing from Kelvin-Helmholtz waves is believed to be one of the most important diffusion processes in the stratified environment in the atmosphere and the ocean. If so, the role of canopy waves in the nocturnal atmosphere-plant exchange processes cannot be ignored. This is especially true for the nighttime CO_2 flux measurement because CO_2 is physiologically active at night, due to the respiration of trees and soil processes.

The objectives of this dissertation research are: 1) to investigate the two-dimensional wave structures by analyzing the existing field observation; 2) to investigate the effect of the canopy drag on the wave dynamics with a simple two-layered linear model; 3) to simulate the two-dimensional flow structure of the wave-like motion with a numerical canopy flow model. In Chapter 1, the current state of knowledge on canopy waves is reviewed. Background knowledge of coherent canopy turbulence and KH instabilities is briefed. In Chapter 2, the flow structure of the wave-like air motion is investigated by analyzing the high-resolution temperature profiles and the sonic anemometer data from a boreal forest. In Chapter 3, a two-layered linear canopy wave model is developed. The effect of the canopy drag on the wave dynamics is investigated. In Chapter 4, a two-dimensional eddy-resolved numerical canopy flow model is used to simulate the flow structure of the canopy wave. The ability of this model to reproduce the salient wave features is demonstrated. Finally, the results are summarized in the Conclusion and future works are suggested.

Chapter 1

The Organized Structures in the Canopy Flow

The surface layer is the lower 5-10% of the atmospheric boundary layer, which is characterized by large gradients of wind speed, temperature and water vapor. But the mean wind direction and the vertical turbulent fluxes of heat, water vapor and momentum remain nearly constant with height. Observations over horizontally homogeneous surfaces have demonstrated that the turbulence characteristics in the surface layer depend on only four scaling parameters, the height above the ground, surface stress, heat flux, and the buoyancy variable. Monin-Obukhov similarity theory states that outside the roughness sublayer (a region influenced by length scales associated with the roughness elements), turbulent motion is independent of the boundary roughness except through its influence on the friction velocity. Mean wind, temperature and water vapor gradients, variances of turbulent fluctuations, etc., when normalized by appropriate combination of the scaling parameters, can be described by unique functions of the stability parameter. By analogy to the molecular diffusion in the laminar flow, turbulent fluxes of surface stress, heat and water vapor can be related to the gradient of the mean wind, potential temperature and humidity by turbulent exchange coefficients, the counterparts of viscosity, conductivity and diffusivity. The extension of the gradient-diffusion concept to the turbulent exchange in the atmosphere surface layer is widely known as the K-theory.

The micrometeorological experiments for establishing the Monin-Obukhov similarity theory were all performed over bare surfaces or surfaces with short vegetations. The observation heights are well above the characteristic heights of the underlying roughness elements. In contrast, over tall forests, for the practical interest and the logistical constraint, the instrument heights in most micrometeorological measurements are usually located within the canopy roughness sublayer. The observed turbulence characteristics in this layer differ greatly from those over bare soil or surfaces with short vegetations. Depending on the proximity to the canopy tops, a departure from Monin-Obukhov similarity theory is expected. Several canopy heights above the canopy tops, Monin-Obukhov similarity relations still hold if plant canopies are conceptually treated as elevated solid surfaces. The departure to surface layer profiles gets larger when approaching the canopy tops. Within canopies, wind is characterized by high turbulence intensity. The downward momentum transfer is mainly done by the organized structures with scales of the canopy heights. The flux-gradient relationships for wind, temperature, humidity, CO_2 and other scalars show erratic patterns as the result of the non-local transport by the canopy turbulence and the temporal and spatial variation of sources and sinks. The commonly used K-theory fails in forest environment because the structure of canopy turbulence differs from that of the surface layer turbulence.

Observations over the last two decades have established that the turbulence in the canopy roughness layer is far from random. It is now widely recognized that, within and just above plant canopies, turbulence is characterized with the intermittent coherent structures, with the length scale of the canopy height. The coherent structure can be identified in time series of wind velocity components as repetitive patterns of ejection-sweep cycles, that is, slow upward air motions (ejections) followed by strong downward motions (sweeps). Numerous observational studies have provided the detailed picture of the daytime coherent structure. It is generally believed that the strong wind shear at the canopy top is responsible for the generation of these coherent structures (Raupach *et al.*, 1996). In contrast with daytime coherent structures, the nocturnal wave-like motion has not attracted much attention yet. The wave-like air motion, by its well-organized structure, is especially suitable for mathematical and theoretical studies. The study of the wave-like air motion will provide further insight into the complex interaction between the airflow and plant canopies.

In this chapter, a brief description of the unique distribution of common meteorological variables in forests is given in the Section 1.1, followed by a review of the observed features of the ramp-like coherent structures and canopy waves. A brief description of Kelvin-Helmholtz instability is given in Section 1.3. The plane-mixing layer analogy for the ramp-like structures and the linear wave models will also be introduced.

1.1 Biophysical Environment in Forests

1.1.1 Leaf Area Index and Leaf Area Density

The crown canopy, the upper part of trees with branches and twigs, is the part that directly interacts with the surrounding air. The structure of canopies is such arranged for optimal exposure of leaves to the environment, especially for the optimal reception of radiation energy for photosynthesis and transpiration. The details of the influence of an individual tree on the distribution of biophysical variables are extremely complex and vary with the stand structures, which makes understanding the canopy flow structures a formidable task.

In opposition to the common intuition, observations have demonstrated that the features of the canopy turbulence might owe more to the properties of the flow structure above the canopy than to the wakes of leaves, stems, branches or even individual trees. For a homogeneous forest, it is possible to characterize the vertical distribution of major meteorological variables with a few parameters. One such parameter describing the canopy structure is the leaf area density $a(z)$. It is the leaf area in the unit volume and is a function of height. The non-dimensional number Leaf Area Index (LAI) is the integral of leaf area density from ground to the treetops h,

$$LAI = \int_0^h a(z)\, dz. \tag{1.1.1}$$

It is the total leaf area in the column above the ground over a unit horizontal cross-section.

1.1.2 Net Radiation

Radiative transfer in forest canopies is extremely complex because of the large variability and inhomogeneity of the stand architecture and the individual tree structure. Other external factors, such as the changes of the direction and the intensity of incident solar radiation, cloud type and amount, and aerosols, only add more complexity. A detailed description of the radiative transfer in the plant canopies can be found in Ross (1975).

Most micrometeorological studies are mainly concerned about the thermal effect of the radiation in plant canopies. Both the shortwave and the longwave radiation must be taken into account for the energy exchange between the atmosphere and the vegetation. At the stand-atmosphere interface, the radiation input consists of the direct solar radiation, the diffusive irradiance, and the downward longwave radiation. The output includes the reflected solar radiation and the upward longwave emission from plant elements and the ground. The shortwave and the longwave components are combined in the net radiation. The net radiation can be measured directly without measuring the individual shortwave and longwave components. The divergence of the net radiation determines the transpiration and the heat exchange between canopy elements and the surrounding air. These exchange processes determine the leaf temperature and the air temperature within canopies.

Figure 1.1 shows the vertical distribution of mean net radiation on a selected day with clear sky in a homogeneous spruce forest with average tree height of about 30 m (Galoux *et al.*, 1981). The diurnal pattern of the net radiation R_n above the canopy

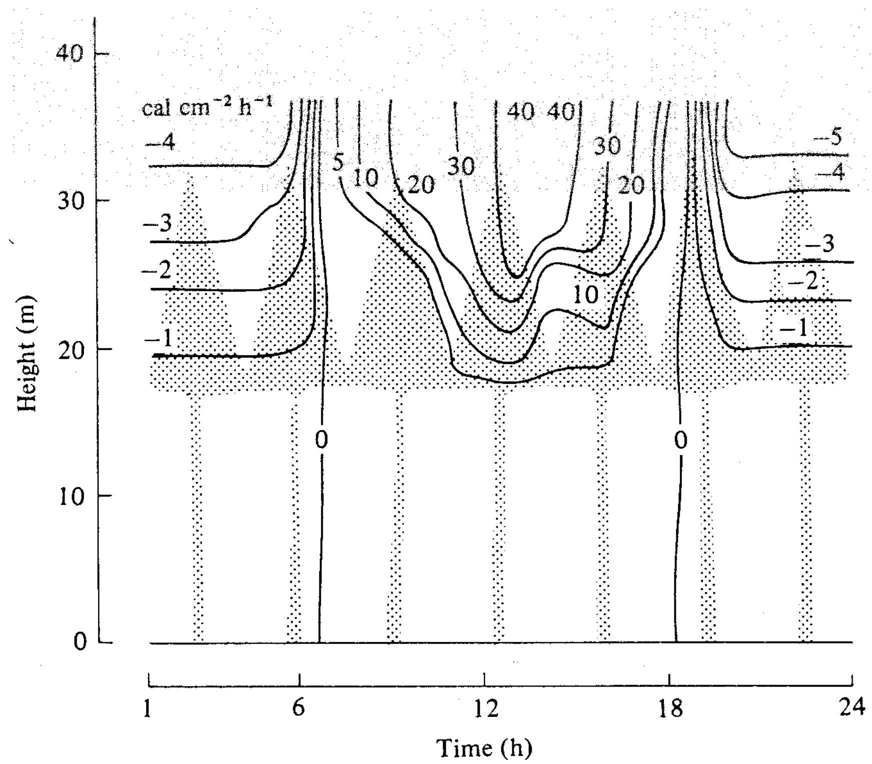

Figure 1.1: The typical daily variation of the net radiation in a forest.

follows the same pattern as that above a open surface. In the daytime, the solar direct irradiance is the dominant radiation component and the R_n variation essentially resembles that of the solar radiation. At night, without the shortwave component, the R_n is determined by the atmospheric longwave radiation and the longwave emission of the canopy (and of the ground, if the forest is sparse). Since the temperature of canopy elements is usually greater than the effective radiative temperature of the sky, the net radiation is negative and the air temperature in the canopy layer keeps dropping throughout the night. Transitions between the nighttime and the daytime patterns occur at sunrise and sunset. The R_n becomes positive shortly after sunrise and negative about one hour before sunset. Within canopies, the reduction of the R_n increases with decreasing height. Much of the reduction occurs at the upper canopy, where the R_n is only 40% of the value at the treetops in the daytime and 20% at night. In the lower canopy and the trunk space, the R_n values might be less than 10% of that at the treetops.

1.1.3 Temperature

The air temperature in plant canopies is determined by the energy balance. The energy balance at a reference level above the ground can be written as

$$R_n = H + \lambda E + G + A + S, \tag{1.1.2}$$

where H is the sensible heat flux, λE is the latent heat flux, G is the soil heat flux, A is the energy used by photosynthesis and S is heat storage of canopy elements. The detailed measurements of the various components in forests (Thom, 1975; Denmead and Bradley, 1985) have demonstrated that A and S are usually small fractions of the remaining terms. The energy budget is dominated by R_n, H and λE.

In closed canopies, the uppermost part of the crown is the place with pronounced daily change of the divergence of the net radiation. As a result, canopy tops experience the largest daily temperature variation. At midday in summer, the temperature near the mid-canopy is usually a few degrees higher than that at the ground level. Below the height of the temperature maximum, there usually is a stable layer. In sparse forests, more solar radiation can penetrate deeper. Stable layers found in closed canopies cannot be established.

On clear nights, canopies emit the longwave radiation almost like blackbodies. The atmospheric longwave radiation is usually smaller than the canopy emission. The net radiation is negative in all layers of the stand and the maximum radiation divergence is located at the upper canopy. It is also the location of the temperature minimum. Temperatures at layers below and at the forest floor are often higher and unstable layer usually exist in the lower canopy layer. Later the temperature may show little difference from ground to the middle of the crown as the result of the convective mixing of the formerly unstable air. In sparse forests, the upward longwave radiation from the ground can escape from the canopies. No unstable temperature structure can be found in sparse forests. The temperature are expected to continuously decrease with height.

Other factors can change the above scenario. Clouds can significantly disturb the net radiation by modifying the shortwave radiation and the atmospheric longwave radiation. In the daytime, clouds affect the energy balance by blocking the direct solar radiation, changing the diffusive shortwave irradiance and enhancing the atmospheric longwave radiation. At night, the radiative cooling of stands can be significantly reduced by the enhanced atmospheric longwave radiation associated with clouds.

1.1.4 Mean Wind

Compared with that above the surrounding bare surface, wind within and just above the treetops is significantly reduced by plant canopies. The wind profile above a canopy has a similar shape to that above a bare surface, except that it is shifted upward. Under neutral conditions, by taking into account of the influence of plant canopies, the famous logarithmic formula for mean wind u can be modified by introducing an extra parameter, d, the displacement height. Thus, mean wind at height z is given by

$$u\left(z\right) = \frac{u_*}{\kappa} \log\left(\frac{z-d}{z_0}\right), \tag{1.1.3}$$

where $\kappa = 0.41$ is the von Karman constant, u_* is the friction velocity, and z_0 is the roughness height. Both d and z_0 depend on the stand density. From the numerical simulation (Shaw and Pereira, 1982), d and z_0 are often estimated to be 0.7 and 0.1 of the plant height. Stability correction for z_0, d or the logarithmic model is also possible.

Within canopies, wind profiles show great variations because of the variability of stand structures and density (Figure 1.2, from Fritschen, 1985). Flow regimes within canopies can usually be divided into three layers according to Campbell and Norman

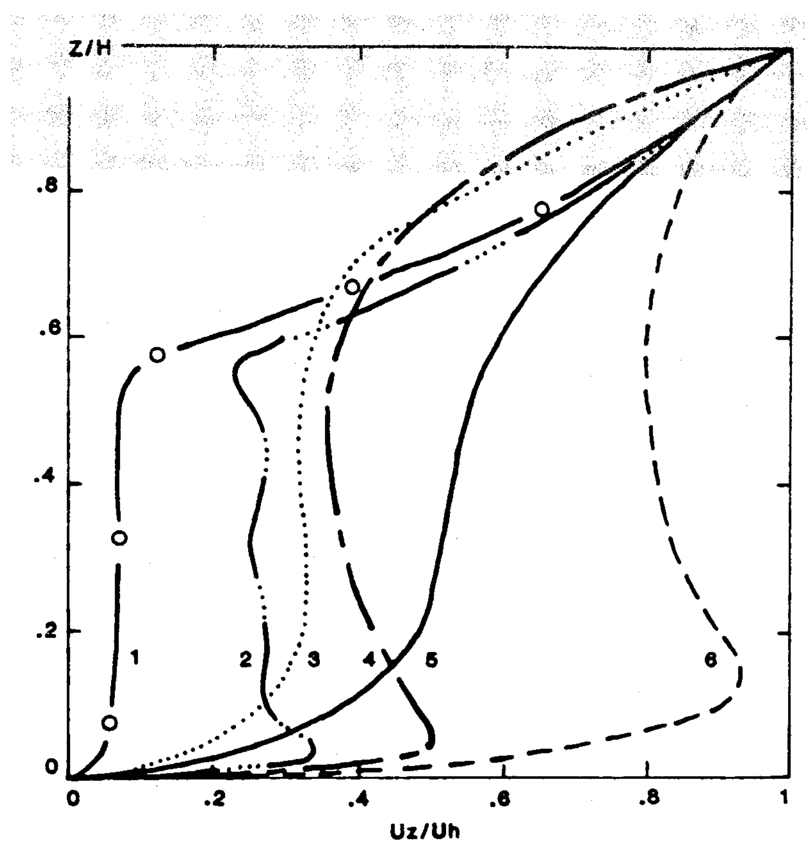

Figure 1.2: Mean wind profiles in various plant canopies, where Z is the height above the ground, H is the height of the top of the canopy, Uz is the wind speed and Uh is the wind speed at the treetop. Line 1 is dense cotton; 2 is Douglas fir forest; 3 is dense conifer with understory; 4 is moderately dense conifer stand with no understory; 5 is dense hardwood jungle with understory; and 6 is isolated conifer stand.

(1998):

1. The top layer ($d < z < h$) is the layer that exerts most of the drag on the wind above canopies. Wind in this layer is usually given by an empirical relation

$$u(z) = u(h)\exp\left[\alpha\left(z/h - 1\right)\right], \tag{1.1.4}$$

where the attenuation coefficient α can be related to the canopy structure.

2. In the second layer ($0.1h < z < d$), wind can be quite unrelated to the wind above the canopy, in both speed and direction. It is believed that the horizontal motion within the canopy is primarily the result of the pressure gradient rather than the shear driven by the airflow aloft. A large within-canopy wind speed is associated with a more open canopy. The presence of an understory affects wind speed within the trunk space. For stands without understories, secondary wind maxima, sometimes called minijets, are often found.

3. In the bottom layer ($0 < z < 0.1h$), the wind profile is similar in shape to the logarithmic profile above the canopy, except for using the forest floor surface roughness.

1.1.5 Carbon Dioxide

Figure 1.3 shows the average CO_2 concentration distributions in an 80-year-old spruce forest for three different months (Galoux *et al.*, 1981). The effects of the different carbon dioxide sources and sinks over time and height can be identified. In April, the activities of CO_2 sources and sinks are moderate and so is the daily variation

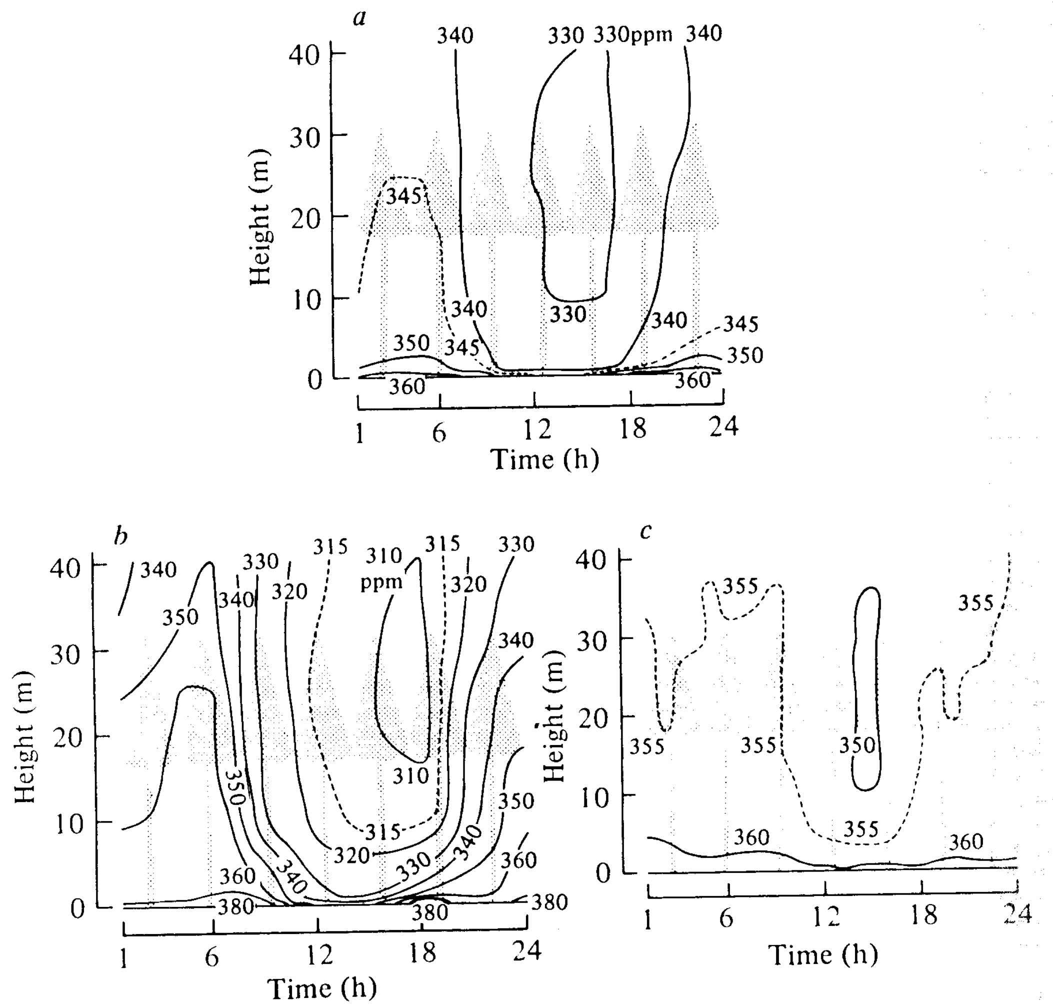

Figure 1.3: Daily CO_2 variation in forests. (a) April; (b) August; (c) December.

of CO_2 concentration. There is a strong photosynthetic carbon dioxide uptake in August, evidenced with the rapid decrease of the concentration after sunrise and the pronounced minimum during the late afternoon. At night, the buildup of the concentration within the canopy is mainly caused by the weak atmospheric mixing of the carbon dioxide from the respiration of stands and the decomposition of the organic matter in the soil. Observations have often found the carbon dioxide concentration twice of that in the free atmosphere. There is no strong sources and sinks in December. Only a slight minimum by photosynthesis occurs during the early afternoon hours. In the next chapter, it is found that CO_2 concentration can be highly changeable during wave events, which has not been paid much attention previously.

1.2 The Organized Structures in the Canopy Flow

Definitions of the organized structures in turbulent flows are somewhat subjective. We refer to both ramp-like structures and wave-like structures in the canopy flow as the organized structures. Generally, the organized structures can be visually identified from the repetitive signal patterns in the time traces of micrometeorological variables or by other flow visualization techniques. In previous literature on the canopy turbulence, the organized structures (sometimes called the coherent structures) are exclusively referred to as the ramp-like structures. Here we use this term inclusively by including the wave-like structure.

1.2.1 The Ramp-like Structure

In the daytime observations, the organized structures in the canopy turbulence manifest themselves as the striking ramp-like patterns in the time traces of scalars, such as temperature, water vapor and CO_2. Typically, a ramp-like structure is characterized by a gradual increase (or decrease) in the magnitude of the scalar followed by a sharp drop (or jump) in just a couple of seconds (Figure 1.4, from Gao *et al.*, 1989). A slow upward motion (ejection, updraft) proceeds the arrival of the scalar front. Following the front, there is a fast downward motion (sweep, downdraft, gust). The duration of these ramps is typically about several tens seconds, with somewhat seasonal variations (Lu and Fitzjarrald, 1994). The ramps occur simultaneously at several levels both within and above the canopy. A series of ramps give time traces a sawtooth pattern.

Th organized structures have been observed over short agricultural fields. Over cereal crops on windy days, the phenomenon of honami, the organized and persistent ocean-wave-like motions, has been documented and named by Inoue (1955). Honami waves appear to be analogous to "catpaws" on open water with the additional property of the plant elasticity conferring some persistence and regularity. Further detailed measurements in a barley field (Finnigan and Mulhearn, 1978a) and in a wheat field by Finnigan (1979a, 1979b) shows visual evidence that the organized structures exist in the canopy flow. When honami waves take place, the field is divided into elongated patches of coherent wavelike structures. There are 2 or 3 individual wave-like structures in each patch. The phase difference between adjacent patches is arbitrary.

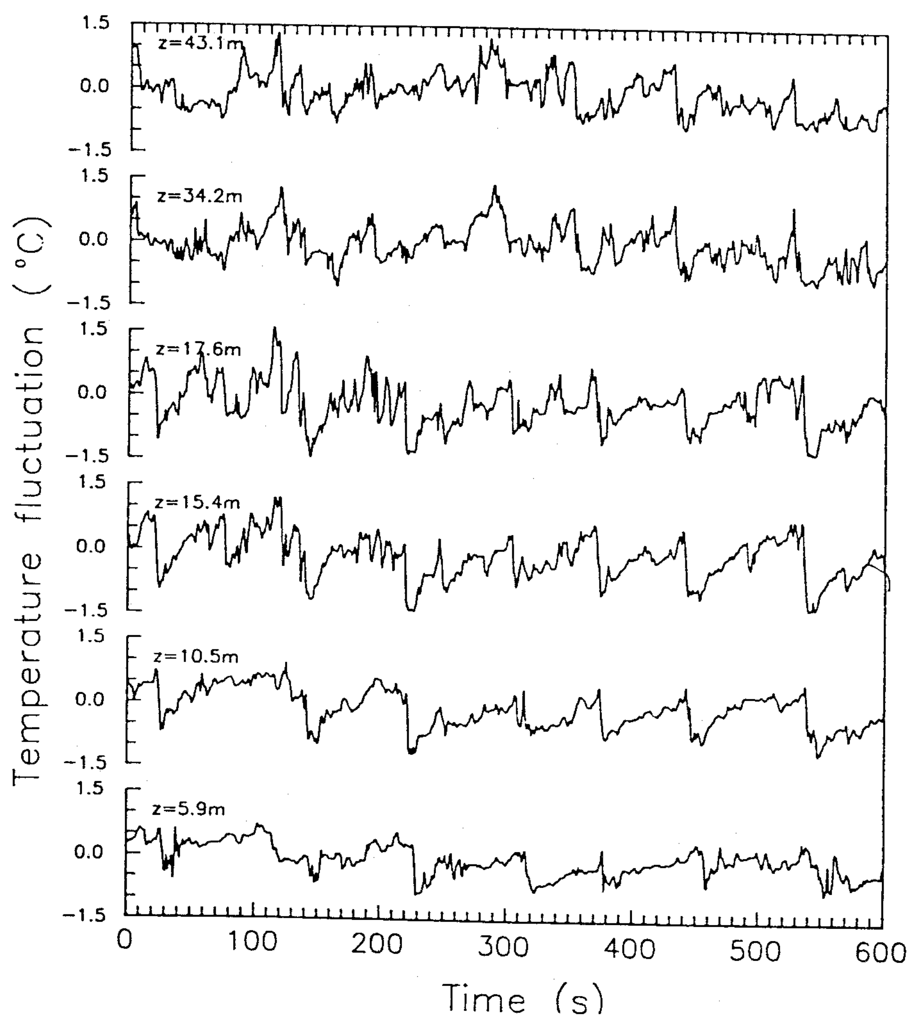

Figure 1.4: Ramp-like structures in the time traces of temperature.

Within patches, individual plants vibrated at their common natural frequency, while the small phase difference between adjacent plants varied smoothly in the streamwise direction, giving the impression of waves moving through the canopy. A patch extends about 20 canopy heights in the streamwise direction and 7 in the crosswind direction. It retains its identity for about 5 s on average. The average phase speed is about twice of the mean velocity at the top of the canopy. Finnigan and Mulhearn (1978b) have proposed that honami waves are records of the passage of gusts with high streamwise momentum. They sweep down to the surface from an outer part of the boundary layer, bending over a succession of stalks in their downwind passage. Almost all of the downward momentum transfer is done by these gusts.

Over tall forests, the coherent structures are best revealed in the time-height plot of temperature and wind fluctuation vectors (Figure 1.5, from Gao *et al.*, 1989). Under unstable conditions, it is clear that the ramp-like structures within and just above forest canopies are scalar microfronts. The temperature drops a couple of degrees in only a few seconds across microfronts. The passage of a microfront at each level lags behind those at higher levels, which makes the microfront tilted to the downwind direction. This can be explained as the result of the wind shear. Near the top of the forest, the vector flow field shows weak upward motions before the arrival of the microfront. After the arrival, the strong downward motion is most noticeable. The shift in the sign of the vertical velocity occurs almost simultaneously at all levels. The measured translation speed is close to the wind speed at the treetop. For a scalar with a negative mean vertical gradient, their time traces show the inverse-ramp structures,

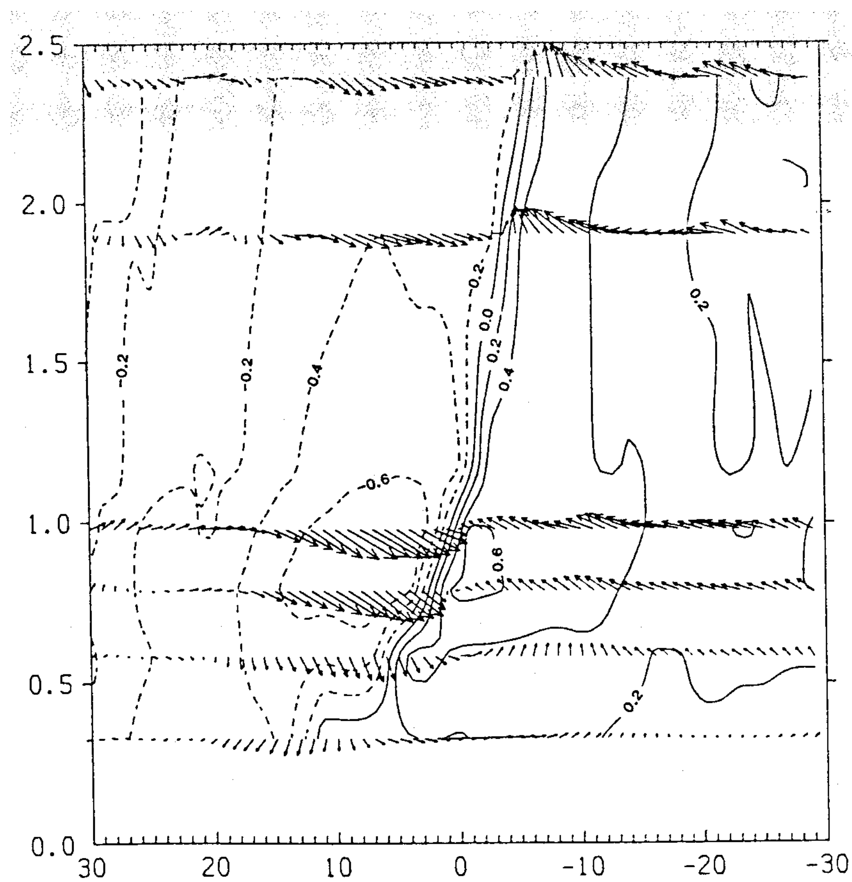

Figure 1.5: Velocity field in a temperature ramp.

which are essentially the mirror images of the ramps described above.

Under neutral conditions, the ramp patterns are not observable in air temperature traces because of the absence of a temperature gradient. However, they can be seen in other scalar fields, such as water vapor and CO_2 (Gao *et al.*, 1989; Paw U *et al.*, 1992). In the daytime, the CO_2 ramps are inverted because this scalar is depleted by photosynthesis during the quiescent ejection periods, whereas, at the same time normal water vapor ramps occur because the atmosphere is humidified by evapotranspiration. This reinforces the concept that the coherent structures occur frequently in the velocity field. It also reinforces the population that the coherent structures are shear-driven eddies rather than convective plumes (Paw U *et al.*, 1992). The patterns have been postulated as the presence of turbulent coherent structures similar to those seen in laboratory flows over rough surfaces or plant models (Raupach *et al.*, 1989).

Paw U *et al.* (1992) have proposed a picture of the nocturnal inverse temperature ramps. At night, under stable conditions, temperature inversion usually occur near the canopy tops. The nighttime ramp-like structures are general believed to be analogous to the inverse scalar ramps described above. The slow temperature drop is a result of the ejection phase of a coherent structure, which is relatively quiescent within the plant canopy, allowing the air to be cooled by the plant elements. When a strong sweep associated with the coherent structure occurs, warmer air from aloft quickly replaces the cooler air, resulting in a sharp rise in the sensed temperature. Quite often the ramp structures are closely associated with wave-like structures. The possible interactions between the two are suggested by Paw U *et al.* (1989, 1990) although the detailed connection has not been established. Lee *et al.* (1998) have demonstrated both ramps and wave-like signals are signatures of the same coherent structures, which is supported by the analysis in the next chapter of this thesis.

Fluxes Associated with the Ramp-like Structures

The role of the ramp-like structures in the turbulent transport of momentum, heat, and mass is of primary interest to micrometeorologists. Observations show that a large fraction of scalar and momentum fluxes occur during the strong intermittent coherent structures, which occur only in a small fraction of the observation period

(Finnigan, 1979a, 1979b; Raupach, 1981; Baldocchi and Meyers, 1988; Gao *et al.*, 1989; Bergström and Högström, 1989). The transfer of momentum, heat and mass occurs both in the ejection and sweep phases. Sweep events dominate flux transport within the canopy, while ejection events become increasingly important above the canopy and become equally dominant above several canopy heights. For example, Gao *et al.* (1989) have found that the ramp structures contribute 50-60% of the momentum and heat flux at the higher level and 70-80% of the fluxes within the canopy. Compared with those in the ejection phase within and just above the canopy, the fluxes in the sweep phase are much larger. At higher levels above the treetops, the contributions from the two become almost equal, like that in the surface layer. These intermittent gusts in the sweep phase are suggested to be responsible for the erratic flux-gradient relationship within canopies (Shaw, 1977; Finnigan, 1979b; Denmead and Bradley, 1985).

1.2.2 The Wave-like Structures

Nighttime micrometeorological measurements over plant canopies often find wave-like fluctuations in the time traces of temperature, wind speed, water vapor, CO_2 and other quantities. The wave mechanism and its connection with the canopy coherent structures have not been fully understood. The fact that wave-like motion is a common nocturnal motion type in forests has not been widely accepted yet. The usual instrument setup in most of the field observations are selected for the daytime conditions. Although the wave-like structures are often observed at certain levels within and above canopies along with ramp-like structures at other levels, the connection between the two could not be readily established with measurements of coarse vertical resolutions.

Phenomena

During the last two decades, there have been sporadic observational studies on the canopy wave. Maitani *et al.* (1984) and Maitani (1989) have reported persistent wave-like fluctuations, most noticeable at the top of crop canopies, in the nighttime wind and temperature measurements over a rice and a sorghum field. Their spectral analysis reveals that the wave-like motions have periods from a few minutes to several tens minutes. Compared with the time scale estimated from the crop height and the wind speed at crop tops, the rather longer periods indicate that a periodical external force drives the wave-like motion near the crop tops. It might be that the gravity wave in the atmospheric boundary layer well above canopy height periodically enhance the wind shear at the canopy tops, in turn, result in intermittent turbulence. The fluctuations would be most noticeable just above the crop tops, the height with large temperature gradients because of the radiative cooling.

Paw U *et al.* (1989, 1990) have demonstrated that waves are frequently observed in a variety of plant canopies, from short crops to tall forests. Wave trains have been found in the temperature and vertical velocity time traces, especially near the time of sunrise or sunset, under low wind conditions. Their observation in an orchard shows that wave-like fluctuations are most noticeable within the canopy. Within the canopy, sometimes the inverse temperature ramps were found to coexist with the wave-like fluctuations at other levels. Above the canopy, there were no discernible wave-like fluctuations, which suggests the waves were localized in the thin layer from the mid-canopy to just above the canopy tops. They have postulated that the waves are gravity waves trapped in the strong inversion layer near the canopy tops.

Fitzjarrald and Moore (1990) have observed wave episodes on clear nights in an Amazonian rain forest about 30 m tall. They found that the waves were triggered by the sporadic increase of the wind above the forest. It seems there was a threshold wind speed for the occurrence of these waves. The periods of these waves ranged from 65 s to 80 s. They were most noticeable in the upper canopy and just above the treetops. The wave patterns were persistent and usually lasted for several tens minutes. The sporadic occurrence of wave episodes seemed to correlate with increase of the wind speed, which was coincident with the appearance of clouds.

The recent observation by Lee and Barr (1998) showed that waves of various intensities were found in over 40% of the nighttime observations in a boreal forest. Striking wave features were revealed by the high-frequency temperature profile measured by fine-wire thermal-couples (Figure 1.6, from Lee *et al.*, 1997). The temperatures in the layer near the treetops were often manifested as inverse ramps. The high correlation between ramp-like patterns and wave-like patterns in the layers above and below indicated that the ramps were parts of the same wave event. Key wave parameters have been directly measured by a horizontally separated thermalcouple array, which was not available in previous observations. Typically, waves propagated along mean wind direction, with a speed matching the background wind speed at a few meters above the treetops. Most of the waves were found on nights when the wind over the

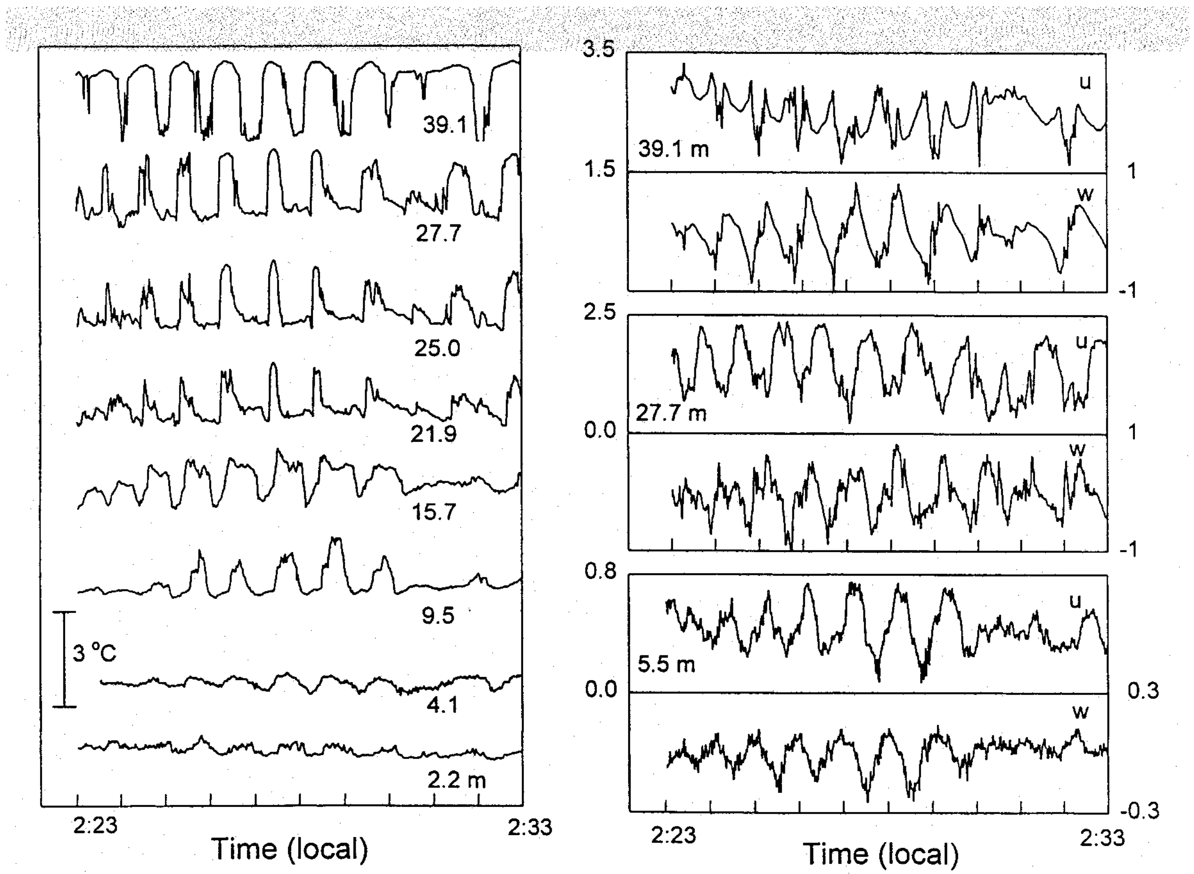

Figure 1.6: Wave-like patterns in the nighttime micrometeorological observation in a boreal forest. The tree height was 21 m. The temperature traces at 8 heights are shown in the left panel. The horizontal velocities and the vertical velocities at 3 heights are shown in the right panel.

forest was moderate and radiative cooling was very strong. The median values of the wave speed, the wavelength, the wave vertical displacement, and the wave frequency are 1.61 ms^{-1}, 75 m, 10 m and 0.02 hz, respectively. Over 90% of the wave events were found when the gradient Richardson number was less than 1.5.

Fluxes Associated with the Wave-like Motions

With the possibility that the canopy wave is a common motion type in forests, its role in the vertical mixing in the canopy sublayer is of great interest. Fitzjarrald and Moore (1990) reported that there were enhanced downward heat fluxes in the upper canopy during wave events. Significant CO_2 efflux occurred in conjunction with these wave episodes. Similar cases with enhanced CO_2 fluxes have also been observed in a temperate forest by Lee *et al.* (1996). Moreover, Lee *et al.* (1996) found the counter-gradient CO_2 fluxes associated with wave events, which is difficult to interpret with current ecophysiological knowledge. They also found that the fluxes measured near the treetops behaved better than those measured at the higher level in terms of flux-profile relations. This is a clear indication of the non-constant vertical fluxes due to the vertical variation of the wave structures. Hu and Lee (1998) have shown a case of a wave with an overturning structure. That the statically unstable structures within the waves suggested that convective instability would lead to irreversible turbulent mixing within the waves. The mixing can also be inferred from the much reduced temperature inversion near the treetops, where usually strong temperature inversion expected as a result of the strong radiative cooling. Fluxes measured at the height of the wave center were significantly larger than those measured at the upper edges of the waves. One can draw the conclusion that turbulent mixing associated with waves is height-dependent even over a short distance above the canopy tops. This rekindles the concern, raised by Fitzjarrald and Moore (1990), that the current profiling systems for CO_2 and other scalars are often too coarse to resolve this vertical variation. It implies that there might be uncertainty in the measured nighttime net ecosystem exchanges (NEE) between forests and the atmosphere during wave events. Considering the high frequency of these waves, the uncertainty is even severe for the long-term measurement of the NEE of carbon dioxide.

1.3 Theoretical Models on the Organized Structures in the Canopy flow

So far, most models treat ramp-like structures and wave-like structures as hydrodynamic instabilities of the Kelvin-Helmholtz type. The basis of these models are well-observed facts in the canopy flow, such as the inflectional wind profile and the turbulence statistics. Some quantitative results are limited in the linear regime and can only be applied to small disturbances in a undisturbed background flow. Even in the laboratory, the direct comparison between theories and experiments is extremely difficult. The applicability of these models to natural flows in canopies is rather limited. Nonetheless, these models are helpful in understanding the complex interaction between the canopy flow and plant canopies.

1.3.1 A Brief Description of the Kelvin-Helmholtz Instability

In a simplified picture, the transition from the laminar shear flow to the turbulent flow begins with a sequence of instabilities. At a sufficiently high Reynolds number, the initial unidirectional shear flow becomes unstable to the growth of long two-dimensional primary waves. The crests of the waves are normal to the shear direction. The waves grow with a rapid redistribution of fluid near the shear center. Fluid accumulates at the centers of the rolls. Narrow braids with large gradients appear to separate the rolls. Later overturning occurs with static unstable structures within billow cores. If undisturbed by further perturbations, the long waves eventually equilibrate at some finite amplitude. This state can be considered as a new basic state. It is unstable to short-wave three-dimensional disturbances. This secondary instability does not equilibrate at finite amplitude, and the flow appears to evolve directly to fully developed turbulence.

In an inflectional flow, the instability typically takes the form of periodically rolled-up clumps of vorticity, called Kelvin-Helmholtz instability (It is Helmholtz who first determined the stability criterion of this type. Kelvin later showed that the streamlines formed a “cat’s” pattern.). The form is robust and has been observed in the ocean (Woods, 1969), in the atmosphere (Altas *et al.*, 1970) and in the laboratory (Thorpe, 1969). The irreversible mixing associated with the turbulent collapse of the KH instability plays important role in the redistribution of momentum, heat, mass, and constituents in the stratified environment. In addition, other motion types can be triggered by the KH instability (Fritts, 1984).

Extensive literature exists concerning the linear stability of parallel shear flows (Drazin and Reid, 1981). After Helmholtz's study of the stability of a vortex sheet, more realistic analyses were performed. The stability diagram for a constant shear layer of finite depth with a continuous density distribution was given by Goldstein (1931)and Miles and Howard (1964). Practical velocity and density profiles were approximated by hyperbolic tangent functions and their stability diagrams were calculated by Hazel (1972). Despite the difference in the details of the profiles, a number of features of the KH instability are proved to be universal if key variables are normalized with the proper velocity and length scales. Without stratification, compared with a vortex sheet, the finite depth of the shear layer effectively suppressed the waves with large wavenumbers. With stable stratification, the increase of Richardson number will suppress both longwaves and shortwaves and their maximum amplitudes at the saturation stage (Fritts and Rastogi, 1985). No instabilities are found when Richardson number is greater that the critical value of 1/4, which is in agreement with Miles' sufficient condition for the stability. Stratification modifies the secondary instability in the free shear layer (Klaassen and Peltier, 1991). The real part of the phase speed of an unstable mode in an unbounded symmetrical shear layer is equal to the flow speed at shear layer center, or the speed of the mean flow. In a reference frame moving with the mean flow, the disturbances are stationary. In this point, it is fundamentally different from a buoyancy gravity wave, which has a phase speed that usually differs from the speed of the medium. The fastest growing mode is expected to dominate the flow structure. The ratio of the wavelength of the fastest growing mode to the shear layer depth is about 7.5.

Besides the shear and the buoyancy, boundaries and the configuration of stratification can alter the above scenario. Hazel (1972) has shown that rigid boundaries can have a stabilizing effect for short waves. However, the boundaries can make long waves less stable. For the atmosphere application, shear flows bounded by the lower rigid ground are more realistic. For a shear flow close to the ground, the growth rate and the phase speed of the KH instability is reduced (Davis and Peltier, 1976), an evidence of the stabilizing effect of the ground. The presence of the ground in a stratified environment may destabilize the flow to modes of an entirely different type (Davis and Peltier, 1979).

1.3.2 Plane-mixing Layer Analogy

Observations have led to the conclusion that the coherent structures are essentially driven by wind shear (Paw U *et al.*, 1992). The same mechanism explains the organized structures in the atmospheric surface layer turbulence (Antonia *et al.*, 1979; Phong-Anant *et al.*, 1980). The ramp structures have been postulated as the presence of turbulent coherent structures similar to those found in laboratory flows over rough surfaces or plant models (Raupach *et al.*, 1989). Raupach *et al.* (1996) have pointed out that, under near neutral or unstable conditions, the turbulence fields in plant canopies resemble the plane-mixing flow because of the instabilities associated with the inflectional mean wind profiles.

Mixing layer turbulence is generated around the inflectional mean wind profile that develops between two co-flowing streams of different velocities. Many observed features of the canopy turbulence resemble those of the mixing layer turbulence, which provide an explanation of the difference between the canopy turbulence and the surface layer turbulence. The supporting evidence includes:

- The mean wind profile has a strong inflection point near the canopy top. The inflectional instability probably determines much of the coherent eddy structure in the canopy roughness layer;
- The observed ratios between the components of the Reynolds stress tensor in the canopy turbulence are similar to those in the plane-mixing layer turbulence;
- The ratio of the eddy diffusivities for heat and momentum in the canopy turbulent flow is similar to those in the plane-mixing layer turbulence;
- The roles of ejections and sweeps in the transport processes are similar;
- The behavior of the turbulent energy balance is similar to that in the plane-mixing layer;
- The length scales of the coherent structures from observations are in agreement with the prediction from the mixing-layer analogy.

The postulated picture is that the canopy turbulence is modulated by large-scale inactive quasi-horizontal turbulence. An inflectional wind profile will be rapidly established by the canopy drag within the large-scale inactive eddy. The primary inflectional instability will develop in such a background flow to a finite amplitude. Then additional secondary instabilities will destroy the primary instability and finally lead to the full turbulence state. The observed organized structures are believed to be the vestiges of the original primary instability.

In the plane mixing layer analogy, buoyancy effects are ignored, even when the air above the canopy is strongly unstable. The justification is that the ratio of shear to buoyant production of turbulence energy varies inversely with height above the aerodynamic ground level or zero-plane displacement (Wyngaard, 1988). Qualitatively the turbulent eddy structures near the top of forest canopies share similar features across a wide range of buoyancy conditions, from weakly stable to neutral, and to unstable conditions. In the daytime, the above inflectional hydrodynamic instabilities grow to finite sizes from infinitesimal perturbations in a rather short time. The subsequent nonlinear development of the mixing layer towards a fully turbulent state includes several additional instability processes, such as three-dimensional instabilities, nonlinear vortex interactions, and background small-scale turbulence (Ho and Huerre, 1984; Thorpe, 1985, 1987; Caufield *et al.*, 1996).

1.3.3 The Canopy Wave Models

A Brief Review of Current Canopy Wave Models

To date, only a couple of models have been developed to interpret canopy waves. These models, all in the linear regime, can explain wave features in certain aspects. By introducing an artificial periodical pressure gradient forcing, the resonance model by Fitzjarrald and Moore (1990) can reproduce salient wave-like signals similar to their observation. Nevertheless, the nature of this periodical forcing is obscure. Furthermore, the model cannot explain the enhanced fluxes of momentum and scalars during the wave events. Together with other assumptions, the model does not provide much insight into the wave dynamics.

In the three-layered model (Paw U *et al.*, 1989), canopy waves are treated as trapped gravity waves in the nighttime inversion layer near the canopy tops. Although wave parameters inferred from their model are in accord with their observation, this simple model has its limitations. First, the canopy effect is not directly included in the wave dynamics. The role of the canopy is limited in maintaining the strong temperature inversion at the treetops to trap the gravity wave. Secondly, Hu and Lee (1998) have presented a wave event with much reduced temperature inversion near the treetops, which contradicts the strong temperature inversion required by the trapping mechanism.

The linear canopy wave model by Lee (1997) extends the plane-mixing layer analogy for the canopy turbulence (Raupach, *et al.*, 1996) to stable conditions. His model shows that canopy waves share features of a Kelvin-Helmholtz (KH) instability. The canopy effect and the proximity to the ground modify the KH instability in several aspects. The main attraction of Lee's model is that it gives a wave generation mechanism, which is not possible with the other two models mentioned above. Furthermore, the irreversible mixing, associated with the subsequent nonlinear processes of KH instability, might explain the often observed enhanced fluxes associated with waves although this is beyond the scope of Lee's linear model.

Lee's Linear Canopy Wave Model

The linear canopy wave model by Lee (1997) furthers the plane-mixing layer analogy to the stable condition. In chapter 4, this model is compared with a two-dimensional numerical model. Here a brief outline is provided. Lee's model takes into account of the canopy drag exerted on the wind components by plant elements and plant-air heat exchange by the temperature oscillation. The linearized inviscid Navier-Stokes equations with the Boussinesq approximation are

$$\frac{\partial u'}{\partial t} + U\frac{\partial u'}{\partial x} + w'\frac{\partial u'}{\partial z} = -\frac{1}{\rho_0}\frac{\partial p'}{\partial x} - C_d A U u', \tag{1.3.1}$$

$$\frac{\partial w'}{\partial t} + U\frac{\partial w'}{\partial x} = -\frac{1}{\rho_0}\frac{\partial p'}{\partial z} + g\frac{\theta'}{\theta_0} - C_d A U w', \tag{1.3.2}$$

$$\frac{\partial u'}{\partial x} + \frac{\partial w'}{\partial z} = 0, \tag{1.3.3}$$

$$\frac{\partial \theta'}{\partial t} + U\frac{\partial \theta'}{\partial x} + w'\frac{\partial \theta_0}{\partial z} = -C_h U A \theta', \tag{1.3.4}$$

where U is the mean wind, u' and w' are the wave components of the horizontal and vertical velocities, θ_0 is the mean potential temperature, θ' is the wave introduced potential temperature fluctuation, C_d is a dimensionless drag coefficient, C_h is the heat exchange coefficient, and A is the plant element area density.

For a small disturbance, the nonlinear interaction between various Fourier components can be ignored. The stability property of the flow can be studied by examining a Fourier mode in the form of

$$f' = \hat{f}(z)\exp\left[i\left(kx - ct\right)\right] + c.c., \tag{1.3.5}$$

where k is the wavenumber, $c = c_r + ic_i$ is the complex phase speed and $c.c.$ denotes the complex conjugate. The stability property of a mode is determined by the imaginary part of the phase speed c_i. A mode is stable if $c_i < 0$, unstable if $c_i > 0$, or neutral if $c_i = 0$. The growth rate, gauging the exponential growth in the linear stage, is defined as

$$\sigma = kc_i. \tag{1.3.6}$$

The reciprocal of this parameter is the time needed for a small disturbance to grow by a factor of e. It is also called e-folding time.

A modified Taylor-Goldstein equation can be derived as

$$\frac{d^2\hat{w}}{dz^2} + \frac{1}{a}\frac{d}{dz}\left(C_d A u\right)\frac{d\hat{w}}{dz} - \left(\frac{N^2k^2}{aa_1} + \frac{ik}{a}\frac{d^2u}{dz^2} + k^2\right)\hat{w} = 0, \tag{1.3.7}$$

with auxiliary variables

$$a = ik\left(u - c\right) + C_d A u, \tag{1.3.8}$$

$$a_1 = ik\left(u - c\right) + C_h A u. \tag{1.3.9}$$

The structure functions are given by

$$\hat{\theta} = -\frac{\hat{w}}{a_1}\frac{d\theta}{dz}, \tag{1.3.10}$$

$$\hat{u} = \frac{i}{k}\frac{d\hat{w}}{dz}, \tag{1.3.11}$$

$$\hat{p} = \frac{\rho}{ik}\left(\frac{a}{ik}\frac{d\hat{w}}{dz} - \hat{w}\frac{d\hat{u}}{dz}\right). \tag{1.3.12}$$

With properly specified boundary conditions, the eigenvalue problem for wavenumber k and complex phase speed c can be solved for a given set of background profiles.

Lee's analysis indicates that canopy waves are generated by the wind shear near the treetops and share features of the Kelvin-Helmholtz wave. The main role of the canopy drag in the wave dynamics is to maintain an inflectional point in the mean wind profile. The ground, which is close to the inflection point of the mean wind profile, exerts a strong stabilizing effect on wave motions, particularly in a sparse forest. The phase speed of the canopy wave is greater than the mean wind speed at the treetop height, where the maximum shear is found. The ratio of the wavelength of the fastest growing mode to the half shear layer depth agrees with previous linear analyses.

Chapter 2

Flow Structures of Nocturnal Wave-like Motions in Forests

A quarter century ago, measurements of turbulence in plant canopies were mainly concerned with the mean turbulence statistics. Much effort has been devoted to relate these means to the boundary conditions of the flow field, the canopy geometry and the reference mean velocity. The canopy transport was simply treated as a gradient diffusion process and characterized by eddy diffusivity, known as K-theory. Later observations raised the question about the efficacy of the K-theory. For example, Wilson and Shaw (1977) and Raupach (1979) have pointed out that the eddy diffusivity would behave erratically in the existence of a vertical downward momentum flux combined with a zero or negative velocity gradient. It implies that there cannot exist a simple first-order "K-theory" flux-gradient relationship for momentum in the canopy layer.

It becomes clear that the failure of the K-theory results from the neglect of the unsteady detail of the canopy flow in the early observations and theoretical works. At the same time, like the trend in the turbulence study in general, the importance of organized structures has been widely recognized (Laufer, 1975). The sweep-ejection cycles have been shown to dominate the smooth surface of the laboratory boundary layer. It is also a feature of the rough-wall boundary layer (Grass, 1971). Close to a rough wall, the dominant mechanism transferring momentum to the surface is the sweep or gust rather than the ejection (Nakagawa and Nezu, 1977). In the atmospheric surface layer, the temperature ramps have been analyzed and the structure of the thermal plume has been depicted (Wilczak and Tillman, 1980; Wilczak and Businger, 1983). However, further measurement indicates that the scalar ramps as signatures of organized structures result from wind shear rather than from differential heating (Antonia *et al.*, 1979). In the experimental studies of canopy turbulence, the importance of coherent structures with scales of the canopy height has been appreciated. Measurements on Honami waves over short crops have provided direct visual evidence of the organized structures in the canopy turbulence (Finnigan, 1979a; 1979b). Over a tall forest, Denmead and Bradley (1986) have depicted intermittent gusts with a sequence of scalar profiles. Their measurement indicates the non-local nature of the canopy turbulent transport, which explains the failure of K-theory. The micro-front structure of the gusts over tall forests has been revealed by further observations (Gao *et al.*, 1989; Bergström and Högström, 1989). The organized structures under various stability conditions have been summarized by Paw U *et al.* (1992). All these observational studies lead to the plane-mixing layer analogy (Raupach *et al.*, 1996), which states that organized structures in canopy turbulence is the manifestation of the shear instability.

The method used by Gao *et al.*, (1989), Bergström and Högström (1989) to analyze organized structures in canopy turbulence was similar to the approach by Wilczak and Tillman (1980). The instrument setups in these observations were mainly for unstable and neutral conditions. At night, in weakly stratified turbulence, temperature inversions were usually found near canopy tops. Inverse ramps identified in temperature traces were usually believed to be the mirror images of those in the daytime conditions (Gao *et al.*, 1989; Paw U *et al.*, 1992). Frequently, wave-like motions coincide with ramp-like structures (Paw U, *et al.*, 1990). The exact connection between the two has not been established yet. The observation by Lee and Barr (1998) indicated that both waves and ramps were the signatures of the same underlying organized structures. They also demonstrated that waves of various strengths dominated the nighttime observation in a boreal forest. The wave-associated mixing was suggested by Hu and Lee (1998). However, unlike daytime ramp-like structures, flow structures for nocturnal wave-like motions over forests remain largely unknown.

In this chapter, the two-dimensional flow structures of nocturnal canopy waves will be investigated by a procedure analogous to those used by Wilczak and Tillman (1980), and Gao *et al.* (1989). Wave structures will be analyzed in detail with the high temporal and spatial resolution temperature measurement. The difference between wave structures and inverse ramp structures will be stressed. The mixing ability by waves and its implication to CO_2 flux measurement will also be discussed.

2.1 Site and Data

The data was collected during the 1994 field campaign of the BOREAS (Boreal Ecosystem Atmosphere Study, Sellers *et al.*, 1995) at Prince Albert National Park, Saskatchewan, Canada (53°42′N, 106°12′W). The forest was an extensive 70-year old stand of trembling aspen (*populus trmuloides*) about $h = 21$ m tall. Canopy base was 15 m, while the stand density was about 530 per hectare. There was a thick understory of hazelnut (*Corylus cornuta*) approximately 2 m high. At the time of the observation, the overstory and understory leaf area indices were 1.8 and 3.2, respectively. There were 3 sonic anemometers mounted at 5.5, 27.7, and 39.1 m from ground level. The fast response water vapor and CO_2 sensors were mounted at 39.1 m for the flux measurement. There were 12 fine wire thermocouples (chromel-constantan, 26 μm diameter) at 2.2, 4.1, 6.4, 9.5, 12.6, 15.7, 18.8, 21.9, 25.0, 27.7, 31.4, and 39.1 m, being sampled at 5 Hz. The precision and the accuracy of the temperature measurements were estimated to be 0.0008-0.0028 K and 0.01-0.033 K, respectively. Detailed information of salient wave structures can be inferred from the temperature profile, supplemented with the velocity field from the 3D sonic anemometers. The details of the observation can be found in Lee *et al.* (1997).

2.2 Flow Structures of Wave-like Motions in Time-Height Dimensions

2.2.1 Background Conditions

Striking wave-like structures can be visually identified in the time-height contour plots of the temperature profiles measured by the thermalcouples. Some of the background conditions favorable to the occurrence of canopy waves are:

1. Radiative cooling is strong (usually when the net radiation above the treetops is less than -40 Wm^{-2}.);

2. Wind above canopies is moderate. Vertical wind fluctuations above canopies are moderately large.

The above criteria can almost serve to predict the occurrence of waves in this data set. In the following discussion, the data for the night between 22:00, 12 July and 05:00, 13 July, 1994 will be presented to illustrate the salient wave features. Waves at other clear nights share similar properties.

Figure 2.1 shows the general meteorological background measured above the treetops from the night on July 12, 1994 to the early morning on July 13, 1994. The measured net radiation at 34 m indicated that the net radiation reached about -70 Wm^{-2} shortly after sunset and remained strong for the whole night, except for the interruptions by clouds at midnight and around 03:00, July 13. Just after sunset the wind was calm. The wind speed was steadily picking up and reached above 3 ms^{-1} just before sunrise. In general, wind was from the NW sector and the variation of the wind direction was moderately small.

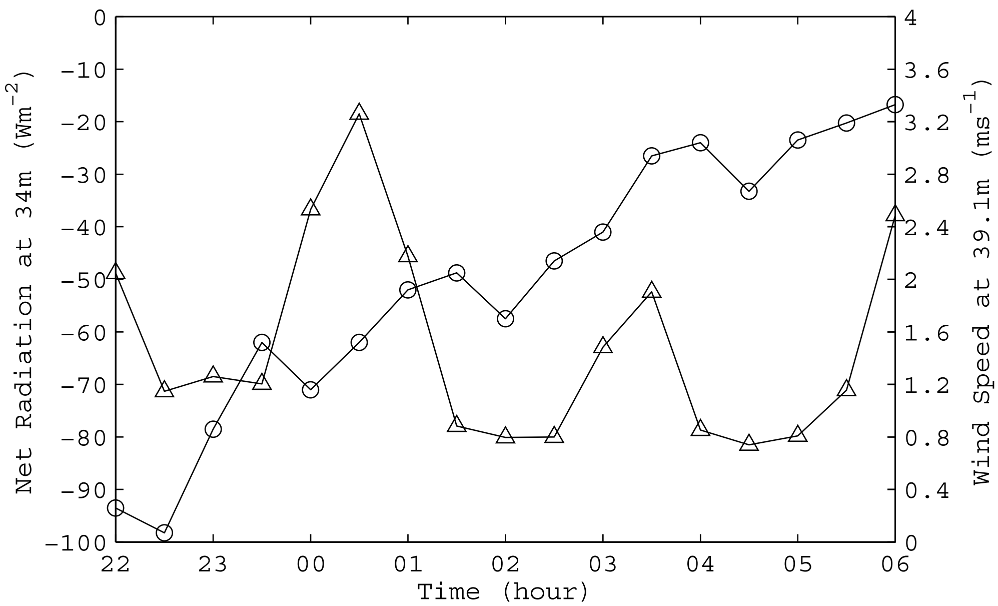

Figure 2.1: Background wind speed (circle) and net radiation (triangle)

Waves were usually found near the treetops when the standard deviations of the vertical velocities σ_w were active (Figure 2.2). In general, σ_w tended toward increasing with the wind speed. The vertical velocity fluctuations measured above the canopy exhibited the characteristics of intermittence. There was good correlation between the peaks of σ_w above the canopy and the well-organized wave patterns in the temperature measurement.

The gradient Richardson number Ri (Figure 2.3) has been calculated with the 5-minute-averaged wind speeds at 39.1 m and 27.7 m and temperatures at 39.1 m and 31.4 m. It is the averaged value for the layer between $1.5h$ and $2h$. Since the maximum wind shear was near the treetops, the minimum Richardson number was expected to be smaller than that in Figure 2.3. The accuracy of Ri before 23:30, July 12 is probably not good since the wind speed was very low. From 23:30, July 12 to

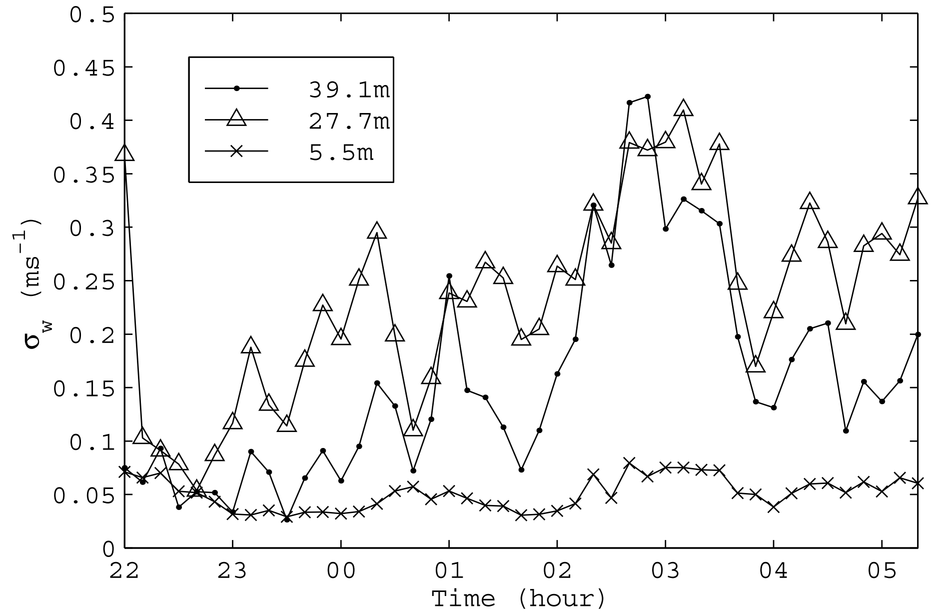

Figure 2.2: The standard deviations of vertical velocities at three levels

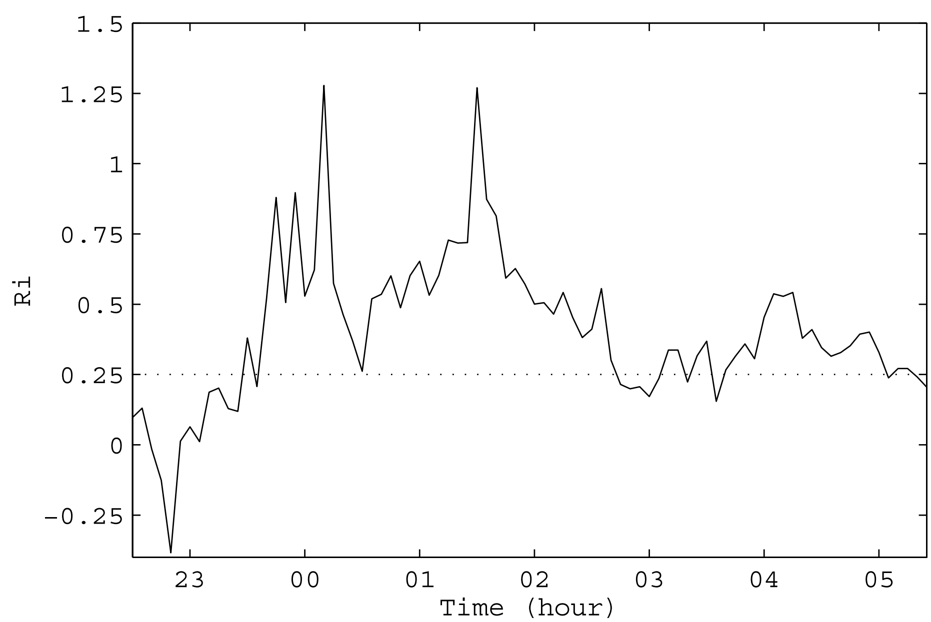

Figure 2.3: Richardson number

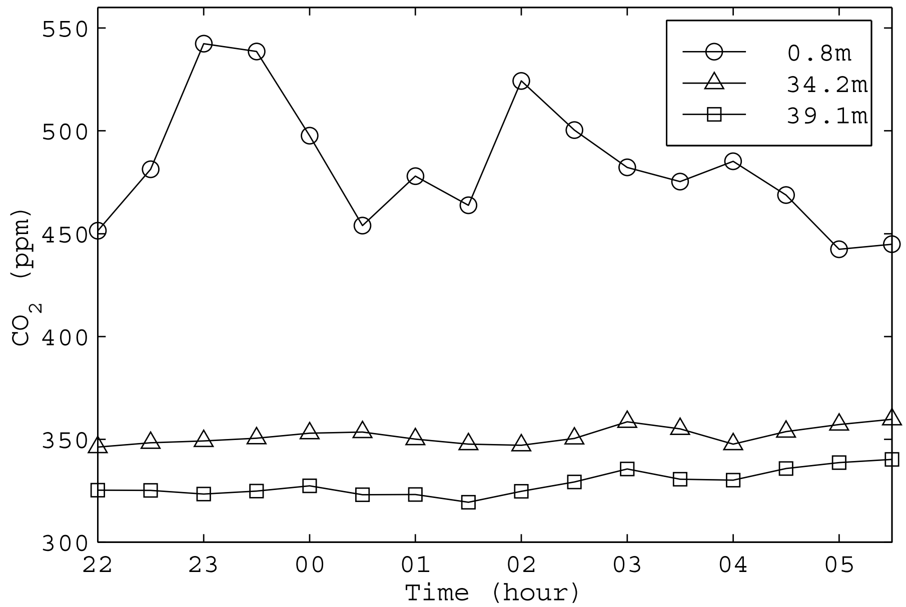

Figure 2.4: 30-minute-averaged CO_2 concentration at three heights

02:40, July 13, Ri was greater than the critical value 0.25. From 02:40 to 03:40, Ri was oscillating around the critical value. After that, it again remained larger than the critical value. The evolution of Ri will be easily understood if one interprets it with the strengths of wave activities, which shall be discussed later.

The 30-minute averaged CO_2 concentration plot (Figure 2.4) shows that CO_2 concentration at 34 m and 39 m were roughly constant throughout the whole night, with a consistent negative gradient. The concentration at the ground level exhibited a large variation. After sunset, it was steadily building up, presumably as the result of the suppressed turbulent mixing. Around midnight it reached its peak value of about 545 ppm. From 12:00 to 02:00, it decreased to 400 ppm. Later another peak of about 530 ppm was found at approximately 02:00, July 13.

2.2.2 The Morphology of the Wave-like Motion

Salient wave structures are best revealed from the time-height plots of tower-based high-vertical-resolution temperature profiles (Figure A.1-A.14 in Appendix A). Wave activities showed a number of distinctive stages in response to the changes of the net radiation and the wind speed above the treetops.

Shortly after sunset, when the wind speed at 39.1 m was low (the 30-minute averaged value was 0.84 ms^{-1}), a strong temperature inversion was found in the thin layer at the treetops (Figure A.1). Above and below the inversion layer, the air was nearly neutral, the signature of the residual layer. The inversion layer was slightly disturbed between 400 s and 600 s. The strength of the inversion layer was enhanced during 600 s to 1200 s as the result of the continuing radiative cooling and little turbulent mixing. As time progressed, the wind speed began to pick up and wavy structures appeared in the thin inversion layer. These wavy structures were confined near the treetops by the near-neutral layers above and below. The inversion layer gradually deepened, and the strength of the temperature inversion was gradually reduced. This might be the result of the mixing associated with the wavy structures, which first appeared when the wind began to increase.

From 22:30, July 12 to 01:45, July 13, wave activities were moderated. This period was characterized by repetitive wave events. The σ_w peaks (Figure 2.2) occurred at the time of well-organized waves (Figure A.1-A.8). The potential temperature fluctuations, which depicted the wave structures, indicated that waves were confined below $2h$. Wind fluctuations at $2h$ had good correlation with those near the treetops.

The σ_w at $1.3h$ was consistently larger than that at $1.9h$. Even with wind fluctuations measured at only three levels, it is speculated that the source of the wind fluctuations was located near the treetops, not from the layer well above.

In Figure A.2 and Figure A.3, a complete life cycle of a wave event can be identified. From 22:50, July 12 to 23:10, July 12, small disturbances appeared in the temperature inversion layer. Its vertical amplitude apparently began to grow. In the same time, the inversion layer was gradually deepened by the temperature gradient was gradually reduced. From 23:10 to 23:20, the wave seemed to reach a steady finite amplitude state. The layer affected by wave activities extended from the mid-canopy to about $2h$. From 23:20 to 23:40, the waves seemed to be destroyed and the treetop inversion layer was re-established. This occurred coincidentally with both the minima of the wind speed (Figure 2.1) and the stand deviations of vertical velocities (Figure 2.2). Similar cycles happened a couple of times until 01:45, July 13. In the later portion of this period, waves were more striking in the time-height potential temperature plots mainly because of the steep temperature gradient at the treetops as a consequence of the enhanced radiative cooling.

Typically, wave events lasted for about several tens minutes. Compared with the duration of each wave episode, the relatively quiescent periods to separate the wave episodes were shorter, typically from several minutes to about 10 minutes. In the quiescent periods, the vertical wind fluctuations were much reduced. The temperature inversion at the treetops was enhanced by the continuing strong radiative cooling and reduced mixing. The peaks and valleys in Figure 2.2 actually revealed the intermittence of the waves. The rather long wave periods observed by Maitani *et al.* (1984) and Maitani (1989) were probably the periods of the external forcing rather than the periods of the waves.

From 02:00 to 04:00, July 13, the reduction in the net radiation and the increase of wind speed implies the occurrence of an outer scale event, likely associated with the appearance of clouds. Wave activities at this time were much stronger than those in the early part of the night. This wave event probably started at 01:45, July 13, when the treetop inversion layer was quiet and the standard deviations of the vertical velocities were at their minima. From 01:45 to 02:20, waves were similar to those described above. During this period, the σ_w at $1.9h$ was smaller than that at $1.3h$. However, the difference was shrinking. Eventually, the σ_w at the two levels were of the same magnitude, coincidentally with the increase of wave amplitudes identified from the time-height temperature contour plots. From 02:20 to 02:45, the layer affected by the wave activities extended above $2h$ and was probably limited to below $3h$. From 02:45 to 03:40, the destruction of the waves began. The remaining temperature field exhibited irregularly-spaced structures, the reminiscence of the original waves. A relatively quiescent inversion layer was found from 03:50 to 04:00.

From 04:00 to 05:30, July 13, the wind at $1.9h$ climbed to 3.2 ms^{-1}, and the net radiation was about -80 Wm^{-2} to -70 Wm^{-2} (Figure 2.1). The σ_w at $1.9h$ was smaller than that at $1.3h$ (Figure 2.2). The waves were again confined below $2h$, and were much like those in the early part of the night, except that the wave periods were much shorter.

2.2.3 Temperature Fluctuations

The temperature fluctuations within the canopy were more or less in phase. At the upper edges of the waves, the temperature fluctuations were also more or less in phase. For vertically propagating gravity waves, tilted phase lines are expected. The observed phase relations obviously exclude the possibility of vertically propagating gravity waves. A phase shift occurred in the thin layer near the treetops, which gave the impression that the waves tilted in the downwind direction. The tilt of the phase lines gave the wave trains a look similar to that of billow waves. These billows were characterized by rather isothermal cores, delineated by steep temperature gradients at both their leading edges and their trailing edges. For some waves, the leading edges were more diffusive, and the temperature gradients at trailing edges were usually steeper.

There were very interesting fine structures within the wave cores. In the core of the wave around 02:22, the warmer air above the canopy dipped into it and then was slowed down by the canopy drag. At the same time, the slow cooler air went up out of the canopy and was sped up by the ambient air. Together, they gave the impression that the warmer air and the colder air were spinning around each other with a positive spanwise vorticity just above the treetops, close to the shear maximum. In the following several waves, the warmer air seemingly went down deeper and was retarded further backward, which resulted in slender, finger-like, warmer stripes at the lower edges of the wave cores. The cooler air was engulfed in the cores and was eventually disconnected from the cooler air within the canopy. Since such overturning structures are statically unstable, turbulence from gravitational instability would be expected, similar to those found in the laboratory experiment by Thorpe (1969). Indeed, in spite of the continuing radiative cooling, the enclosed air in the subsequent cores was actually getting a bit warmer. It might be the consequence of the turbulent mixing associated with the wave overturning if the advection effect could be excluded.

In most micrometeorological observations in the canopy roughness layer, measurements are usually limited at several levels. A variety of patterns, including ramp-like and wave-like structures, has been frequently found in the time traces of scalars and wind fluctuations at night. The various signal patterns in the temperature time traces were really the manifestations of underlying wave structures. Temperature traces seldom assume sinusoidal shape, as expected for linear waves. At about $2h$, square-wave-like signal patterns are often found. These waves had rather flat tops, with various intervals separating them. The short separating intervals generated downward spikes in the time traces of temperatures. A conjecture can be made that there were little disturbances in the layer of the air above $2h$ in this particular half-hour. Temperature traces from sensors located in this layer would be flat lines. The underlying motions would periodically bring cool air up, which would generate dips in the time traces and result in the square-wave-like patterns. Apparently, the disturbance did not originate from the layer well above the canopy, and the motion was confined in the layer below $2h$.

For some waves, the temperature gradients in both the leading edges and the trailing edges had opposite signs and were roughly of the same strength. The cores of the waves were rather isothermal. Temperature sensors detected square-wave-like patterns when these waves passed the tower. From the mid-canopy to just above the treetops, ramp-like structures were typical. They differ from the daytime ramps by their persistence and well-defined periodicity. Usually just above the treetops, at the centers of some of the waves, the temperature gradients at the leading edges were more diffused than those at the trailing edges. Such wave structures would result in the inverse ramps in the temperature traces measured at that level. The strength of the temperature fluctuation within the canopy was closely related to the strength of the wave trains. At the middle of the canopy and lower, the structures were more or less of sinusoidal waves.

It deserves to be pointed out that, in previous observations (*e.g.* Paw U *et al.*, 1989; 1990; 1992), the coincidence of waves and ramps at different levels have been noticed and the interactions between the two have been suggested. However, they were treated as different motion types. Here, the example supports the argument by Lee and Barr (1998) that both of the signal patterns are manifestations of the same underlying canopy waves.

2.2.4 Velocity and Scalar Fluctuations

In this section, the wind velocity fluctuations will be examined by superimposing the horizontal and vertical fluctuations of velocity vectors on the time-height temperature contours. The coordinate rotation has been performed to align the x-axis to the mean wind direction. Five five-minute segments of the data from 01:45 to 04:00, July 13, when the wind fluctuations at both $1.3h$ and $1.9h$ were strong enough to give meaningful results, will be presented. The time traces of CO_2 and water vapor measured at $1.9h$ during the same periods will also be presented for reference.

Example I

Judged from Figure 2.5, the wave activity was weak in this example. The temperature fluctuations were found mainly below $2h$. Although the magnitude of the wind fluctuations at $1.9h$ was small, the distinctive periodical pattern can still be visually identified. At $1.3h$, wind fluctuations were also weak. Nevertheless, it was bigger than that at $1.9h$. Larger wind fluctuations and distinctive patterns were associated with temperature microfronts (for example, between 01:46 and 01:47). The leading edge of this wave was characterized with a steeper temperature gradient than its trailing edge. The temperature sensors near $1.3h$ would detect inverse ramp-like signals. It is interesting that this temperature microfront, unlike the daytime coherent structures, tilted backward to the direction of the mean flow. Before the arrival of the microfront, the air motion shared features of a sweep. Following the front, the motion was similar to an ejection. In contrast to the daytime ramps, where sweeps are dominant, the ejection and the sweep had similar magnitude in this case. The remarkable constant concentrations of CO_2 and H_2O at $1.9h$ could indicate that little vertical displacement of air parcel at that height; it could also indicate that the sensors were located in a previously well-mixed layer. Together with the behavior of the measured wind fluctuations, it may be inferred that the source of the disturbance was located near the treetops, rather than from above.

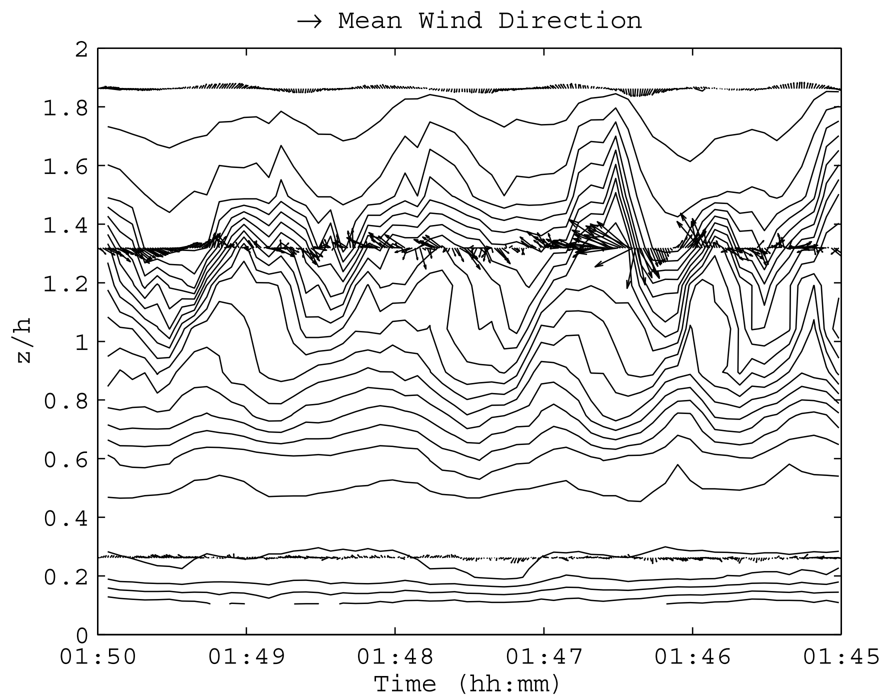

(a) Wind fluctuations superimposed on temperature contours. The magnitude of the maximum wind fluctuation is 0.79 ms^{-1}. The contour interval is 0.2K.

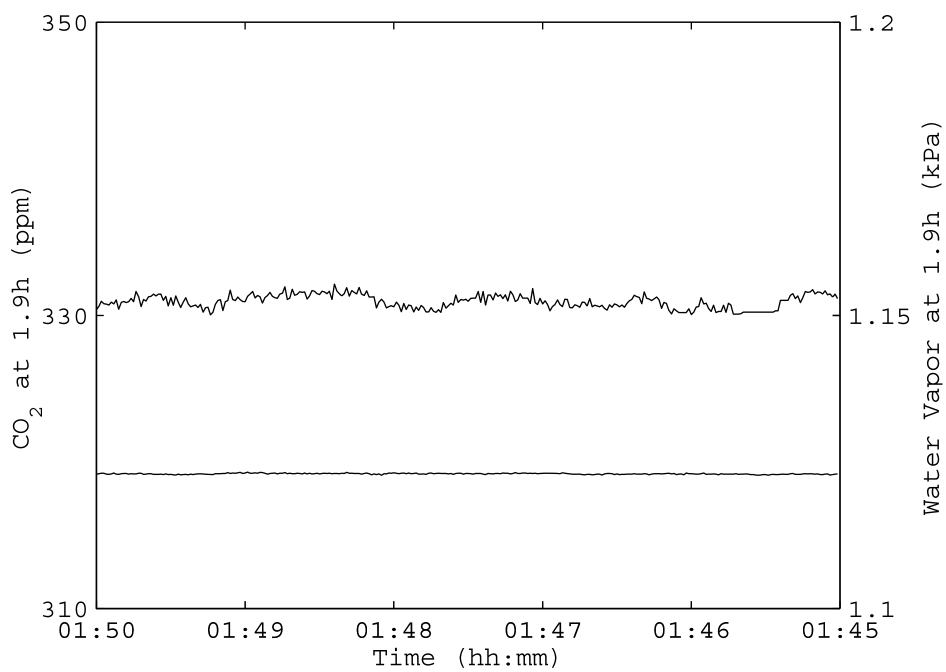

(b) Scalar fluctuations

Figure 2.5: Velocity and Scalar Fluctuations (I)

Example II

For waves with moderate strength (Figure 2.6), the wave cores were confined below $2h$. The sonic anemometer at about $1.9h$ was located above the upper edge of the wave cores, away from the maximum shear. The vector pattern indicated that the vertical velocity fluctuation w' was approximately in quadrature with the horizontal velocity fluctuation u'. More specifically, u' led w' by $\pi/2$. In spite of the relatively large magnitude of the wind fluctuations, little net momentum flux would be resulted in if the instant momentum flux $u'w'$ is averaged over one wavelength. The temperature fluctuation was also roughly in quadrature with the vertical velocity fluctuation, which means little net sensible heat flux too. The phase relations here bear the resemblance to those of evanescent waves.

The disturbances in CO_2 and H_2O time traces (Figure 2.6(b)) at $1.9h$ were closely associated with the strength of the wave activity revealed by the temperature contour plot. The flat baselines in CO_2 and H_2O plots suggested that the sensor at this level was in a previously well-mixed layer. Waves with large amplitude would bring air parcels with high CO_2 and less humidity to the instrument height and would result in spikes in the scalar time traces. Since a high CO_2 concentration is expected within the canopy by the respiration of trees, understory bushes and the soil, waves would certainly generate positive spikes in the CO_2 trace measured above the canopy. The negative spikes in water vapor measurement indicated a downward gradient, which can be interpreted as the result of condensation on the ground and plant elements on this clear night.

The sonic anemometer at $1.3h$ was situated near the center of the wave cores. Compared with those at the upper level, wind fluctuations at $1.3h$ were larger and messier. Patterns of sweeps and ejections can be identified at this level. The phase relations between the horizontal component and the vertical component are favorable to generate a large downward momentum flux. Unlike in the daytime ramps, where sweeps dominate, here the sweeps and ejections associated with waves are of the same order in the momentum transport. It should be noted that the moderate correlation between the vertical velocity and the temperature was positive. The heat flux at $1.3h$ during this five-minute period was upward, which was apparently counter-gradient. The momentum flux at $1.9h$ was also against the background wind gradient. Similar erratic gradient-flux patterns associated with waves have been previously reported by Lee *et al.* (1996). Clearly, a better understanding of these waves would be instrumental to interpret the erratic behaviors of the measured fluxes.

Example III

Strong wave activity was found in Figure 2.7. The sonic anemometer at $1.9h$ measured the wind alternatively in the wave cores and outside the cores. Outside the wave cores, u' and w' were in quadrature as were those in the previous example. Part of the measurement inside the billow cores in general has the sweep-ejection pattern. At the leading edges where temperature gradients were steeper, wind fluctuations were comprised of sweep patterns. Following the sweeps were ejections located mainly in the wave cores. It was these sweeps and ejections that effectively generated downward momentum flux at this height. In other words, momentum flux is generated only at

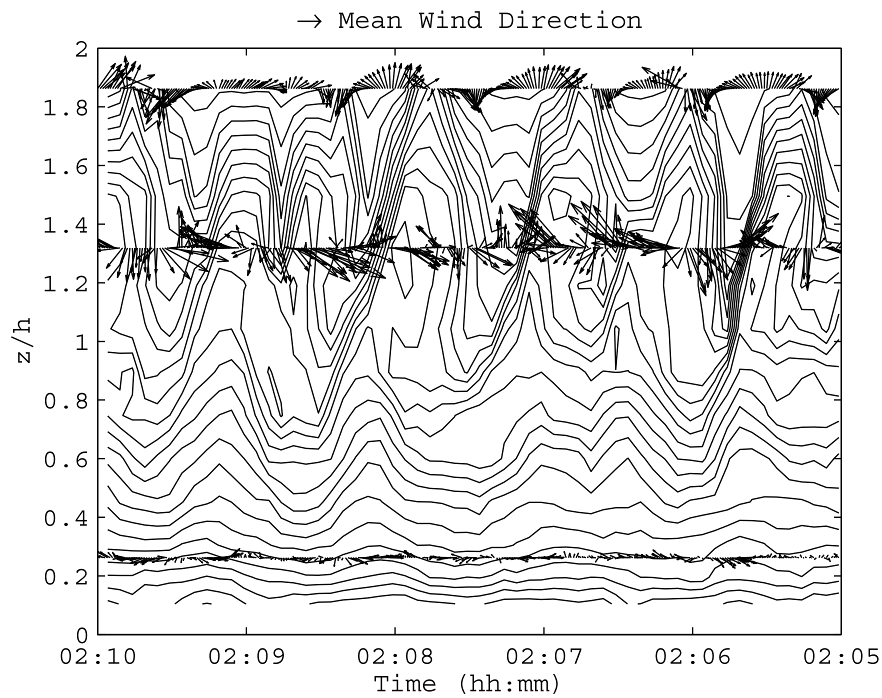

(a) Wind fluctuations superimposed on temperature contours. The magnitude of the maximum wind fluctuation is 1.01 ms^{-1}. The contour interval is 0.2K.

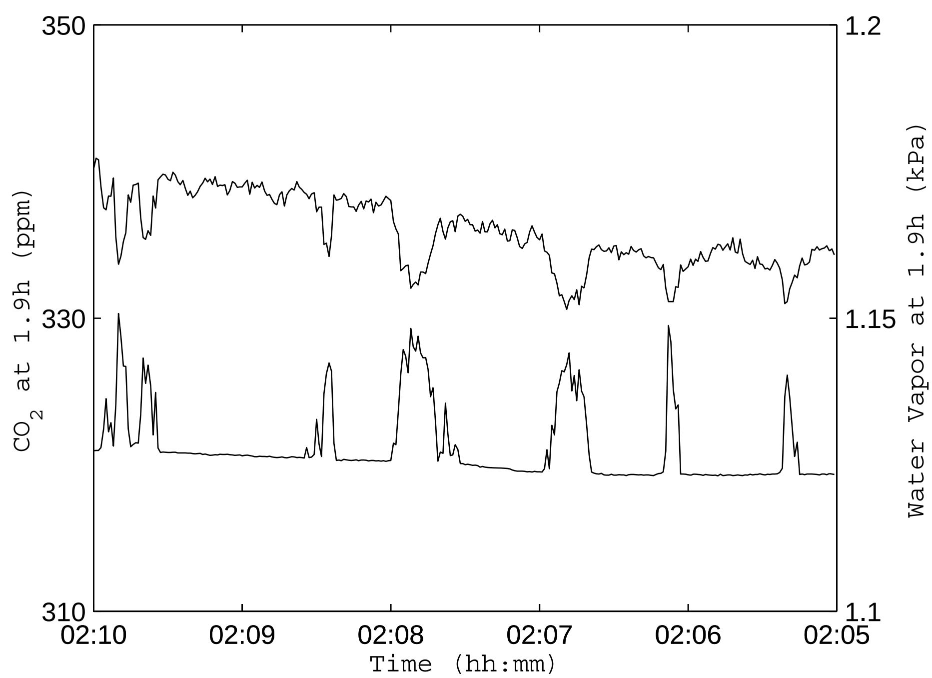

(b) Scalar fluctuations

Figure 2.6: Velocity and Scalar Fluctuations (II)

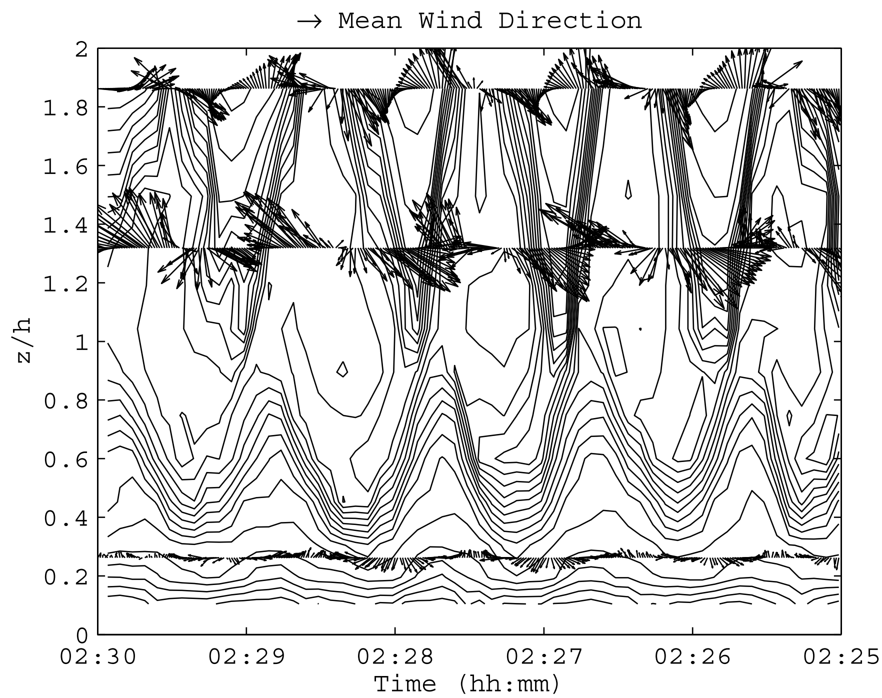

(a) Wind fluctuations superimposed on temperature contours. The magnitude of the maximum wind fluctuation is 1.29 ms^{-1}. The contour interval is 0.2K.

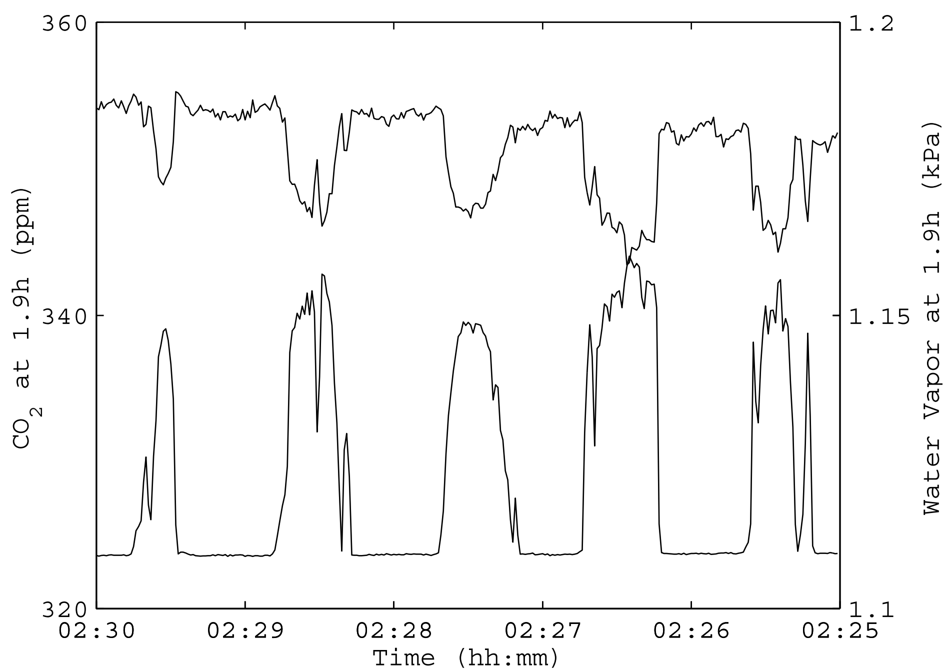

(b) Scalar fluctuations

Figure 2.7: Velocity and Scalar Fluctuations (III)

a fraction of a wave cycle at this height.

At $1.3h$, the level in the middle of the wave cores, velocity fluctuations were of a distinctive pattern. In the leading half of the wave cores, sweeps were noticeable. In the trailing half of the cores, motions were of the ejection type. Sharp transitions between sweeps and ejections occurred roughly in the center of the core regions. The phase difference between u' and vertical w' was approximately π. Qualitatively, the wind fluctuations more or less resembled that found in the shear center of a KH instability. The highly correlated wind components generated large downward momentum fluxes. There were generally slow upward motions in the region of cooler air in cores. Such a pattern of the velocity field supports the conjecture that cooler air and warmer air spin around each other to generate overturning structures.

The wind during this period was strong and the measurement from the sonic anemometer at 5.5 m ($0.26h$) was meaningful. Visually inspecting the wind vector fluctuations, one can infer that u' lag w' by approximately $\pi/2$. Thus, at the lower part of the canopy layer, waves are of an evanescent type. Together with the discussion above, the polarization relations between u' and w' are in accord with the prediction from the linear canopy wave model by Lee (1998), which is qualitatively similar to that of the classical KH wave.

Waves in this figure had larger amplitudes than those in the previous figure. The well-mixed wave cores with high CO_2 and low humidity could touch the sensors at $1.9h$ for a considerable fraction of a wave period. As a result, much broader disturbances were found in the time traces of CO_2 and water vapor.

Example IV

Another example shown in Figure 2.8 is from the period between 02:55 and 03:00 on July 13, 1994. During this period, wind at $1.9h$ was getting strong. The vertical velocity fluctuation reached the maxima of the night (Figure 2.2). The steep temperature gradient, which delineated the waves, began to disappear. Irregularity was introduced as the waves were being destroyed. The wind fluctuations at $1.9h$ were of similar magnitude as those at $1.3h$. The dominant organized structures in the temperature field were the reminiscence of the previous waves. A downwind tilted temperature front was found around 02:58. The temperature traces measured above the treetops assumed the patterns of inverse temperature ramps. Before the arrival of the microfront, at both levels above the canopy, the air motion was of the ejection type. Following the microfront, air motion was more or less of the sweep type. The strength of the sweep was stronger than that of the ejection. In general, this event was in accord with the inverse temperature ramp described by Paw U *et al.* (1992).

The time traces of CO_2 and H_2O reflected the wave activity. As the turbulence zone originated from the wave cores vertically expanded and horizontally merged, the scalar fluctuations at $1.9h$ were rather chaotic. The flat baseline in CO_2 and H_2O time traces disappeared. However, their patterns were closely correlated with the temperature field. The remarkable negative correlation between CO_2 and water vapor indicated that the gradient of water vapor was continually opposite to that of CO_2.

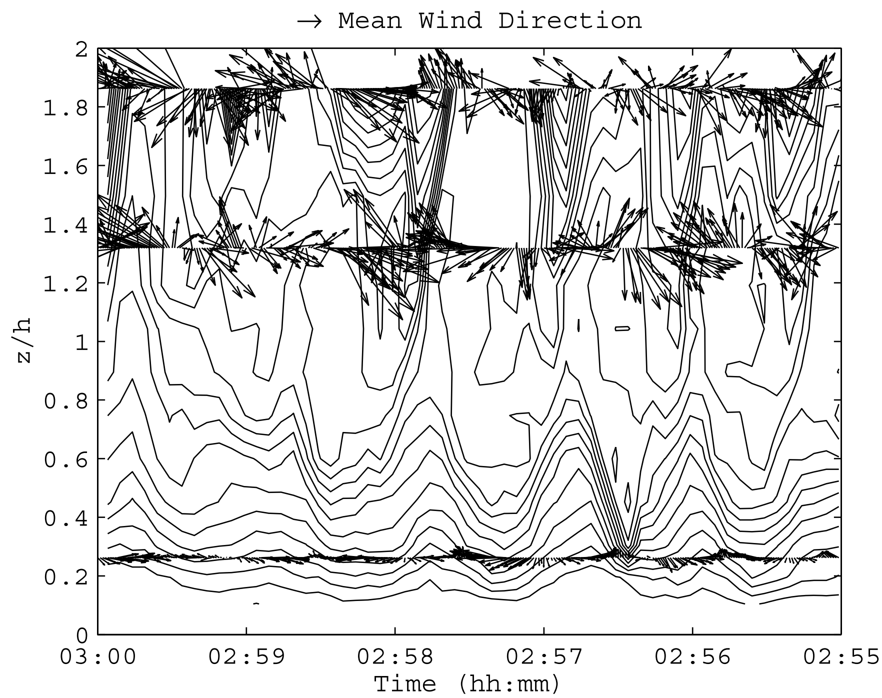

(a) Wind fluctuations superimposed on temperature contours. The magnitude of the maximum wind fluctuation is 2.08 ms^{-1}. The contour interval is 0.2K.

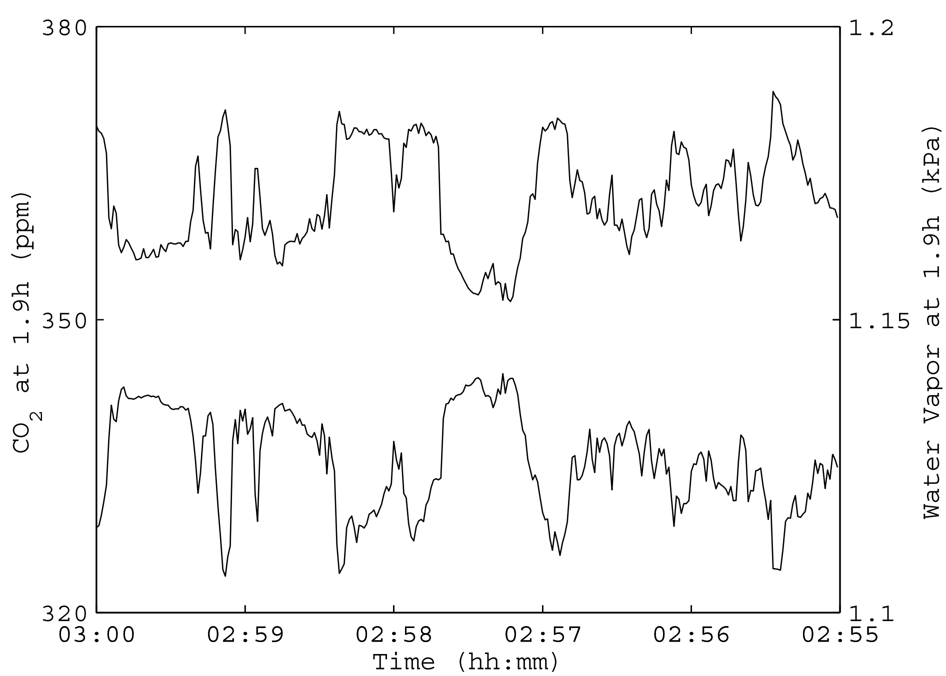

(b) Scalar fluctuations

Figure 2.8: Velocity and Scalar Fluctuations (IV)

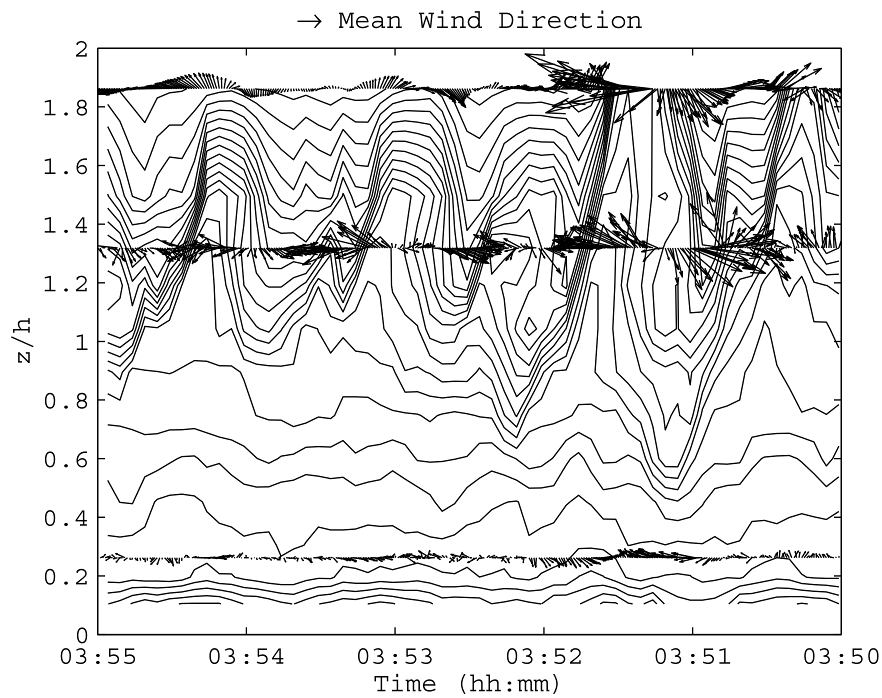

(a) Wind fluctuations superimposed on temperature contours. The magnitude of the maximum wind fluctuation is 1.62 ms^{-1}. The contour interval is 0.2K.

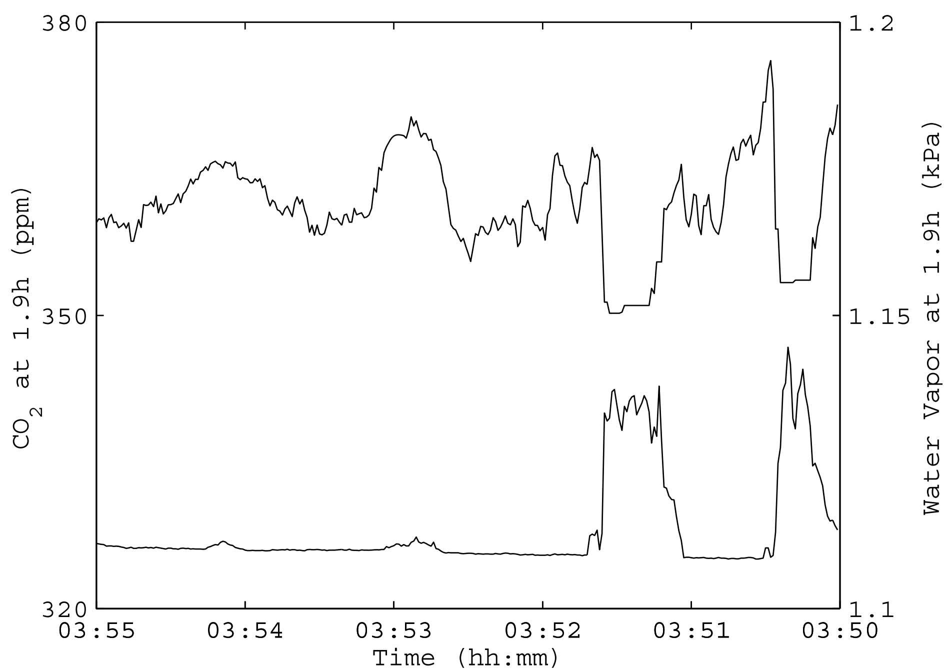

(b) Scalar fluctuations

Figure 2.9: Velocity and Scalar Fluctuations (V)

Example V

In the final example (Figure 2.9), the waves were weakening. Wind fluctuations at $1.3h$ and $1.9h$ was similar to those discussed in Figure 2.6. The disturbances in scalar fluctuations were also reduced at $1.9h$. The flat baselines in CO_2 and water vapor indicated that waves were weak and could not influence the air layer at $1.9h$.

The examples above cover the various stages of a wave event. It is interesting to note that the baseline concentration of CO_2 during the two-hour period gradually increased from 319.2 ppm to 326.0 ppm. This increase of background atmospheric CO_2 concentration might be the result of the mixing associated with the previous wave events or turbulence events. But this one-point tower measurement cannot address this issue.

2.3 Discussion

2.3.1 The Mechanism of Canopy Waves

The data presented above shows that wave-like motions of various strengths dominated the canopy roughness layer in a boreal forest. By surveying the wave events at other nights at this site, two background conditions were essential for the occurrence of canopy waves. First, the wind above the canopy was moderately strong, about 2-3 ms^{-1} . Second, the radiative cooling was strong with the net radiation below -40 Wm^{-2} . The two conditions are usual for boreal forests on clear nights. Lee and Barr (1998) have proposed that the nocturnal wave-like motion is a common motion type in forests. Indeed, in this study, the straightforward visual inspection of the time-height temperature contours and other supporting measurements reinforces their postulation.

With the frequent occurrence of wave-like motions, the mechanism of canopy waves is of great interest. The wind and scalar fluctuations measured at about two tree heights have indicated that the waves are localized in the thin layer near the treetops. The possibility that waves are generated from the layer well above is excluded. One may suspect that canopy waves are trapped gravity waves generated by topography. Although there are no direct observations against it, there are a number of arguments that are not favorable to topographical effects. The setup of the instruments of this observation satisfied the fetch requirement for eddy covariance flux measurement (Businger, 1984). The upwind fetch for the tower measurement system was about 5 km at this site. It was not likely that any obstacles within the homogeneous fetch generate the disturbances. Since the disturbances in the stable boundary layer can propagate several kilometers downstream, the tower-based sensors might experience the effect of forest edges or obstacles in the upstream far beyond the edges. However, the trapped lee wave by topography should be stationary and cannot be detected by the tower based time-height measurement. In addition, waves were observed to travel with the mean flow (Lee and Barr, 1998). Moreover, there was no evidence that waves were from some preferential directions, as expected for lee waves.

Another candidate often popping up is the roughness structure of forests. Surely, forests create background conditions favorable to the wave-like motions. Waves are not likely to be generated by the direct obstacle effect. The spatial observation by Lee and Barr (1998) has found that waves travel at the mean wind direction at the speed matching the wind speed a couple of meters above the treetops of a forest about 21 m tall. With an observed mean wave period of about 1 minute and moderate wind above canopies, the order of the wavelength is about 100 m. It is much larger than the tree height and the length scale characterizing the horizontal separation of trees. Furthermore, canopies are more porous than rigid. The possibility of generating waves from the obstacle effect by canopies is not a likelihood.

A more plausible explanation is that canopy waves originate from hydrodynamic instability of the Kelvin-Helmholtz type (Lee, 1997), which extends the plane-mixing layer analogy (Raupach *et al.*, 1996) to stable conditions. The data analyzed in this study supports Lee's argument in several aspects. Firstly, clear cycles of wave generation, growth, saturation and destruction have been identified, which bear resemblance to the laboratory experiments (*e.g.*, Thorpe 1969; Delisi and Corcos, 1973) and radar observation in the atmosphere (Atlas *et al.*, 1970). The measured gradient Richardson number was above the critical value 0.25 in most wave events, apparently against KH instability. One should notice that the measurement was taken outside the layer with maximum wind shear. The minimum Richardson number at the shear maximum was likely below the critical value.

Secondly, the polarization relation among wind fluctuations and scalars are in accord with Lee's model (1997), which embeds the KH instability. Specifically, away from the treetops, where the maximum shear is found, w' is in quadrature with u' and θ'. Near the treetops, there are examples showing the π phase difference between

w' and u'. Such phase relations have been predicted by Lee's linear model (Lee, 1997, Figure 9).

Thirdly, the observed thermal structures of canopy waves are similar to the numerical simulation of KH instability (*e.g.*, Patnaik *et al.*, 1976; Peltier *et al.*, 1978; Chapter 4 of this thesis), wind tunnel experiment (Delisi and Corcos, 1973) and laboratory experiment (Thorpe, 1969). The waves cores, delineated by the steep temperature gradient, are nearly isothermal, caused by wave folding and overturning. There are evidences showing that cool air from the canopy layer and warm air from above spin around each other. Statically unstable superadiabatic structures have been found in the cores during the overturning. Turbulence from convective instability, similar to that found in the tilting tank experiment (Thorpe, 1969) is expected. This is corroborated by the turbulent wind fluctuations in wave cores.

Even in the laboratory, it is very difficult to track the details of the evolution of the KH instability. The observations in forests have demonstrated that canopy waves share broad features of KH waves. Further dedicated observations would provide more detailed information. Based on current knowledge on canopy waves, it is postulated that the wave evolves in several distinctive stages:

1. **Quiescence Phase**

   On clear nights, when the wind is calm, a thin inversion layer develops at the treetops. Then the wind speed above the treetops is accelerated by outer scale motions, sometimes associated with the appearance of clouds (Fitzjarrald and Moore, 1990). The wind within the canopy layer is greatly reduced by the canopy drag.

2. **Growth Phase**

A wind shear is rapidly established at the treetops by the canopy drag. Small disturbances grow on such background shear. The wind shear, the proximity to the ground and temperature inversion will be favorable to the wave of certain wavelength, and this wave has the largest growth rate. It will eventually dominate the flow structure. This fastest growing wave will break the original parallel shear flow and create periodical vorticity maxima. Cool air within the canopy layer and warm air above will spin around each other as the wave grows. This will raise the potential energy field of the stably stratified flow. The growth of the wave is fed by the energy extracted from the background flow, which is partitioned among the kinetic energy, the wave potential energy and the dissipation of the wave.

3. **Saturation Phase**

Since the available energy is finite and the stable stratification is strong, the wave will saturate eventually. The finite amplitude wave will be confined below two or three tree heights. During the growth, distinctive isothermal cores appear as a result of the wave folding, which is enhanced by the convective mixing introduced by overturning. The cores will travel at the speed of the mean flow, matching the wind speed near the treetops. In this aspect, KH waves differ from propagating buoyancy gravity waves whose speeds do not give them a critical level.

4. **Destruction Phase**

   If the wind above is strong and the temperature inversion is not strong enough to suppress the instability, the finite wave will be further destroyed. The statically unstable structure formed during the wave overturning is first found in the leading edge of the wave. Turbulence will first destroy the leading steep temperature gradient. The surviving trailing edge exhibits the downwind tilting microfront-like temperature structures, which will be the typical inverse ramps described in the previous studies (*e.g.*, Gao *et al.*, 1989; Paw U *et al.*, 1992). The persistence of the observed wave trains indicates that the strong stable stratification and moderate wind above the canopy may inhibit the destruction. Thus, the long-lasting primary wave structures are preserved.

2.3.2 The Role of Forest Canopies in the Wave Dynamics

This study and previous observational works strongly suggest that the nocturnal wave-like air motions are manifestations of KH waves. For the KH instability, it is well-known that the shear is to destabilize the flow while the stable stratification is to stabilize the flow. The role of canopies in wave dynamics would be easy to understand in terms of generating and modifying the two competing factors. In addition, the proximity of the shear center to the rigid ground can modify the dynamics to a certain extent.

It is well established from observations that a strong wind shear is usually found near the canopy top. The process to establish the shear at the canopy top deserves to be clarified. Initially, the wind within and above canopies is calm and the temperature inversion is found near the canopy tops. Sporadic external events, such as the breakdown of the nocturnal low-level jets, would speed up background wind in the canopy roughness layer. This background flow initially could be treated as a laminar flow since little small scale turbulence would exist in the beginning. The absorption of momentum by the canopy elements will create a wind shear near the canopy tops. The time scale of establishing the shear can be estimated with the empirical formula for the canopy drag, which is slightly different from the formulation in Shaw and Shumman (1992), that is,

$$F_c = c_d a u^2 = u/2\tau, \tag{2.3.1}$$

where c_d is the drag coefficient, a is the leaf area density, u is the horizontal wind speed. The $\tau = 2/c_d a u$, can be called the half time, is the time needed for the wind being reduced by a half. For a forest that is 20 m tall with a leaf area index of 5, leaves uniformly distributed from ground to treetops, initial wind speed of $u = 2$ ms^{-1} and canopy drag coefficient $c_d = 0.15$, the estimated τ is about 10 s. Thus, in a very short time the wind shear at the treetops would be established. The initial wind shear generated by the canopy drag would be found in the thin layer in the upper canopies. Although the temperature inversion is strong due to the strong radiative cooling, the strong wind shear can bring the Richardson number below the critical value of 0.25. The initial instabilities would be of a smaller scale than the observed waves since the initial shear layer is thin. As the initial instability grows to the finite stage and finally are destroyed, the initial shear layer is broadened. Instabilities with a larger scale might be triggered in the broadened the shear layer or by the merging of previous smaller waves. Since the background flow is always being modified, the choice of the basic flow for linear stability analysis is not straightforward.

2.3.3 The Implication to the Eddy-Covariance Flux Measurement

Of most practical interest is the mixing ability associated with canopy waves. From the observation, the turbulent wave cores extend to about 2 tree heights. Presumably, the CO_2 within canopies can be mixed with the air above the treetops. Since these wave cores travel with the background mean flow, the escaped CO_2 will be advected in the downwind direction. Because the waves have limited finite amplitudes, the irreversible mixing occurs only in the thin layer below 2 or 3 tree heights. Although the mixing is limited in the vertical direction, the result is expected to be significant, considering the large CO_2 gradient maintained by the nighttime respiration.

Canopy waves deserve more attention from experimentalists doing eddy-covariance flux measurements. This study has demonstrated that erratic flux-gradient relations are associated with the overturning and mixing in the wave cores. A thorough knowledge of wave dynamics will shed light on understanding the apparent counter-gradient nocturnal fluxes.

Another problem often bothering researchers is the underestimation of the nocturnal exchange of CO_2 when there is little apparent turbulence effluxes at the instrument heights. For example, Schmid *et al.* (2000) found that the CO_2 storage buildup in the early night was significantly reduced at midnight with little measured friction velocity. Others have developed empirical methods to estimate the CO_2 release for low friction velocity conditions (*e.g.*, Goulden *et al.*, 1996b; Yang *et al.*, 1997). There are several explanations of such missing CO_2 flux at low friction velocity conditions. The often-ignored canopy waves might be responsible for it. Since most of the flux measurements have instruments mounted at about two or three tree heights, the instruments simply cannot detect the underlying weak wave activities and the associated CO_2 effluxes. For waves with moderate strengths, although considerable wind and scalar fluctuations can be detected at instrument heights, the polarization relations similar to evanescent waves would generate little momentum, that is, little friction velocity. Nevertheless, the examples shown in this study suggest that certain amount of CO_2 could be flushed out of canopies by the wave-introduced irreversible mixing to the thin layer just above the canopy, which might be below the instrument height. Clearly, the current setup of instruments cannot adequately quantify this mixing process. Given the frequent occurrence of wave events, the accumulated effect would be significant. It raises great uncertainty regarding the long-term measurement of the net ecosystem exchange of CO_2 between forests and the atmosphere by eddy-covariance systems.

2.4 Summary

In this descriptive study, the salient flow structures of wave-like air motions in forests have been analyzed in the time-height dimensions. The results show that wave-like air motions were dominant in the canopy roughness layer on clear nights when the wind above the treetops was moderate. The life cycles of wave events bore resemblance to those of KH waves. The wave were characterized by their intermittence in response to the changes of the background wind and the radiative cooling. The temperature fields of the waves resembled those of finite-amplitude KH waves. A variety of signal patterns in time traces, including both wave-like and ramp-like signal patterns, could be associated with the distinctive wave structures. The polarization relations measured at limited heights were in accord with those of KH waves. The statically unstable structurehas been found inside the overturning waves. The conjecture of turbulent mixing from convective instability is corroborated with the measured turbulent wind fluctuations within the waves.

The turbulent mixing associated with canopy waves has been discussed. There is evidence that counter-gradient fluxes are associated with the highly non-linear overturning and mixing inside the waves. It has been pointed out that wave-introduced irreversible mixing can flush CO_2 out of canopies to the layer just above the treetops with a depth of 1 to 2 tree heights. This flux cannot be satisfactorily quantified by current instrument setups. Thus, it raises the potentially significant uncertainty in the estimation of the long-term net ecosystem-atmosphere CO_2 exchange by using the popular eddy-covariance technique.

Chapter 3

A Two-layered Canopy Wave Model

3.1 Introduction

Lee's linear wave model indicates that canopy waves share many features of the KH instability. The key linear parameters, such as growth rate and phase speed, are essentially determined by the strength of the wind shear and the temperature stratification. The analytical profiles used in Lee's analysis are of realistic shapes, which are often observed in the unstable or neutral conditions in the canopy sublayer. However, his model relies on turbulent mixing to maintain the inflectional wind profile. In this point, it is not consistent to use such inflectional profiles and at the same time assume infinitesimal disturbances. In addition, some results from Lee's model depend on the empirical relation between the leaf area index and the wind profile. The interaction between the two makes it hard to separate the effect of each individual factor.

In this chapter, a two-layered canopy wave model will be developed to investigate the major features of canopy waves. Gossard and Hooke (1975) have demonstrated that layered models provide a remarkably good prediction of observed wave phenomena over limited regions of the atmosphere. Their simplicity greatly aids in the physical interpretation of observations. In this canopy wave model, with the same belief, the simple flow configuration and the simple canopy structure will make it much easier to identify the role of the canopy drag in the wave dynamics.

3.2 Model Description

The canopy layer is of height h, with uniform leaf area density a from the ground to the treetops h and the leaf area index $L = ha$. Within the canopy, the wind speed is u_1 and the wind speed in the layer above is u_2. The air densities in each layer are constant. Within the canopy the air density is ρ_0 and there is a density jump of $-\triangle\rho$ at the treetops.

The governing equations with the canopy drag term is linearized as

$$Du' = -\frac{1}{\rho_0}p'_x - Fu', \tag{3.2.1}$$

$$Dw' = -\frac{1}{\rho_0}p'_z - \frac{\rho'}{\rho_0}g, \tag{3.2.2}$$

$$u'_x + w'_z = 0, \tag{3.2.3}$$

$$D\rho' + w'\bar{\rho}_z = 0, \tag{3.2.4}$$

where u and w are the horizontal and the vertical velocities, p is the pressure, ρ is the air density, and g is the gravitational acceleration. The primed quantities are the wave-introduced fluctuations. The canopy drag term F is given by

$$F = \begin{cases} c_d a u_1 & z \leq h \\ 0 & z > h \end{cases}, \tag{3.2.5}$$

where $c_d = 0.15$ is the canopy drag coefficient, given by the observation (Shaw, 1988).

Substitute the wave fluctuations in equations 3.2.1-3.2.4 with their normal modes in the form of

$$f' = \hat{f} \exp\left[i\left(kx - ct\right)\right] + c.c., \tag{3.2.6}$$

where $\hat{f}$ is the structure function and $c.c.$ denotes the complex conjugate. After substitution, a modified Taylor-Goldstein equation can be derived as

$$\hat{w}_{zz} - l^2 \hat{w} = 0, \tag{3.2.7}$$

where

$$l^2 = \begin{cases} k^2 & z > h \\ \frac{(u_1 - c)k^2}{(u_1 - c) + F/ik} & z \le h \end{cases}. \tag{3.2.8}$$

Based on the observation (Chapter 2), the evanescent wave solution is chosen for the layer above the canopy [1], that is,

$$\hat{w} = B \exp\left[-k\left(z - h\right)\right], \tag{3.2.9}$$

where B is a constant and will be determined later. Within the canopy, the solution is in the form of

$$\hat{w} = A\left\{\exp\left[-l\left(z - h\right)\right] - \exp\left(2lH\right) \exp\left[l\left(z - h\right)\right]\right\} \tag{3.2.10}$$

which satisfies boundary condition at the rigid ground $\hat{w}_{z=0} = 0$.

The vertical displacement of the interface at the treetops η is of the form like that in equation 3.2.6. The continuity of η at height h requires

$$B/\left(u_2 - c\right) = A\left[1 - \exp\left(2lH\right)\right]/\left(u_1 - c\right) \tag{3.2.11}$$

[1] Prof. Ronald B. Smith has investigated the stability property of the same flow system with a propagating gravity wave solution in the upper layer (personal communication).

The dynamic boundary condition at the interface requires

$$p_1 = p_2 + \rho_0 g' \eta, \tag{3.2.12}$$

where the reduced gravitational acceleration is given by

$$g' = \frac{\triangle \rho}{\rho_0} g. \tag{3.2.13}$$

By manipulating the matching conditions (equation 3.2.11 and 3.2.12), the dispersion relation is given by

$$(u_1 - c)\left[(u_1 - c) + F/ik\right] l + \left[(u_2 - c)^2 k - g'\right] \tanh(lh) = 0. \tag{3.2.14}$$

Without the canopy, that is, $F = 0$, if $lh \gg 0$, the above equation is reduced to

$$(u_1 - c)^2 k + (u_2 - c)^2 k = g'. \tag{3.2.15}$$

In the coordinate moving at the speed of the mean flow $(u_1 + u_2)/2$, we have

$$c^2 = \frac{g'}{k} - \left(\frac{\triangle u}{2}\right)^2, \tag{3.2.16}$$

which describes an instability of the Kelvin-Helmholtz type.

For a long wave, lh is small and $\tanh(lh) \approx lh$, equation 3.2.14 is simplified to

$$\left[(u_1 - c)^2 + (u_1 - c) F/ik\right] + \left[(u_2 - c)^2 k - g'\right] h = 0. \tag{3.2.17}$$

For the reference frame moving at the speed of u_1, the above equation is transformed to

$$c^2 (1 + kh) - cF/ik - 2 \triangle uckh + \triangle u^2 kh - g'h = 0 \tag{3.2.18}$$

With the assumption that $kh = 1$, the above equation is simplified to

$$c^2 - c \triangle u + \frac{icc_d L u_1}{2} = \frac{g'h}{2} - \frac{\triangle u^2}{2}. \tag{3.2.19}$$

Hereafter, in the following discussion we will use normalized velocities

$$\begin{aligned} U_1 &= u_1 / \triangle u, \\ U_2 &= u_2 / \triangle u, \\ C &= c / \triangle u. \end{aligned} \tag{3.2.20}$$

Equation 3.2.19 becomes

$$C^2 + (i\beta - 1)\, C + \frac{1}{2} - R = 0, \tag{3.2.21}$$

where

$$R \equiv g'h / \left(2 \triangle u^2\right) \tag{3.2.22}$$

is a stability parameter, analogous to the Richardson number. The canopy drag parameter is defined as

$$\beta \equiv c_d L U_1 / 2. \tag{3.2.23}$$

3.3 Results and Discussion

The phase speed $C\,(R, \beta)$ is a function of both the stability parameter R and the canopy drag parameter β. The dispersion relation with the canopy drag is quite complicated. The analytical form of the phase speed is hard to solve. Here the phase speed for the same flow configuration but without the canopy drag will be serve as the reference state. In the absence of canopy term, that is, $\beta = 0$, we have the familiar solution

$$C\left(R,0\right) = \frac{1}{2} \pm \left(R - \frac{1}{4}\right)^{1/2}. \tag{3.3.1}$$

When $R > 1/4$, the equation will give two neutral wave solutions. One moves faster than the other one. When $R < 1/4$, there are two modes according to the equation. The two modes move at the speed of the mean flow. One of them is unstable and the other is stable. The transition occurs at the critical Richardson number $R_c = 1/4$. It is conspicuous that the inclusion of the canopy term in equation 3.2.21 will always result in a complex phase speed. Thus, the neutral waves in the absence of the canopy will become unstable if the imaginary part of the complex phase speed is positive. For the classical KH instability in the absence of the canopy, the canopy drag will modify the stability property by altering both the real and imaginary part of the phase speed.

For a given Richardson number and a canopy drag parameter, there are two possible solutions for C. We will numerically solve

$$C = C_r + iC_i \tag{3.3.2}$$

over a range of Richardson numbers for several typical canopy drag parameters. The results are presented in two figures. Figure 3.1 shows the first reference state (the faster neutral wave mode when $R > 1/4$ and the decaying mode when $R < 1/4$) and those departures from this base state by introducing canopy drags of various strengths. Figure 3.2 shows the second reference state (the slower neutral wave mode when $R > 1/4$ and the growing mode when $R < 1/4$) and those departures from this base state by introducing canopy drags of various strengths. In both of the figures, the solid curves are cases without the canopy drag. They will serve as the reference states for the following discussion.

In Figure 3.1(a), compared with the reference state, the inclusion of the canopy drag increases C_r, the real part of the phase speed, in the range $0 \leq R < 1/2$. Larger canopy drags bring larger increases. For very strong stratification, there is no significant modification of C_r. In Figure 3.1(b), when $R > 1/4$, the imaginary part of the phase speed is negative and the modification increases with the increase of the canopy drag. The faster neutral wave in the absence of the canopy would be damped out after introducing the canopy. Dense canopies with large drags will be more effective removing the original faster neutral wave. When R is large, C_i is almost insensitive to the increase of R. When $R < 1/4$, canopy drags increase the magnitude of the original negative imaginary part of the phase speed. Thus, the decaying of the original decay mode is even faster. Overall, the canopy drag in this case is to stabilize the flow. Figure 3.2 illustrates much more interesting features. In 3.2(a), contrary to those in the previous figure, phase speeds are decreased by canopy drags in the range $0 \leq R < 1/2$. Larger canopy drags cause more reductions. The original slower moving neutral wave becomes stable when $R > 1/2$. However, in the range $1/4 < R < 1/2$, the original slower moving neutral wave becomes unstable. Larger drags cause larger growth rates. The original neutral waves become more and more unstable when approaching the critical Richardson number 1/4. Since the instability

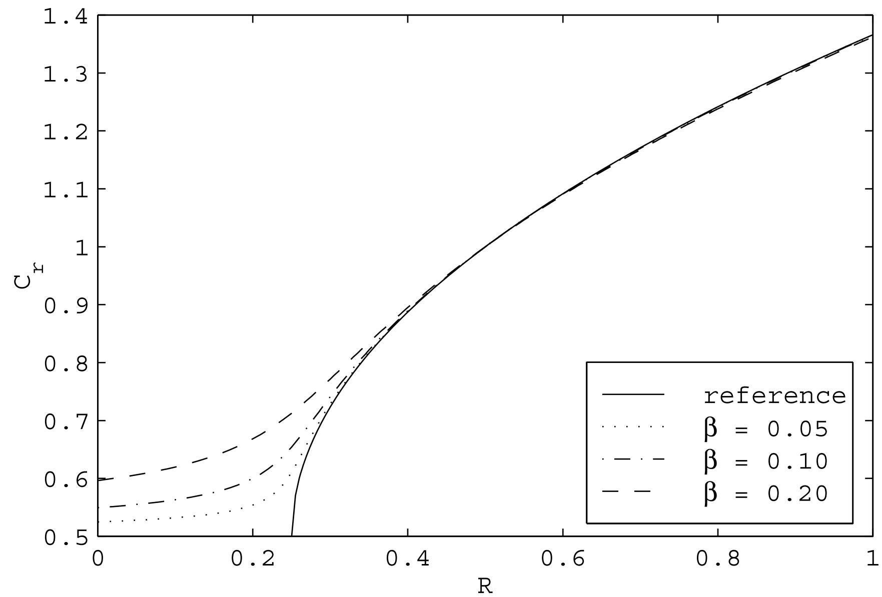

(a) The real part of the complex phase speed.

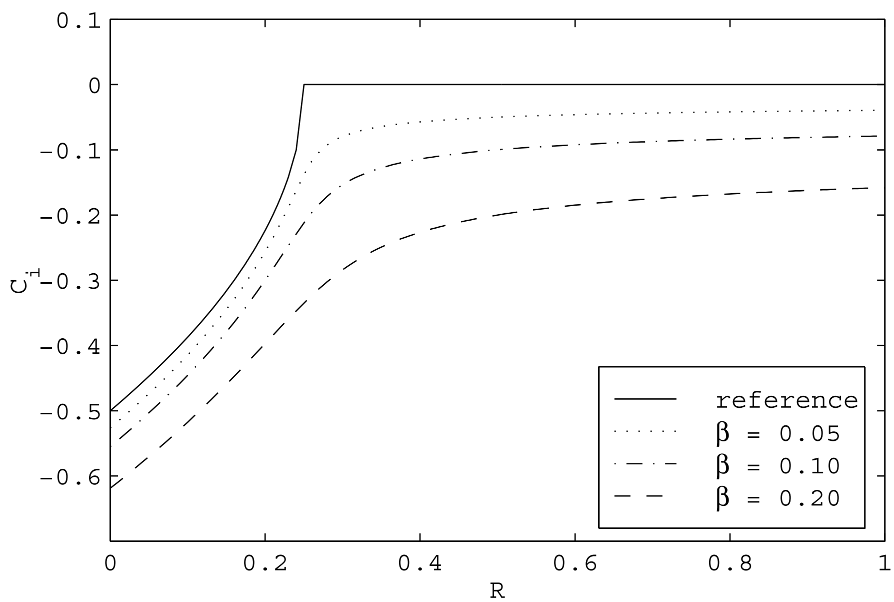

(b) The imaginary part of the complex phase speed.

Figure 3.1: The influence of canopy drag on phase speed. The reference state is the faster neutral wave mode when $R > 1/4$ and the decaying mode when $R < 1/4$.

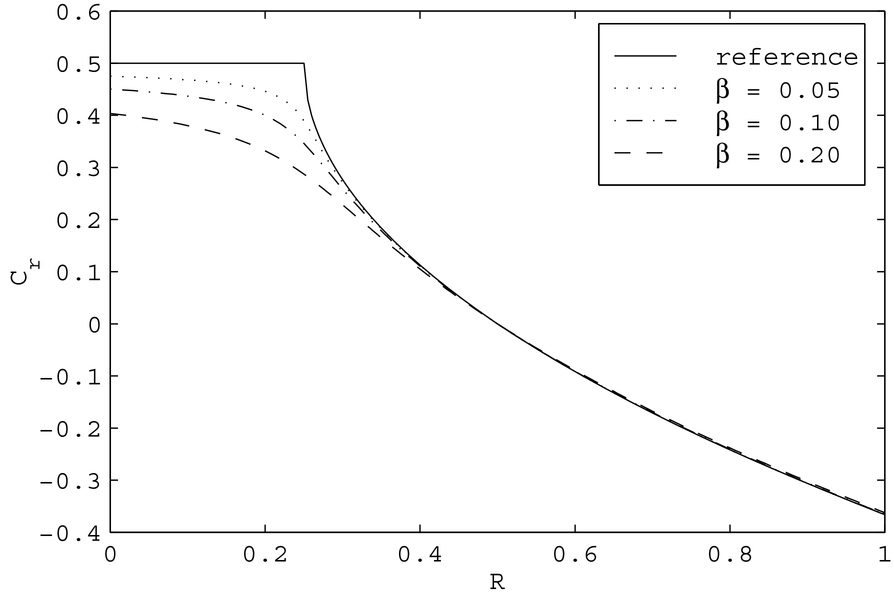

(a) The real part of the complex phase speed.

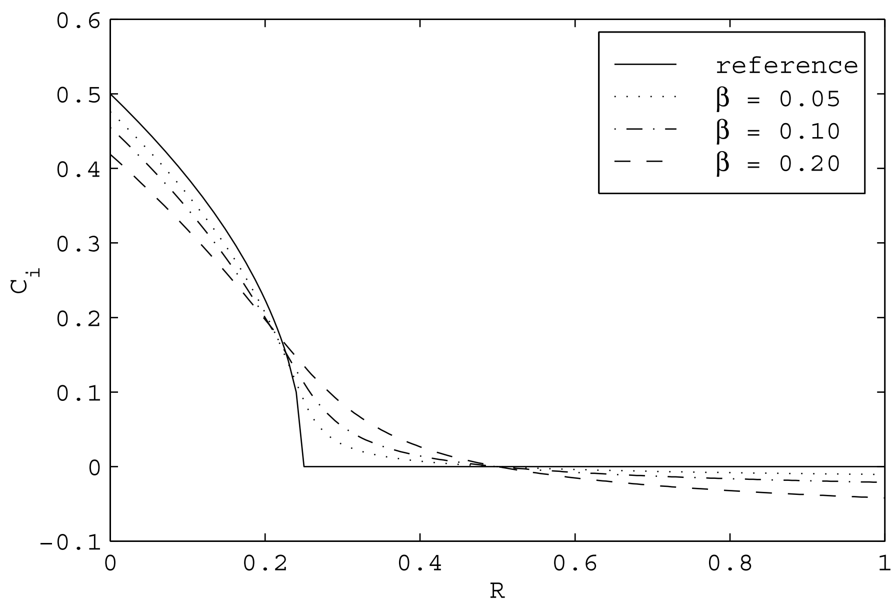

(b) The imaginary part of the complex phase speed.

Figure 3.2: The influence of canopy drag on phase speed. The reference state is the slower neutral wave mode when $R > 1/4$ and the growing mode when $R < 1/4$.

in the above Richardson number range appears solely as the result of introducing the canopy drag, it is tentatively called the canopy drag instability. At $R = 1/2$, according to equation 3.2.21, the two solutions are

$$C_1 = 1 - i\beta, \tag{3.3.3}$$

$$C_2 = 0. \tag{3.3.4}$$

The C_1 is just the stability from the original neutral faster wave. It decays according to the canopy drag strength. The zero C_2 separates the canopy drag instability and the stability. Thus, the critical value 1/2, tentatively called the critical Richardson number for the canopy drag instability, shares the feature of the critical Richardson number 1/4 for the stability property of the flow without canopies.

In the range $0 \leq R < 1/4$, the canopy drag can either enhance or reduce the growth rate of the original unstable mode. Close to the critical value $R_c = 1/4$, the increase of C_i by the canopy drag is conspicuous. The growth rate of the original unstable mode in this range is enhanced until R is less than 0.22, roughly constant for the range of canopy drag parameters considered here. Further reduction of R will result in the reduction of C_i, compared with the original unstable mode. The reduction depends on the magnitude of the canopy drag. Larger drags cause more reductions. To summarize, depending on the stability parameter, the canopy drag can either destabilize or stabilize the flow.

3.4 Conclusion

In contrast to the flow system without the canopy, this linear analysis indicates that the phase speed of a normal mode is generally complex because of the canopy drag. Specifically, the canopy drag causes following changes:

- When $R > 1/2$, no neutral waves are allowed with the canopy drag. In this sense, the canopy drag is to stabilize the flow.

- When $1/4 < R < 1/2$, the canopy drag instability appears solely as a result of including the canopy drag. The canopy drag instability moves more slowly than the mean speed of the flow and the speed increase with the decrease of Richardson number.

- When $0 < R < 1/4$, the original stable mode is further stabilized by the canopy drag. When the stability parameter is close to the critical value $1/4$, the unstable mode is further destabilized by the canopy drag. For even smaller Richardson numbers, the canopy drag may stabilize the flow by reducing the growth rate of the unstable mode. The unstable mode is slowed down by the drag and moves at a speed less than that of the mean flow.

This two-layered canopy wave model indicates that the canopy drag can trigger instabilities in the otherwise stable background conditions without canopies. This is contrary to the common intuition that the canopy drag would damp out disturbances and stabilize the flow. Several simplifications have been adopted in the formulation of this model, which make it unable to predict the fastest growing mode. The model might not be suitable for direct comparison with realistic canopy flows. Further research should focus on the choice of background states on which the linearization is made and the modeling of the canopy drag.

Chapter 4

A Numerical Simulation of Wave-like Motions in Forests

4.1 Introduction

The observational study by Lee and Barr (1998) has demonstrated that wave-like air motions are common on clear nights in a boreal forest. Enhanced turbulent fluxes have been found during the wave episodes in an Amazonian forest (Fitzjarrald and Moore, 1990). But the flux-gradient relations exhibit erratic behaviors (Lee *et al.*, 1996). Unstable thermal structures have been found in the overturning waves (Hu and Lee, 1998), which may lead to the irreversible mixing. A better understanding of the transport mechanism associated with canopy waves is of great practical interest in quantifying the nighttime forest-atmosphere exchange of CO_2 and other biologically important gases.

To date, several linear models have been developed to interpret canopy waves (Paw U *et al.*, 1990; Fitzjarrald and Moore, 1990; Lee, 1997). The basic wave parameters derived from these models are in accord with observations. Among these models, the linear canopy wave model developed by Lee (1997) is more realistic. His model extends the plane-mixing layer analogy for the canopy turbulence (Raupach *et al.*, 1996) to stable conditions. It shows that canopy waves share features of the Kelvin-Helmholtz (KH) instability. Canopy effects and the proximity to the ground modify the KH instability in several aspects. One of the main attractions of this model is that it gives a wave generation mechanism, which is not possible with other linear models. The irreversible mixing process in the nonlinear development stage of KH billows is expected to be an important transport mechanism on clear nights in forests.

Linear wave models describe the evolution of small wave-like disturbances in a constant background flow. However, the observed wave patterns seldom resemble pure sinusoidal waves assumed by the linear analysis. It might be the result of non-linear processes, which is beyond the scope of linear models. Furthermore, the measured profiles have shown the evidence of turbulent mixing (Hu and Lee, 1998), which is a highly nonlinear phenomenon. In reality, wave-like motions can be visually identified only after wave-like fluctuations have grown to the finite amplitude stage. In another word, observed waves are probably not in the linear regime described by the linear models. For example, the numerical simulation by Patnaik *et al.* (1976) has found that nonlinear processes favor the development of waves longer than those that grow fastest in the linear range. Thus, the applicability of linear analysis to interpret field observations is limited.

A suitable next step, beyond the linear framework, is a two-dimensional numerical canopy wave model. The justification for a two-dimensional model is that the primary

KH wave is two-dimensional and quite persistent in the initial stage. Three dimensional motions appear only after primary waves reach the saturated stage (Werne and Fritts, 1999). Even then the coherent large-scale structure is observed to persist in the presence of small-scale fluctuations. These structures are commonly believed to be the vestige of the primary instability in the early stage in the transition from laminar flows to turbulent flows (Klaassen and Peltier, 1985). Two-dimensional numerical simulations of the instability of a parallel shear flow (*e.g.*, Patnaik *et al*, 1976; Peltier *et al.*, 1978) have substantiated the predictions of the linear analysis, such as the phase speed and the growth rate of the primary mode. The structure of the growing waves has been calculated by these early numerical studies. In the two-dimensional numerical study by Sykes and Lewellen (1982), a second-order closure scheme has been employed to describe the three-dimensional small-scale turbulence within KH billows. The breakdown of the rolled-up vortex layer and the subsequent spread and decay of the turbulence can be reasonably simulated. The goal of this chapter is to reproduce major canopy wave structures with a two-dimensional numerical model, in which a crude turbulence closure scheme will be used. Since the macro-structures of primary interest are essentially determined by initial profiles and boundary conditions, the quality of the turbulence closure model is not crucial for this purpose.

From the point of view of observation, some features of two-dimensional flow structures can be revealed by the tower-based profile measurement. For example, daytime coherent structures have been revealed as scalar microfronts by presenting the data in time-height contour plots (Gao *et al.*, 1989). The same method has been applied to the nighttime high-frequency temperature profile measurements (Lee and Barr, 1998; Hu and Lee, 1998; Chapter 2 in this thesis). It has been demonstrated to be a powerful tool in visualizing organized flow structures. We expect that this two-dimensional model, coded in the current understanding of the interaction between the atmosphere and canopies, could reproduce the major observed features of the canopy waves.

Here a sequence of numerical simulations of the instability of a parallel shear flow in a stably stratified boundary layer will be presented. Specifically, the lower boundary is covered with trees. Several aspects of the KH wave growth will be investigated, particularly the modification of the classical KH instability by the canopy elements, and by the proximity of the critical level to the ground. The detailed thermal structures and velocity fields are compared with observations. Some of the preliminary results can be found in Hu and Lee (2000).

4.2 Model Description

4.2.1 Basic Equations

This two-dimensional eddy-resolved model solves motions with scales larger than the grid size explicitly, and the effects of the sub-grid-scale motions are modeled. The formulation is similar to that of the large eddy simulation of canopy flows (*e.g.*, Shaw and Shumman, 1992), except that the computation is performed in $x-z$ dimensions in space. The Boussinesq approximation has been made to simplify the Navier-Stokes equations for momentum, heat and mass balance. Within the canopy, additional terms are included to account for the canopy drag and the heat exchange between the air and trees. Major variables are located in the center of grid cells in the $x - z$ plane. The grid-cell-averaged governing equations are:

$$\frac{\partial \bar{u}_i}{\partial t} + \frac{\partial}{\partial x_j}\left(\bar{u}_j \bar{u}_i\right) = -\frac{1}{\rho_0}\frac{\partial p'}{\partial x_j} + g\frac{\theta'}{\bar{\theta}_0}\delta_{i3} + \frac{\partial \tau_{ij}}{\partial x_j} + F_i, \tag{4.2.1}$$

$$\frac{\partial \bar{\theta}}{\partial t} + \frac{\partial}{\partial x_j}\left(\bar{u}_j \bar{\theta}\right) = \frac{\partial}{\partial x_j}\left(\overline{u_j' \theta'}\right), \tag{4.2.2}$$

$$\frac{\partial \bar{u}_i}{\partial x_i} = 0, \tag{4.2.3}$$

where u_i $(i = 1, 3)$ is the velocity component in the x_i direction, θ is the potential temperature, p is the pressure, ρ is the air density, and g is the gravitational acceleration. The overbar denotes the grid cell average. The p' and θ' are the deviations from the adiabatic background. The drag force by canopy elements F_i is modeled as that in Shaw and Schumann (1992),

$$F_i = -c_d a V \bar{u}_i, \tag{4.2.4}$$

where V is the instant scalar total velocity, a is the leaf area density. The drag coefficient c_d is set to be 0.15, based on the field measurement (Shaw *et al.*, 1988).

The subgrid-scale momentum flux can be written as

$$\tau_{ij} = \bar{u}_i \bar{u}_j - \overline{u_i u_j} = K_m \left(\frac{\partial \bar{u}_i}{\partial x_j} + \frac{\partial \bar{u}_j}{\partial x_i}\right) - \frac{2}{\delta_{kk}} E \delta_{ij}, \tag{4.2.5}$$

where K_m is the subgrid eddy viscosity of momentum, and $E = \overline{u_i'^2}/2$ is the subgrid-scale turbulent kinetic energy. The eddy viscosity is obtained from the Prandtl-Kolmogorov relation

$$K_m = c_m l E^{1/2}, \tag{4.2.6}$$

where empirical constant $c_m = 0.15$s. The characteristic length scale l is related to the horizontal and vertical grid sizes $\triangle x$ and $\triangle z$ by

$$l = (\triangle x \cdot \triangle z)^{1/2}. \tag{4.2.7}$$

The turbulent kinetic energy is computed by solving the following prognostic equation

$$\begin{aligned} \frac{\partial E}{\partial t} + \frac{\partial(\bar{u}_j E)}{\partial x_j} = \frac{\partial}{\partial x_j}\left(K_m \frac{\partial E}{\partial x_j}\right) + K_m\left(\frac{\partial \bar{u}_i}{\partial x_j} + \frac{\partial \bar{u}_j}{\partial x_i}\right)\frac{\partial \bar{u}_i}{\partial x_j} \\ - K_h \frac{g}{\theta_0}\frac{\partial \theta'}{\partial x_j}\delta_{j3} - c_\epsilon \frac{E^{3/2}}{l} + c_d a V^3, \end{aligned} \tag{4.2.8}$$

with empirical constant $c_\epsilon = 0.93$. The canopy drag effect is included in the last term in the above equation.

4.2.2 Numerical Method

The MATLAB flow solver for solving the model equations is developed by Stevens *et al.* (2000). The same algorithm has been used to study the small-scale entrainment processes in a stratocumulus marine boundary layer (Stevens *et al.*, 2000). The numerical scheme is based on the algorithm developed by Almgren *et al.* (1996, 1998), which is a variation of the original projection formulation (Chorin, 1969). This modified projection method is a fractional step scheme. It first solves the advection-diffusion equations to predict the intermediate velocities, and then projects these velocities onto the space of approximately divergence-free vector fields. A specialized second-order upwind method is adopted to discretize the nonlinear advection terms, which avoids any cell Reynolds number stability restriction for high Reynolds flow. Compared with standard upwind differencing methods, the scheme couples the spatial and temporal discretization to attain second order accuracy in both space and time. It leads to a robust higher order discretization with excellent phase-error properties. Unlike the widely-used staggering grid layout, all of the primary variables to be computed are located in the centers of the grid cells. One of the benefits is that no interpolation is needed to compute model statistics, such as momentum flux and heat flux. The time-step constraint is the common Courant-Friderich-Levy condition

$$\max\left(\frac{|u| \triangle t}{\triangle x}, \frac{|w| \triangle t}{\triangle z}\right) \leq 1. \tag{4.2.9}$$

4.2.3 Boundary Conditions, Initial Profiles and Initialization

The lateral boundaries are periodical, which is suitable for the simulation of waves. The length of the computation domain is set to be one wavelength of the fastest growing mode predicted by the linear wave model (Lee, 1997). The upper and lower boundaries are treated as rigid walls and no-flux conditions are implemented. The computation domain height is set to be 6 tree heights. The upper boundary is sufficiently far away from the maximum shear. It has negligible effect on the flow development.

The same profiles in the linear canopy wave model (Lee, 1997) are used to set up this two dimensional simulation. A Gaussian distribution describes the leaf area density

$$a(z) = \frac{Lh}{0.125\sqrt{2\pi}} \exp\left[-\left(z/h - 0.65\right)^2 / \left(2 \times 0.125^2\right)\right], \tag{4.2.10}$$

where z is height, h is the tree height, and L is leaf area index. The tree height in the following calculation is assumed to be 20 m. The initial mean wind speed is given by

$$u = \begin{cases} u_h \exp\left[\alpha_2 \left(z/h - 1\right)\right] & z \leq h \\ u_h \left\{\alpha_1 \tanh\left[\left(\alpha_2/\alpha_1\right)\left(z/h - 1\right)\right] + 1\right\} & z > h \end{cases}, \tag{4.2.11}$$

where the wind at the treetop $u_h = 1\ \mathrm{ms}^{-1}$, α_1 and α_2 are empirical constants given by

$$\alpha_1 = 3, \tag{4.2.12}$$

$$\alpha_2 = -0.0296L^2 + 0.6565L + 0.7010. \tag{4.2.13}$$

The temperature profile is set up to make the Brunt-Väisälä frequency profile assume the following form

$$N^2 = 0.003\left\{(1-\gamma_1)\exp\left[-\gamma_2\left(z/h - 1\right)\right] + \gamma_1\right\}, \tag{4.2.14}$$

where $\gamma_1 = 0.2$ and $\gamma_2 = 2$.

The parameters used in the simulation are listed in Table 4.1. The minimum Richardson number of 0.112 is found just above the treetop, which is below the critical value of 0.25.

Parameter		Value
$\triangle x$	horizontal grid size	3.28 m
$\triangle z$	vertical grid size	1.88 m
h	tree height	20 m
L	leaf area index	4
u_h	wind speed at the treetop	1 ms^{-1}
λ	wavelength of the fastest growing mode	210 m
L_x	length of the computation domain	λ
H	height of the computation domain	$6h$

Table 4.1: The parameters used in the numerical simulation.

Simulations are initiated with small-amplitude white noise added to the initial potential temperature field. Other variables adjust themselves gradually to the perturbation. At about 200 s after the initiation, the flow field locks into the fastest growing mode. The initial perturbation is chosen to be sufficiently small so that it does not influence the flow structure at the finite-amplitude stage. Previous studies (*e.g.*, Peltier *et al.*, 1978; Sykes and Lewellen, 1982) have demonstrated the insensitivity of the result to the exact form of the initial perturbation.

4.3 Results and Analysis

4.3.1 Comparison with the Linear Theory

For the parameters listed above, simulations have been performed for the flow with canopy and without canopy respectively. The amplitude of the initial perturbation is chosen to be sufficiently small and the linear growth stage can be captured by the 2D simulation. The apparent growth rate and phase speed can be compared with the linear theory (Lee, 1997). To estimate the apparent linear growth rate, the horizontal mean of the horizontal velocity u in the two dimensional $x-z$ plane is defined as (Patnaik *et al.*, 1976)

$$\langle u \rangle = \frac{1}{\lambda}\int_0^\lambda u\,(x,z)\,dx, \tag{4.3.1}$$

where the λ is the wavelength of the primary mode. The total perturbation kinetic energy is given by

$$E\,(t) = \int_0^H dz\left(\int_0^\lambda \frac{1}{2}\left[(u-\langle u \rangle)^2 + w^2\right]dx\right). \tag{4.3.2}$$

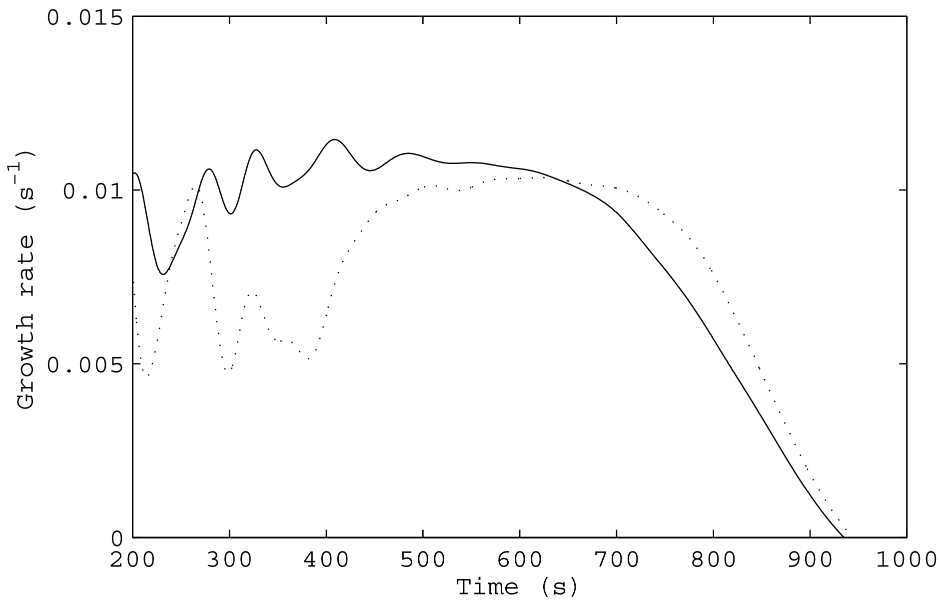

Figure 4.1: The linear growth rates for the flows with canopies (solid line) and without canopies (dashed line).

The growth rate σ, defined in equation 1.3.6, of the primary mode can be estimated by

$$\sigma = \frac{1}{2}\frac{d}{dt}\left(\ln E\right). \qquad (4.3.3)$$

The result is shown in Figure 4.1.

Inspection of Figure 4.1 shows that linear growth stages, characterized with constant growth rates, can be identified (between 400 s and 700 s) for simulations with the canopy drag and without the canopy drag. The initial oscillations in the growth rates are the result of the initialization with white-noise, similar to those observed by Peltier *et al.* (1978). The steady growth rate for the simulation without the canopy drag has been established after about four linear time constants. The growth rate for the simulation without canopies is about 0.01 s^{-1}, nearly identical to the prediction

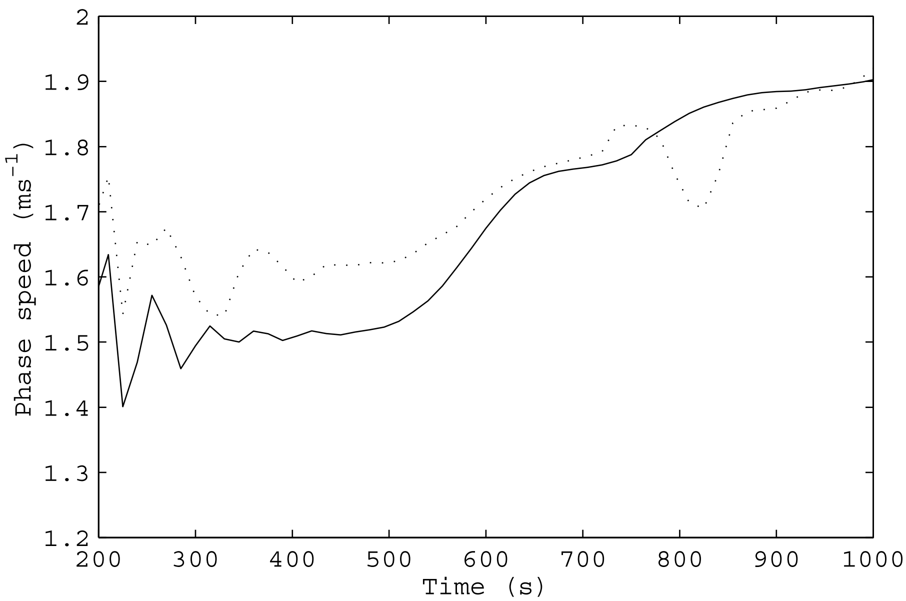

Figure 4.2: The phase speeds for the flows with canopies (solid line) and without canopies (dashed line).

of the linear stability analysis (Lee, 1997). For the simulation with the canopy drag, it takes less time to establish the normal growth curve. Two dimensional simulations show that the growth rate with canopies is slightly larger than that without canopies. Nonetheless, Lee's linear wave model (Lee, 1997) predicts a smaller growth rate of 0.067 s^{-1} for the flow with canopies.

The phase speed in Figure 4.2 is calculated by a cross-correlation algorithm (Appendix B). Lee's linear wave model predicts that the phase speeds for the flows with canopies and without canopies are almost equal, about 1.60 ms^{-1}. In the 2D computations, the phase speed for the flow without canopies is about 1.61 ms^{-1} in the linear growth stage, which is in agreement with the linear analysis. For the flow with canopies, the phase speed is about 1.50 ms^{-1}, smaller than the prediction of the linear stability analysis.

For the flow without canopies, the agreement of the linear growth parameters between this 2D simulation and linear stability analysis are similar to previous studies on the KH instability (Patnaik *et al*, 1976; Peltier *et al*, 1978). It is indicative of good performance of this 2D flow solver. For the simulation with canopies, the discrepancy might be understood in terms of the changing background flow. In the linear analysis, the background flow is assumed constant with time. However, in the 2D numerical simulation, as discussed in Chapter 2, the half time to reduce the wind within canopies is much shorter than the linear time constant. The wind within and just above the canopy is significantly reduced by the canopy drag during the growth of small disturbances. As the result, the instability grows on a background wind profile whose wind shear would be larger than the initial shear given in equation 4.2.11 and a larger growth rate is not unexpected. The speed of the modified mean flow is slower than that of the initial wind profile because of the reduction of wind speed by the canopy drag. Since the instability moves with the mean flow, the phase speed is expected to be smaller. In addition, non-linear processes caused by the proximity to the ground can also reduce the phase speed (Peltier *et al.*, 1978). Thus, a larger growth rate and a slower phase speed are expected in the 2D simulation. In general, wind speed within the canopy is low and the discrepancy is not too severe. However, it reminds one that the results from linear stability analysis should be used with caution.

Beyond the linear growth stage, the growth rates decrease to zero rapidly within a couple of linear time constants. The inspection of the flow structures shows that the wave becomes saturated in amplitude. At the same time, the phase speed increases to about 1.9 ms^{-1}. It could be understood as the result of the saturated wave moves at the increased speed of the mean flows of a broadened shear layer.

4.3.2 The Two-dimensional Wave Evolution

Potential Temperature and Wind Fluctuations

Figure 4.3 shows a time sequence of potential temperature field for a growing wave for the simulation with the canopy drag. The result is qualitatively similar to the classical KH wave simulations reported by Patnaik *et al.* (1976) and Peltier *et al.* (1978). The prominent qualitative feature of this process is the rolling-up of potential temperature contours in the region called the "core", which is rather isothermal. The crowding of these contours along inclined bands is called the "braid", which connects the bottom of one core to the top of the next.

At the starting time, a small disturbance is added to the background potential temperature field. As the amplitude of the wave grows, the horizontally homogeneous stratification is gradually distorted. In the center of the wave, vertical temperature gradient is reduced. It is most noticeable just above the treetops, where wind shear is of maximum strength. From 700 s to 900 s, the amplitude of the wave achieves its maximum amplitude and becomes saturated. At 740 s, the overturning structure, which results in the statically unstable structure, is found in the center of the core. Finger-like overturning structures are found at both the leading and trailing edges of the core. Later, as the overturning structure develops, the finger-like structures are getting narrower and more adjacent to the edge of the core. As for the braid, which

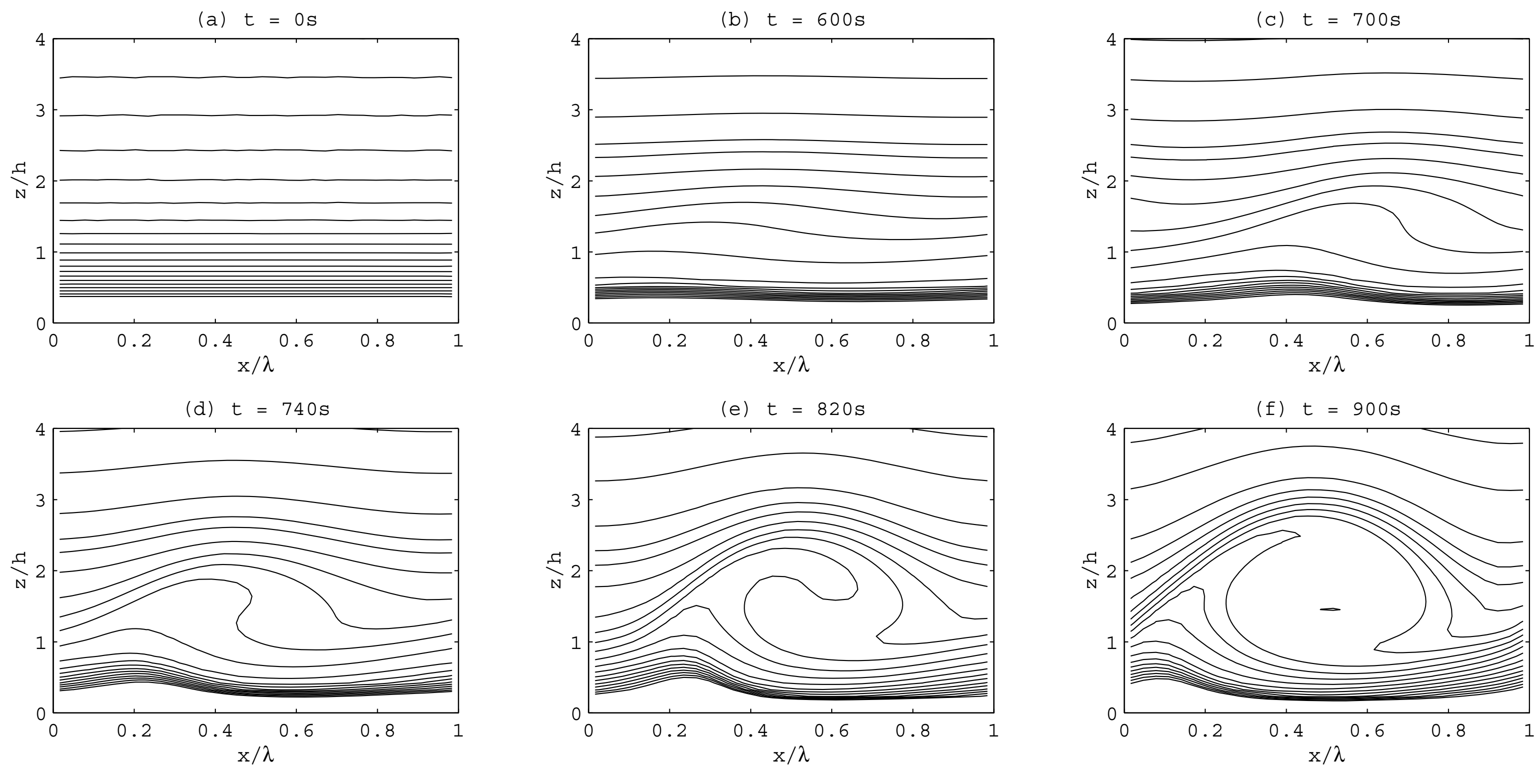

Figure 4.3: The evolution of a canopy wave in the potential temperature field. The contour interval is 0.2 K.

delineates the core, the leading edge is more diffusive and the trailing edge is more compact. With such thermal structure, an imaginary instrument tower would record signal patterns similar to those discussed in Chapter 2.

In Figure 4.4, wind fluctuation vectors are superimposed on the potential temperature field at the time when the wave reaches its maximum amplitude. Above the wave core, the vertical velocity is in quadrature with the horizontal velocity and potential temperature, which would generate little vertical momentum and heat fluxes. This evanescent wave feature is expected because of the way in which initial fields are specified. Large wind fluctuations are found at the layer where the wave core is located. Near the treetops, before the arrival of the braid, the slow upward motions are similar to the ejections observed in the daytime coherent structures. Following the braid are the fast downward motions whose counterpart would be the sweeps. The transition between the ejection and the sweep occurs at the braid, which would be the counterpart of the microfronts found in the daytime coherent structures. The sweep-ejection pattern is prominent from the upper canopy to about two tree heights. Further above, motions of the ejection type persist throughout the braid. There is no sweep following the ejection after the braid. The rather larger wind fluctuations near the ground are probably unrealistic since the lower boundary condition in the calculation does not provide a momentum sink.

In the unbounded KH instability simulations (Patnaik *et al.*, 1976; Peltier *et al.*, 1978), vertical symmetrical temperature structures have been found, since the velocity profile is symmetrical and the speed of the mean flow is found at the shear

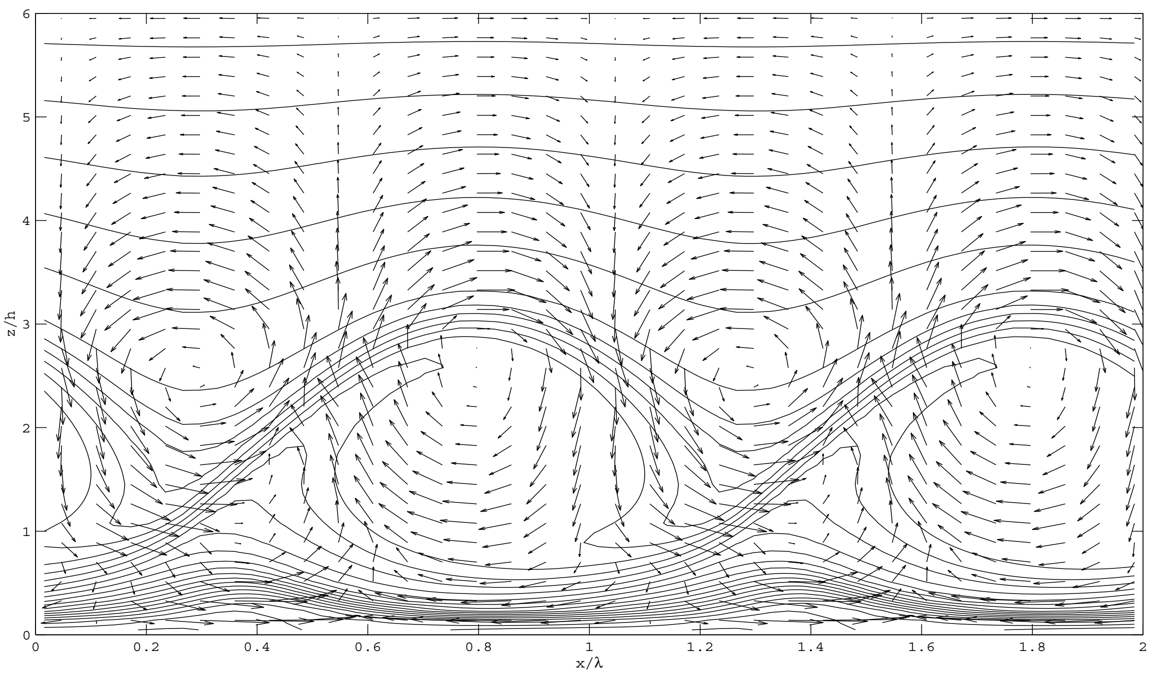

Figure 4.4: Wind fluctuation vectors and potential temperature contours. The contour interval is 0.2K.

maximum. This simulation differs from the two in several aspects. First, the wind profile is anti-symmetrical. Second, the shear maximum at the treetops is close to the ground. The growth of the lower half of the wave is significantly limited by the rigid ground. Furthermore, by visual inspection it is found that the center of the wave core is at about 1.3 tree heights, a few meters above the shear maximum. The phase speed calculated in section 4.3.1 is coincident with the background wind speed at the height of the core center. This is in agreement with the observation by Lee and Barr (1998).

Streamline Pattern

In the reference frame moving with the mean flow, the classical KH instability is characterized with a closed streamline pattern, which is widely known as the "cat's eye" (Drazin and Reid, 1982). Here the streamlines for the simulated canopy wave will be checked. In the coordinates moving with the wave, the stream function is defined as

$$\phi = \int (u - c)\, dz, \tag{4.3.4}$$

where u is the horizontal velocity, and c is the phase speed given by Figure 4.2.

A sequence of streamlines is presented in Figure 4.5. The closed streamlines initially appear at $1.35h$, where the minimum Richardson number is found. In the reference frame moving with the mean flow, the fluid circulates in the same fashion as the vorticity associated with the initial shear. As the wave grows, the center of the closed streamlines gradually moves upward. At the later stage of the linear growth,

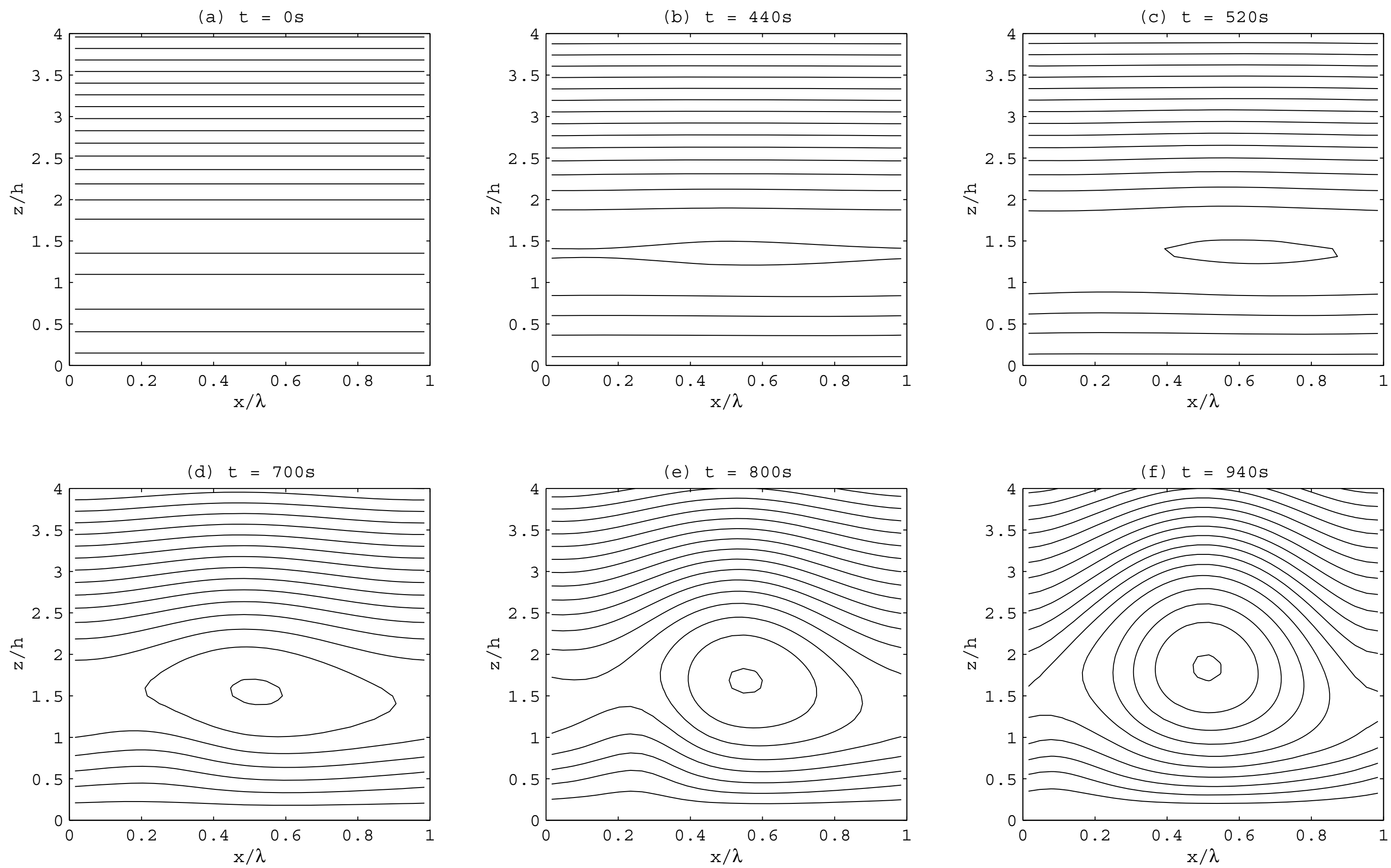

Figure 4.5: The evolution of streamlines.

the closed streamline pattern looks like the so-called "cat's eye" pattern. The pattern is not symmetrical as the result of unsymmetrical wind profiles. In addition, the amplitude of the lower half of the closed streamlines is limited by the proximity to the ground. The major axis is turned slightly clockwise from the horizontal line.

4.4 Wave-Mean Flow Interaction and Wave Introduced Mixing

Figures 4.6(a) and 4.7(a) illustrate the modification of the mean horizontal wind profile and the mean potential temperature profile until the wave reaches its maximum amplitude. The modification becomes prominent as the wave grows to the maximum amplitude. The ranges that the two profiles are modified in correspond approximately to the first closed streamline at that time (Figure 4.3). At the maximum amplitude, the reduction of horizontal wind speed in the layer below $3h$ is noticeable. The most reduction is found at about $2h$, the height with the maximum divergence of Reynolds stress (Figure 4.6(b)). Just above the treetops, the slope of the momentum flux profile remains zero throughout the growth phase. Thus, the wind speed just above the treetops changes little. The direct result of this reduction is to reduce the shear strength near the treetops. Within the canopy, the reduction of the wind speed is primarily done by the canopy drag. Since the half time of the wind speed reduction by the canopy drag (Equation 2.3.1) is related to the distribution of canopy elements, the Gaussian distribution used in this model (Equation 4.2.10) and the open trunk space creates secondary wind maximum within the canopy (at 600 s in Figure 4.6(a)). The reversal flow near the ground at the maximum stage is intriguing. The momentum

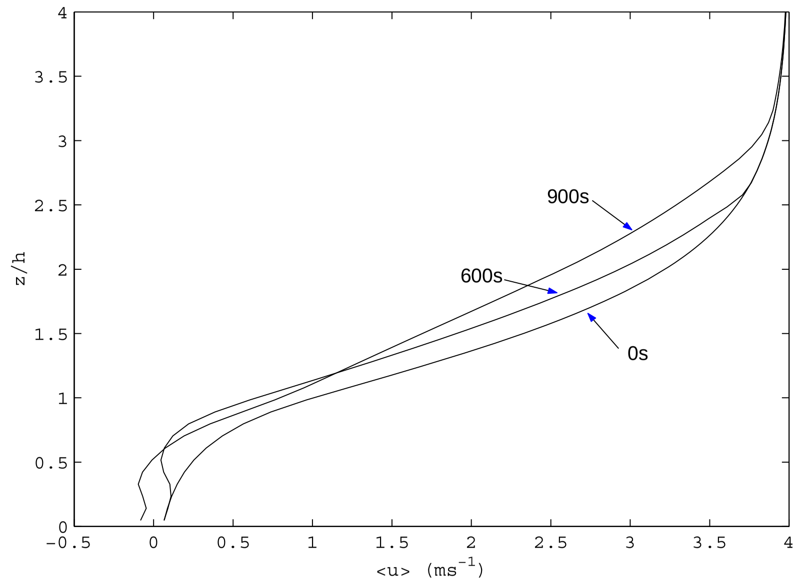

(a) Background horizontal wind profile.

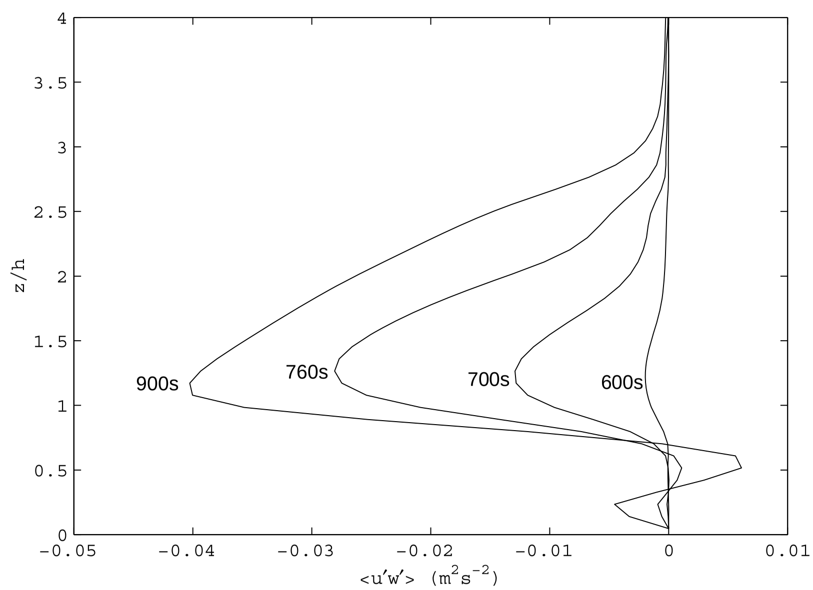

(b) Horizontally averaged momentum flux.

Figure 4.6: Background horizontal wind profile and horizontally averaged momentum flux.

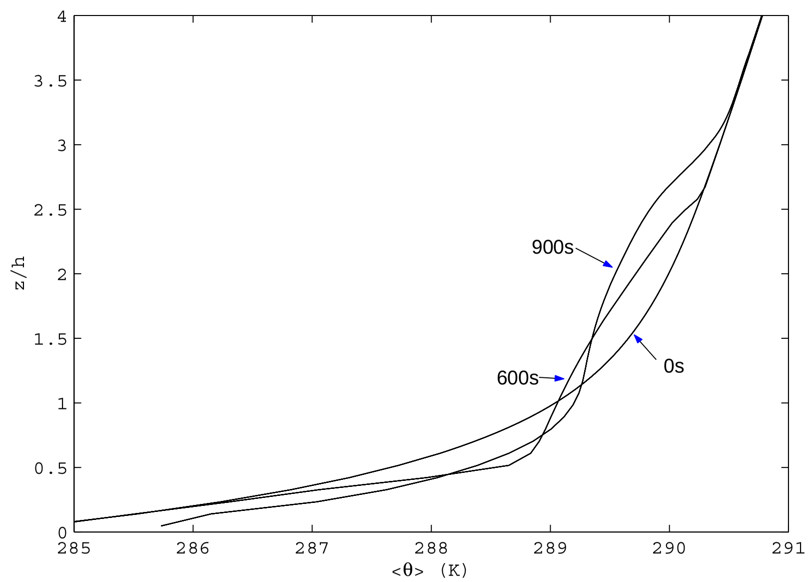

(a) Background potential temperature profile.

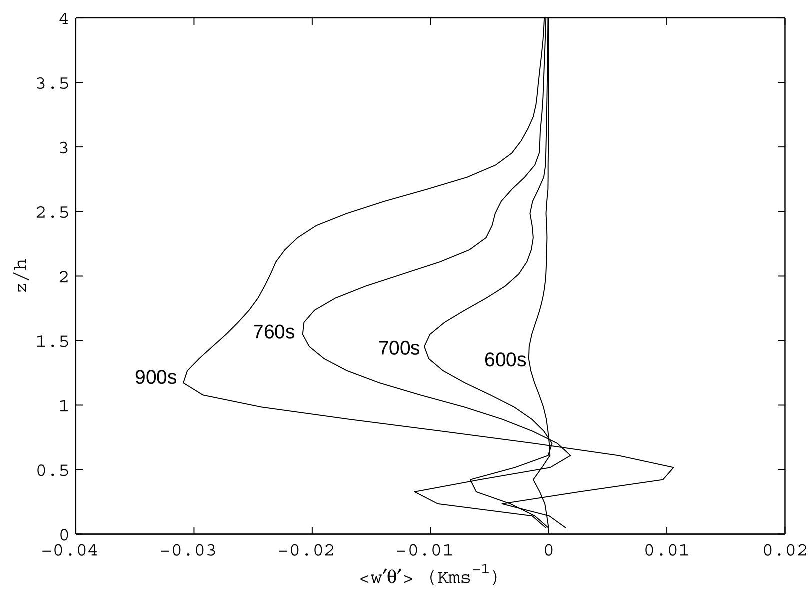

(b) Horizontally averaged heat flux.

Figure 4.7: Background potential temperature profile and horizontally averaged heat flux.

flux at the same time exhibits a zigzag pattern. This might be the effect of the entrainment of the fast-moving fluid into the slow-moving lower layer similar to that observed by Peltier *et al.* (1976). It could also possibly be the numerical effect from the lower no-flux rigid boundary.

The heat fluxes (Figure 4.7(b)) responsible for the potential temperature profile (Figure 4.7(a)) modification are qualitatively similar to the momentum fluxes. The modification of the original potential temperature profile by the eddy heat flux is associated with the growing wave. The divergence of the heat flux above the treetops brings the air temperature down. The air within the canopy is heated by the the downward heat flux. At the maximum amplitude, the temperature gradient in the layer between the upper canopy and about two tree heights is much reduced. As a result, two secondary inversion layers appear both above the canopy and in the lower canopy, similar to the splitting of the original inversion layer reported by Peltier *et al.* (1976). The zigzag pattern of the heat flux near the ground is similar to that found in the momentum flux. It is probably created by the statically unstable structure formed during the overturning of the wave. But the numerical effect cannot be excluded either. Above three tree heights, the background profiles of both wind and potential temperature are completely unaffected by the wave.

4.5 Discussion and Summary

If one compares Figure 4.4 with Figure 2.6 and Figure 2.7 in Chapter 2, obvious commonalities will be revealed. They are:

- The simulated potential temperature field at the maximum amplitude bears major resemblance to the observation. The observed isothermal wave cores which are delineated by steep temperature gradients are similar those of the KH wave at the growing and saturated stages.

- The observed polarization relations at the level above shear maximum is similar to those of evanescent waves, which are reproduced by the numerical simulation.

- Within the wave core, certain fine scale structures are reproduced. For example, finger-like statically unstable overturning structures are found both in the observation and the numerical simulation.

- Near the treetops, motions of sweep and ejection types, similar to those found in observations, are reproduced by the numerical model.

However, this two-dimensional numerical simulation has its limitations. Further development of span-wise secondary instability in the braids and gravitational instability in the cores is three-dimensional in nature, which cannot be resolved by this two-dimensional model. For example, this model cannot reproduce the observed turbulent wind fluctuations in the wave cores in Figure 2.6 and Figure 2.7. Nonetheless, it is the macro-structures, which are essentially determined by the initial profiles and boundary conditions, that are of primary interest at the present time. The qualitative resemblance between the numerical simulation and the tower based field observation suggests that the observed canopy waves are shear-generated KH waves.

The mixing of scalars, especially the nocturnal respiratory CO_2, can be inferred from the modification of wind profile and potential temperature profile by canopy waves. The simulation indicates that considerable mixing occurs during the growth of the KH wave below three canopy heights. The potential temperature in the thin layer above the canopy is reduced by the downward transport of sensible heat. At the same time, the air in the canopy layer, most noticeable in the upper canopy layer, is heated up. The role of the canopy wave is to entrain warmer air above into the canopy layer and simultaneously flush cooler air out of the canopy. The irreversible mixing, by the secondary convective instability in the statically unstable structures, will reduce the strength of the temperature inversion. On clear nights, similar to that of the potential temperature profile, a large positive CO_2 concentration gradient across the forest-atmosphere interface is usually found. The mixing process associated with the wave is expected to flush CO_2 out of the canopies and mix it with the air above. But the mixing is limited to the thin layer just above the treetop and below 2 to 3 tree heights. The escaped CO_2 might be advected down-stream by the mean flow. If such a scenario is true, most of the current tower-based eddy-covariance systems cannot capture this CO_2 efflux. Erratic nocturnal flux behaviors, which differ from normal flux-gradient relations, are not unexpected. Most worrisome is the uncertainty of the estimate of the long-term net ecosystem exchange of CO_2 measured by such systems.

Although this numerical model, with a crude sub-grid turbulence closure scheme, can produce flow structures that qualitatively bear resemblance to observations, the quantitative details of the evolution of the fluid field and turbulence statistics are not realistic. Within the 2D frame work, further improvement in sub-grid turbulence closure can be done, such as the second-order closure scheme employed by Sykes and Lewellen (1982). The improved turbulence statistics can be used by Lagrangian transportation models (*e.g.*, Raupach, 1988) to investigate the wave-introduced mixing, similar to the study of the particle dispersion due to KH instability in the lower stratosphere (Schilling and Janssen, 1992). Ultimately, the simulation should be done in a three-dimensional large-eddy simulation. Much is expected with the advance of the large-eddy simulation of the nocturnal canopy flow.

Conclusion

In this dissertation, the flow structure of the wave-like air motion in forests has been analyzed in time-height dimensions. The results show that wave-like air motions are dominant in the canopy roughness layer on clear nights when the wind above the treetops is moderate. The life cycles of wave events bear resemblance to that of a Kelvin-Helmholtz wave. Wave activities are characterized by intermittence in response to the changes of the background wind and the radiative cooling. The temperature field of the wave resembles that of a finite-amplitude KH wave. The polarization relation measured away from shear maximum is in accord with that of a KH wave. Statically unstable structures by the wave overturning have been found. The conjecture of turbulent mixing from the convective instability is corroborated with the measured turbulent wind fluctuations within waves. There is evidence that counter-gradient fluxes are associated with the overturning structures. It is first pointed out that the irreversible mixing associated with the waves can flush CO_2 out of canopies to the thin layer with a depth of 1 or 2 tree heights. This flux cannot be captured by most current instrument setups. Thus, it raises the uncertainty of the measurement of the long-term ecosystem-atmosphere exchange of CO_2 by using the eddy-covariance technique.

A two-layered linear canopy wave model has been developed to investigate the wave mechanism. The inclusion of the canopy drag changes the stability property of the flow system. By modifying the growth rates, the canopy drag can either stabilize or destabilize the flow in reference to the flow with the same configuration but without canopies. A new type of instability has been found solely as a result of the canopy drag in the otherwise stable background conditions without canopies. The model results indicate that the forest environment is favorable to the occurrence of wave-like air motions of KH type on clear nights.

In an effort to reproduce flow structures of canopy waves, a two-dimensional numerical model has been developed. With the prescribed initial profiles and a crude turbulence closure scheme, the detailed flow field information of the wave evolution is computed. The numerical results bear major resemblance to the observation. Specifically, the temperature field is characterized with isothermal cores delineated by steep temperature gradient. Away from the shear maximum, the observed phase relations among the wave components is reproduced in the numerical computation. The observed fine structures look like those resulting from the wave overturning in the numerical simulation. The numerical model also indicates that motions of sweep and ejection types are reminiscent of KH waves. The numerical simulation also reveals the non-stationary property of the mixing process associated with the wave. The implication of these results to the field observation has also been discussed.

Appendix A

Wave-like Air Motions in Time-height Dimensions

Salient wave structures are best revealed by the time-height plots of tower-based high-vertical-resolution temperature profiles. In these plots, the time axes are reversed to give the impression that the mean wind is blowing from left to right. The vertical axis is normalized with the tree height h=21 m. The treetop is located approximately in the middle of each plot. The contour interval in the following plots is 0.2 K.

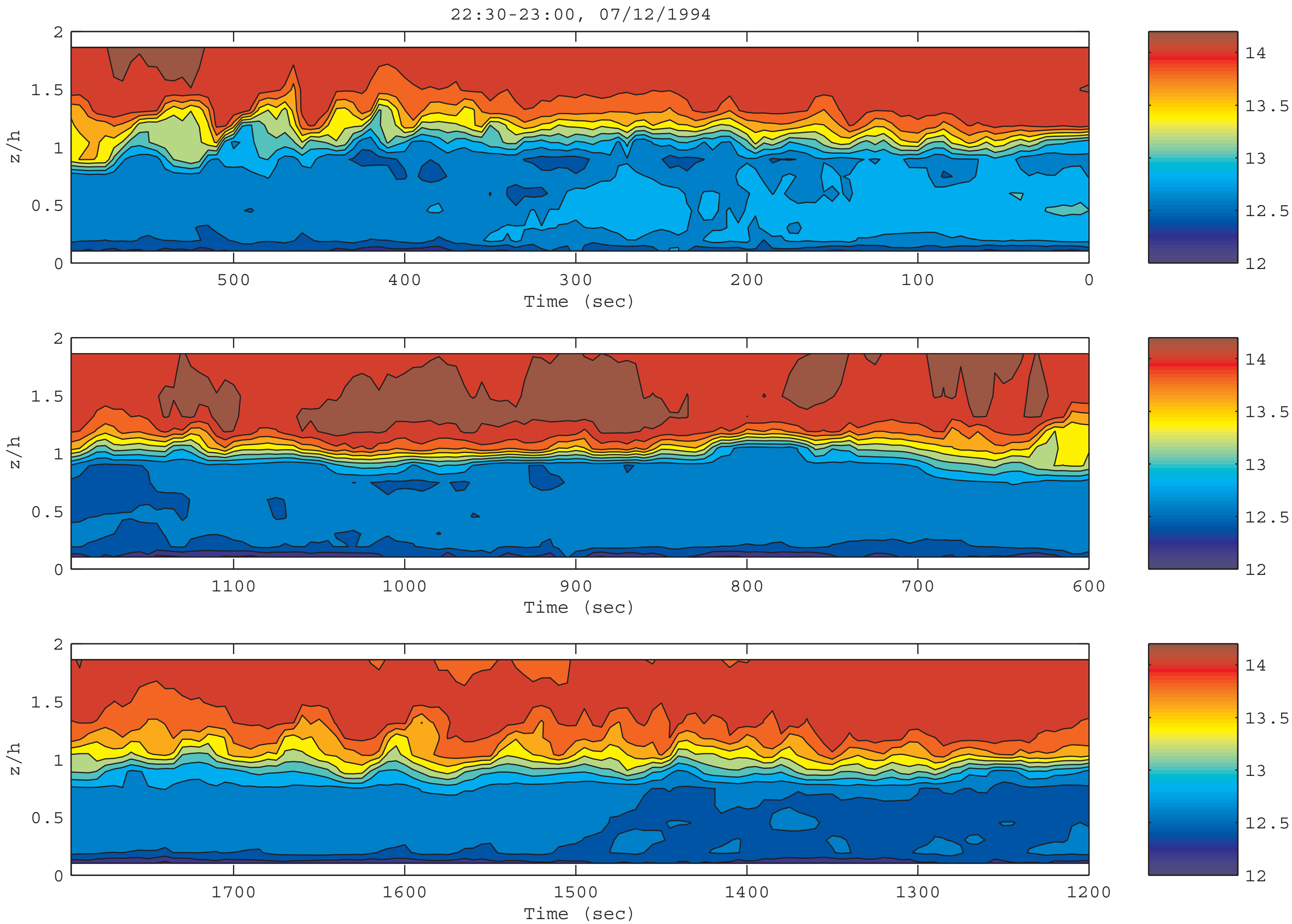

Figure A.1: Time-height potential temperature contour plot (22:30-23:00, July 12, 1994).

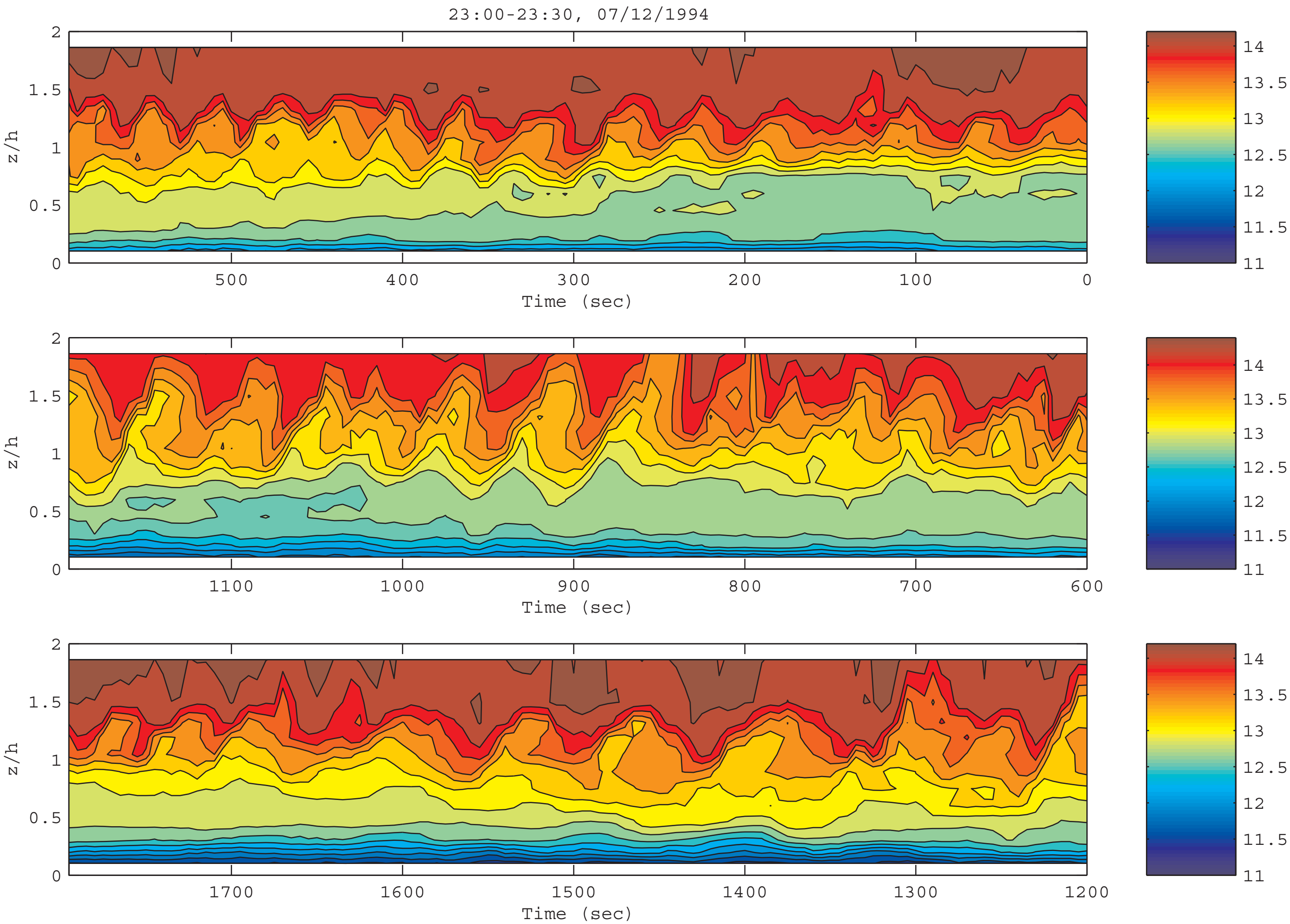

Figure A.2: Time-height potential temperature contour plot (23:00-23:30, July 12, 1994).

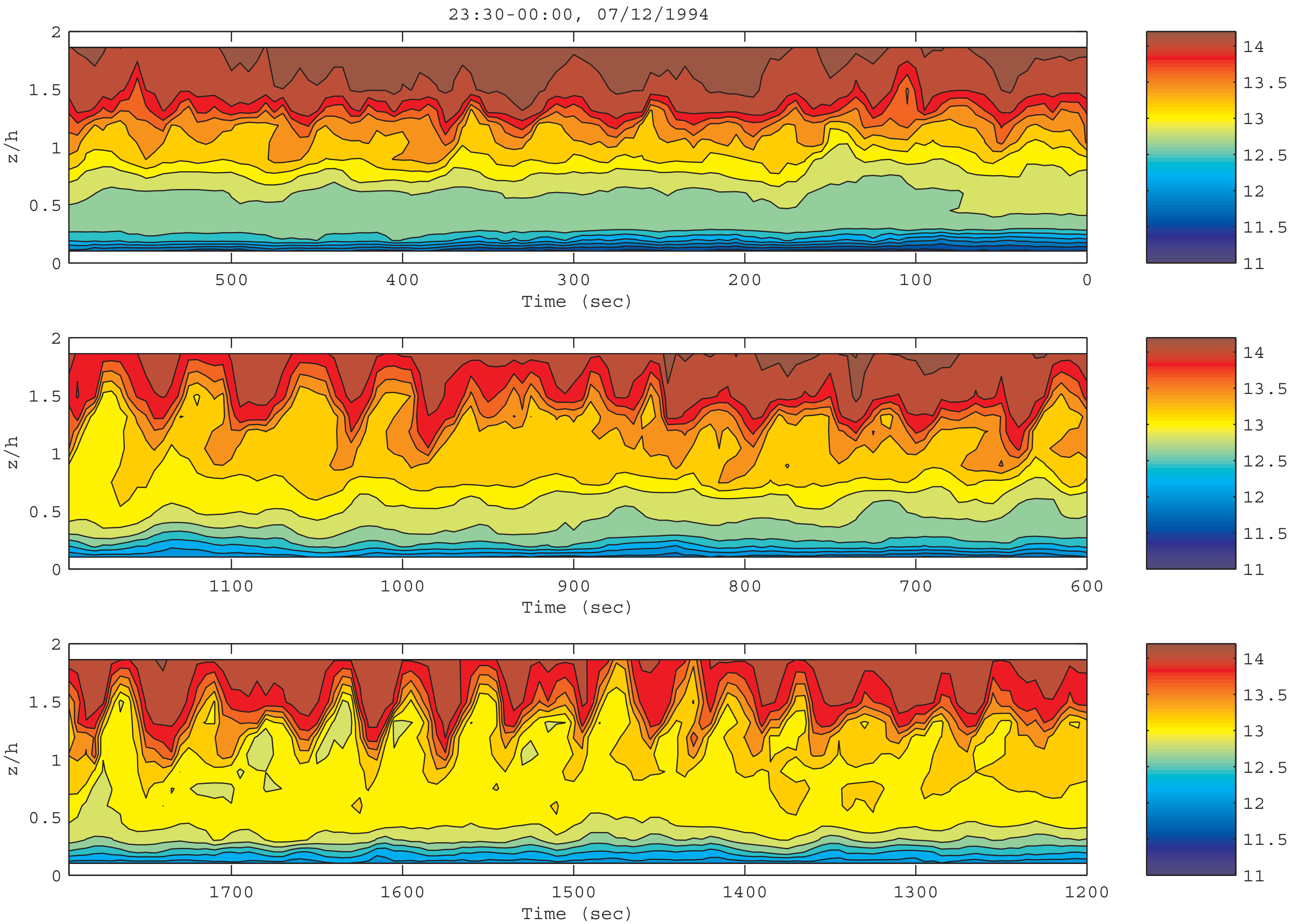

Figure A.3: Time-height potential temperature contour plot (23:30-24:00, July 12, 1994).

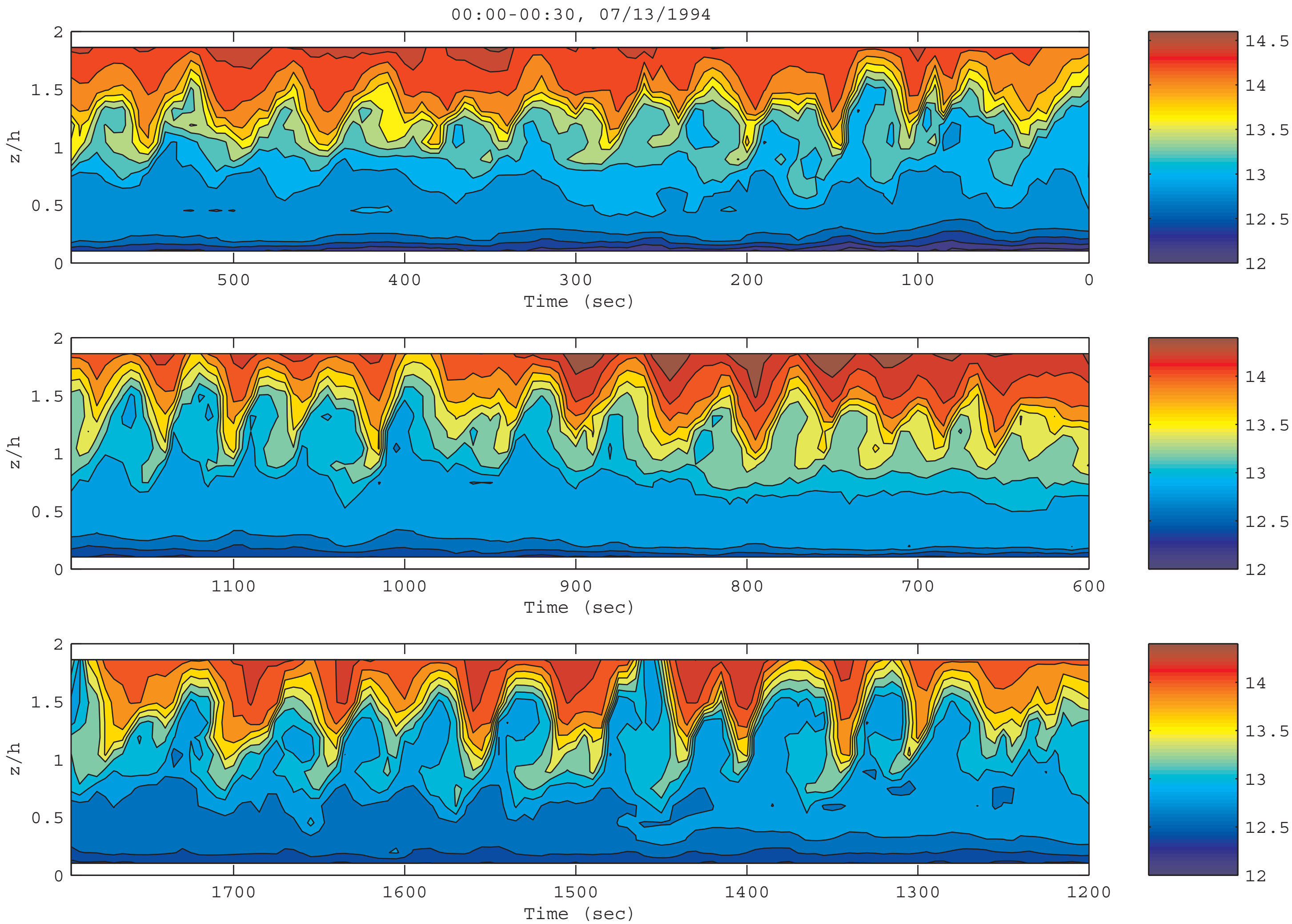

Figure A.4: Time-height potential temperature contour plot (00:00-00:30, July 13, 1994).

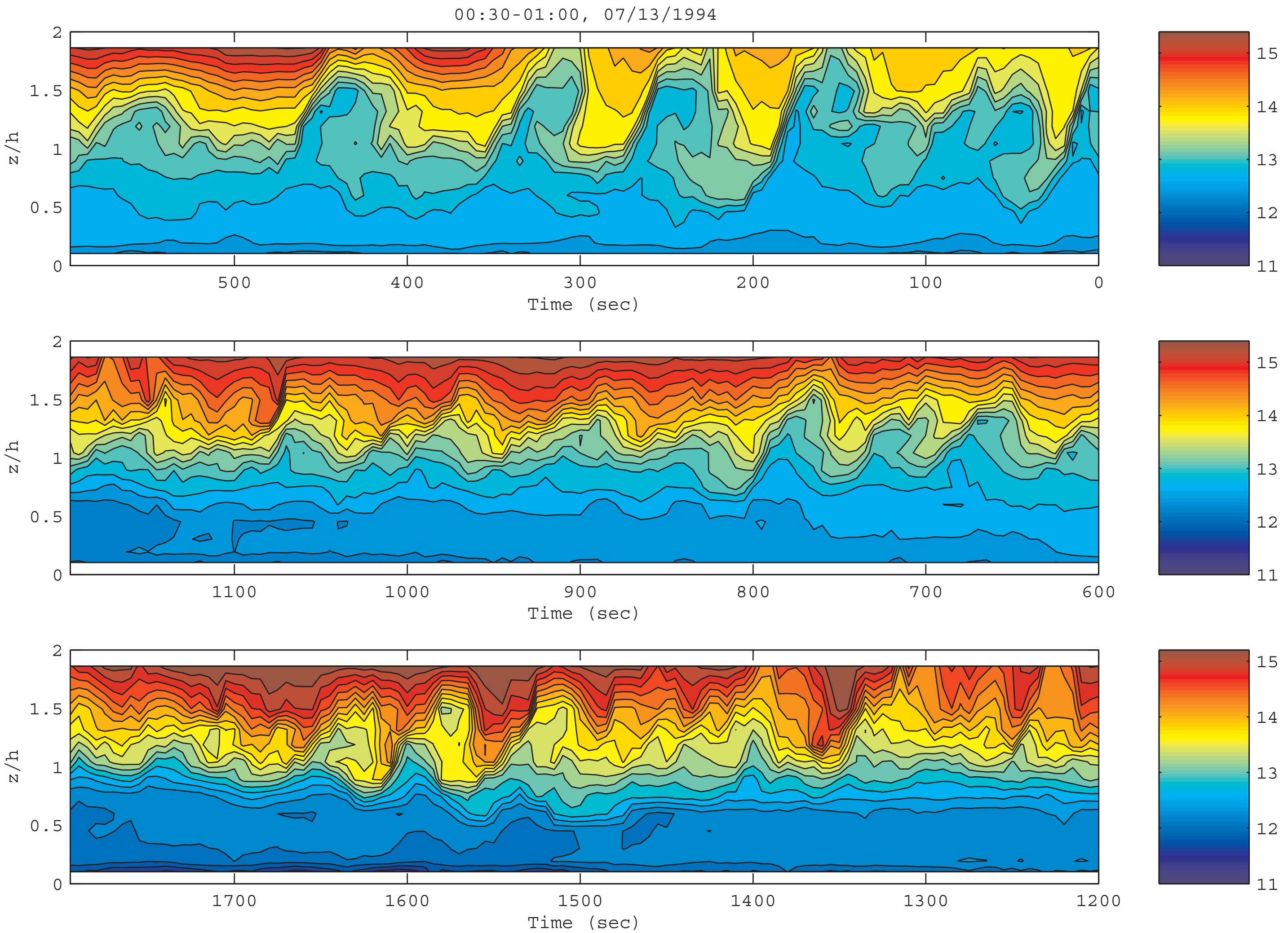

Figure A.5: Time-height potential temperature contour plot (00:30-01:00, July 13, 1994).

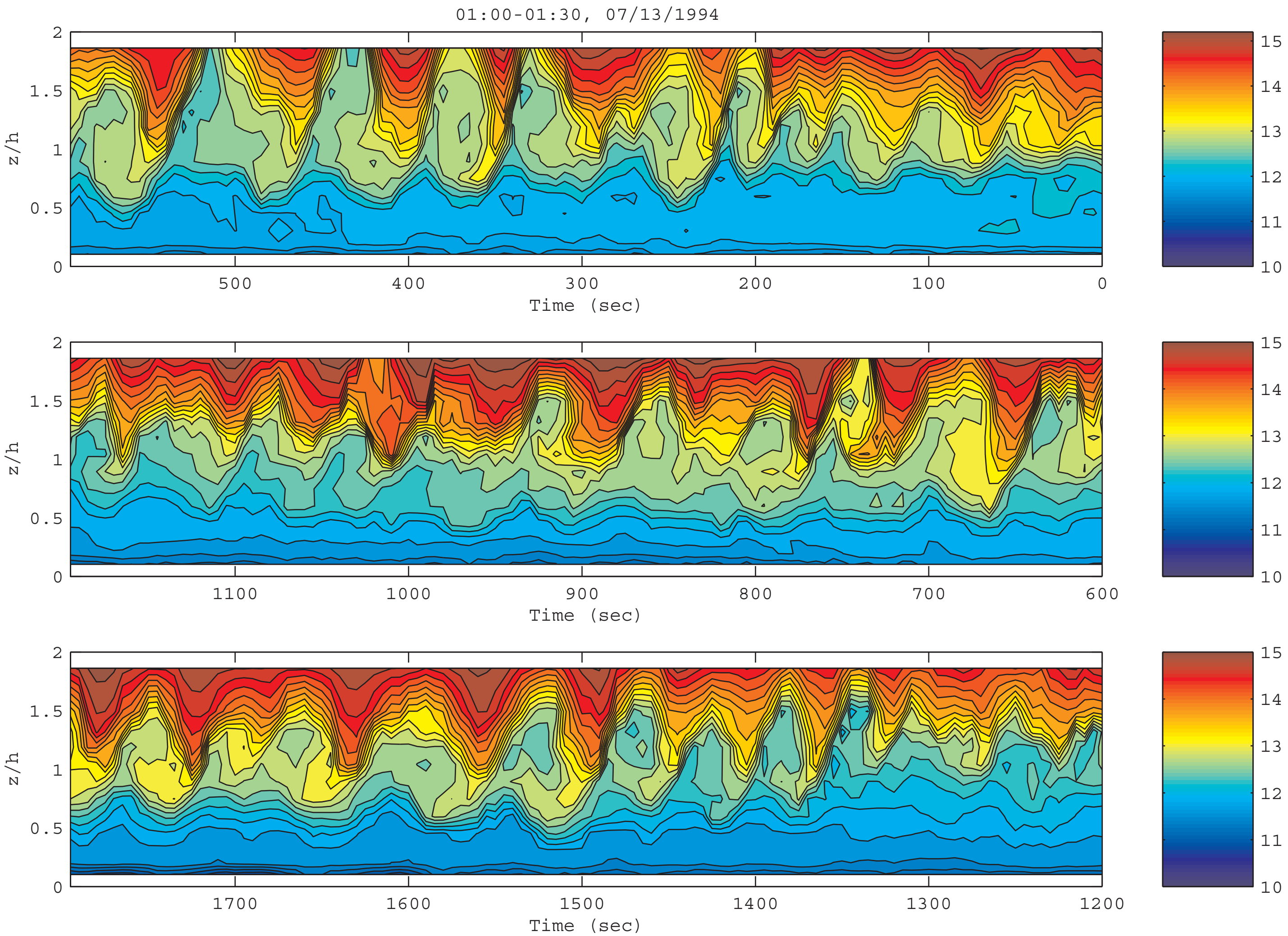

Figure A.6: Time-height potential temperature contour plot (01:00-01:30, July 13, 1994).

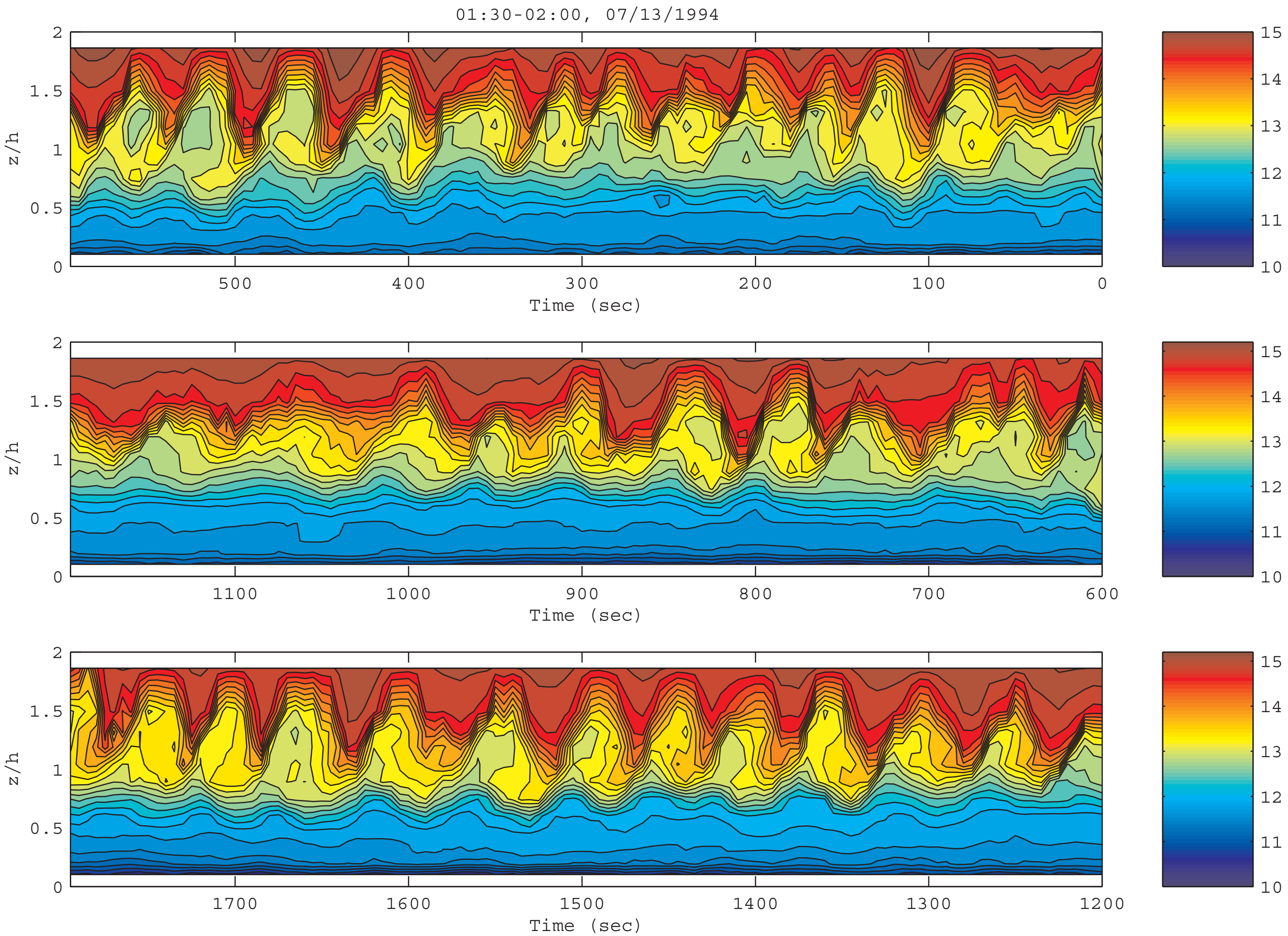

Figure A.7: Time-height potential temperature contour plot (01:30-02:00, July 13, 1994).

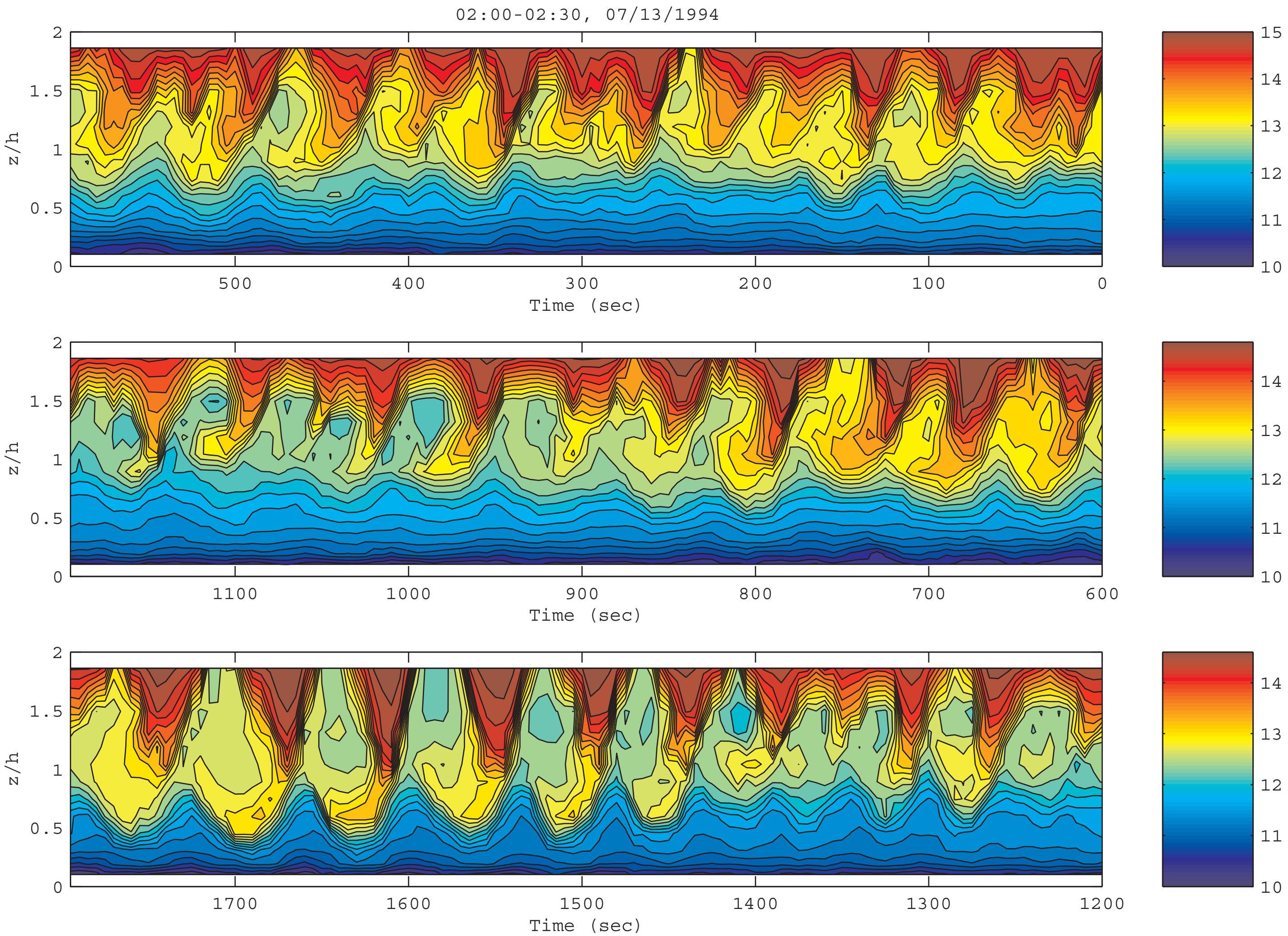

Figure A.8: Time-height potential temperature contour plot (02:00-02:30, July 13, 1994).

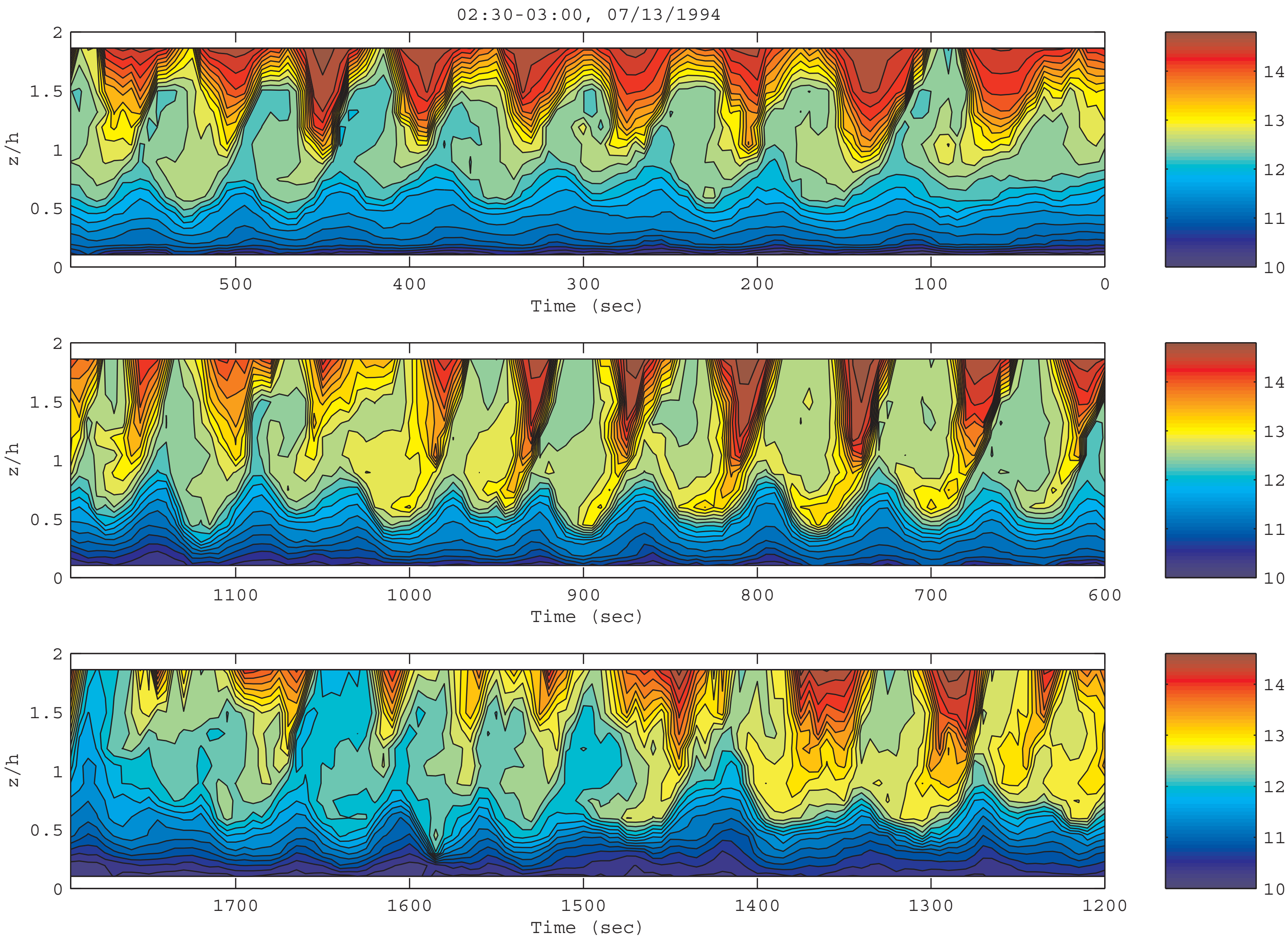

Figure A.9: Time-height potential temperature contour plot (02:30-03:00, July 13, 1994).

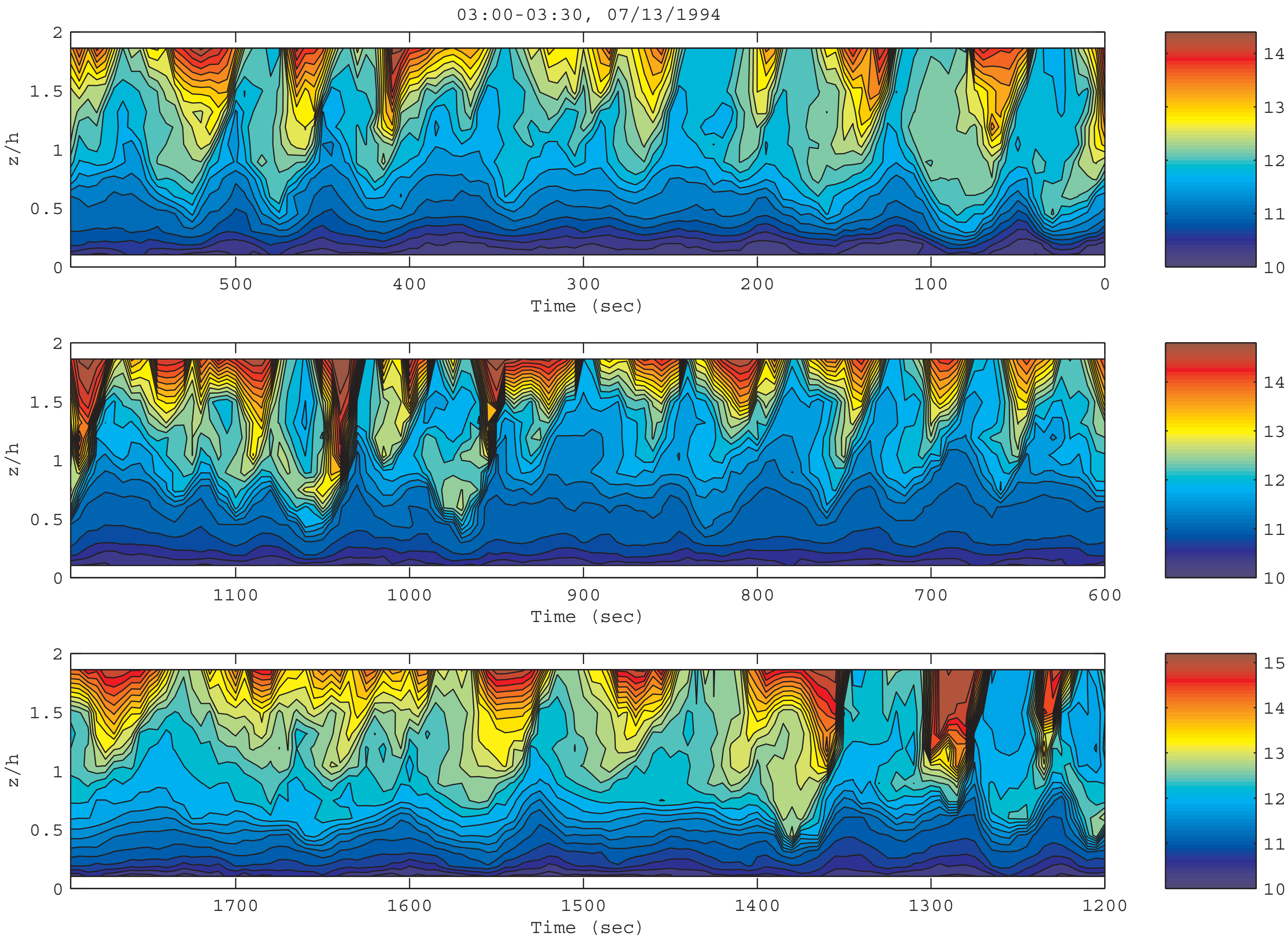

Figure A.10: Time-height potential temperature contour plot (03:00-03:30, July 13, 1994).

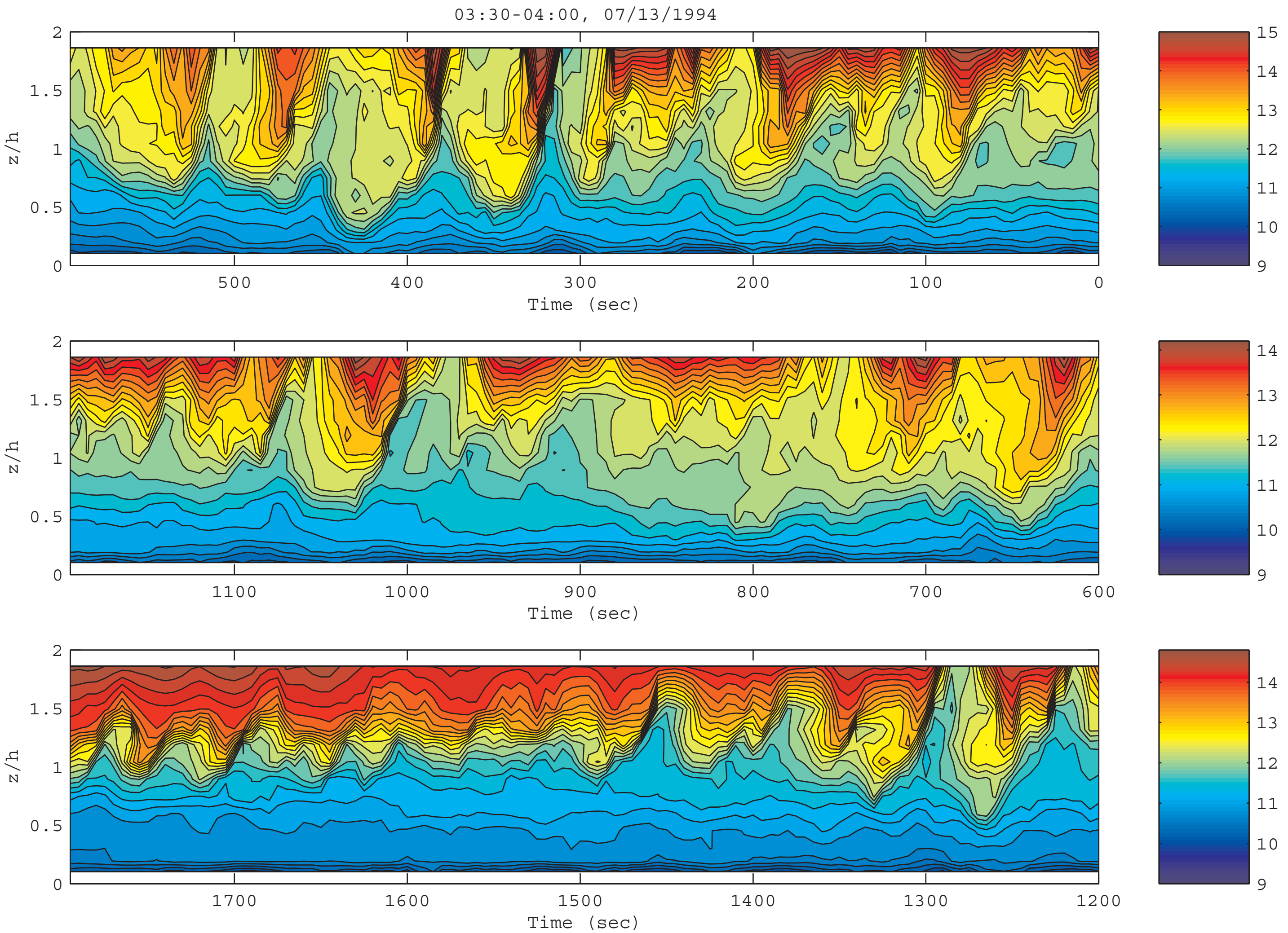

Figure A.11: Time-height potential temperature contour plot (03:30-04:00, July 13, 1994).

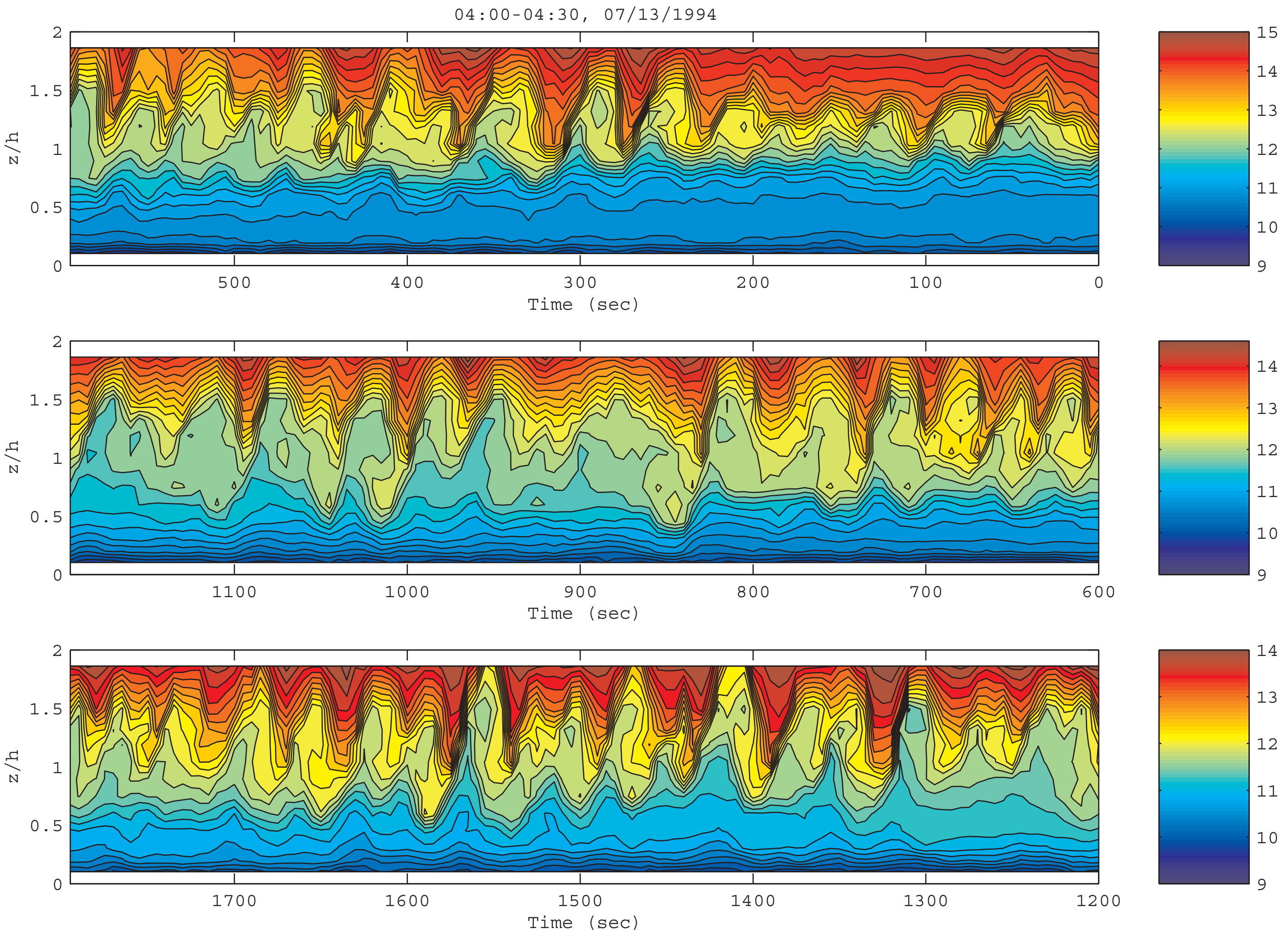

Figure A.12: Time-height potential temperature contour plot (04:00-04:30, July 13, 1994).

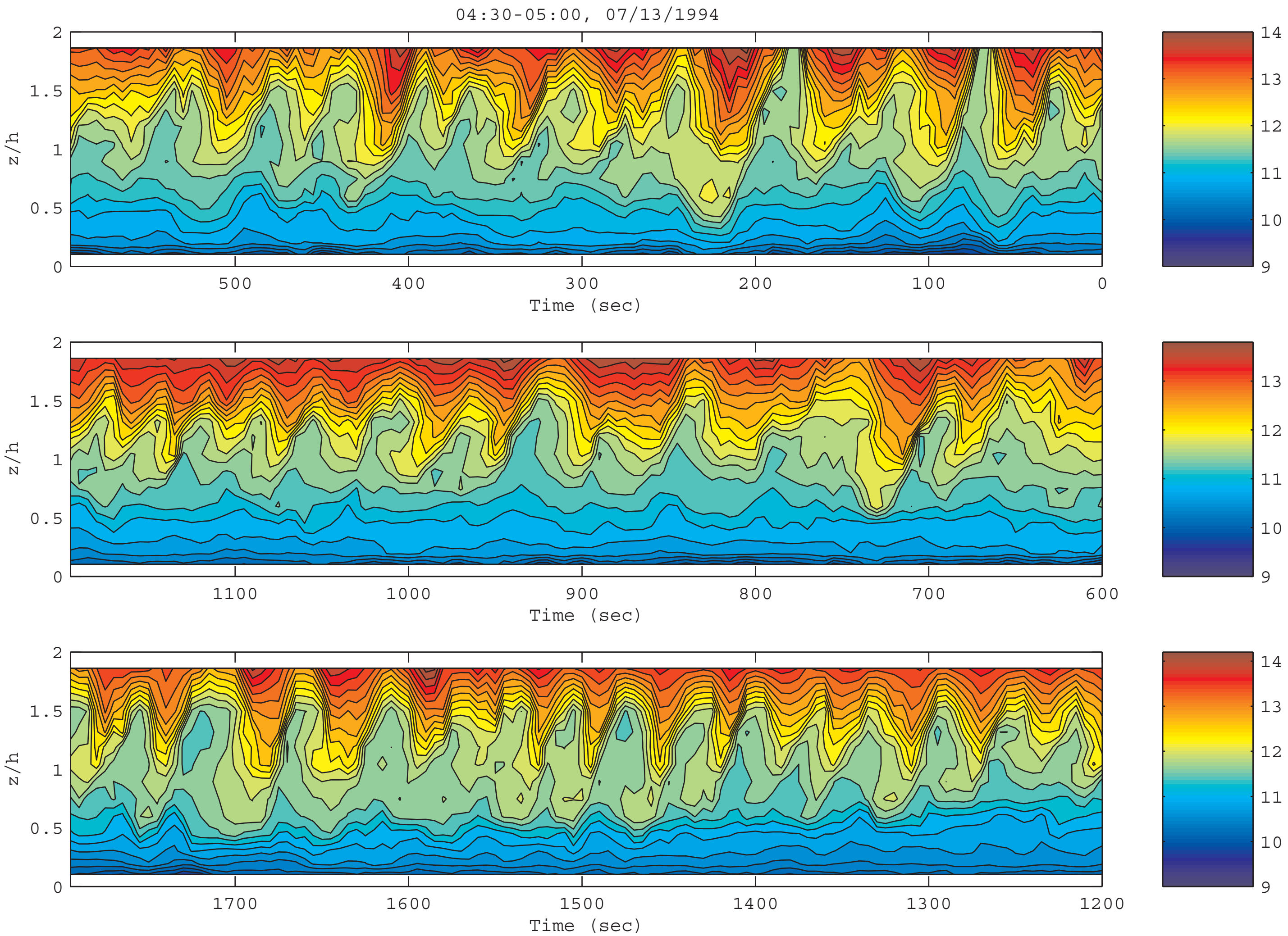

Figure A.13: Time-height potential temperature contour plot (04:30-05:00, July 13, 1994).

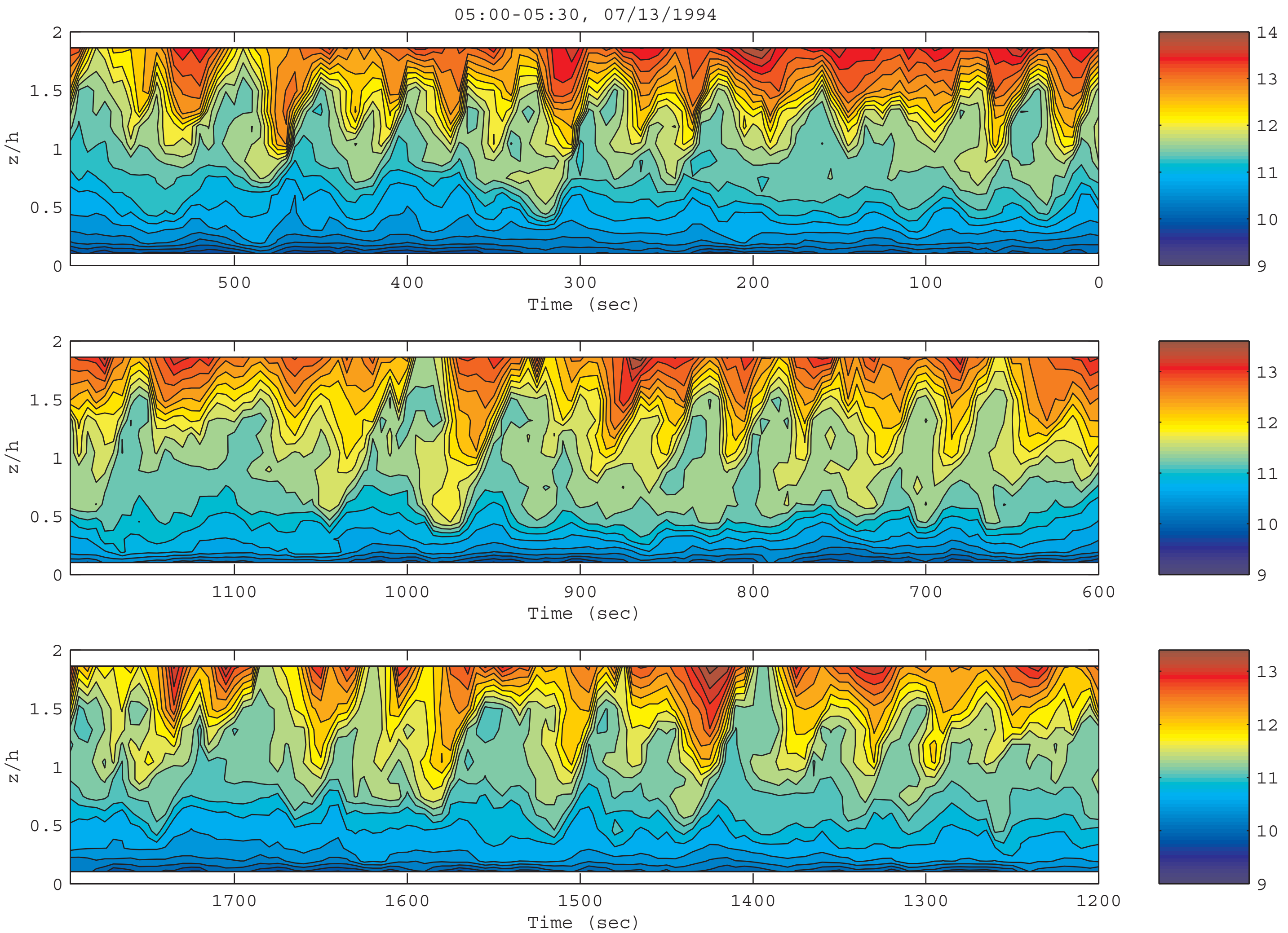

Figure A.14: Time-height potential temperature contour plot (05:00-05:30, July 13, 1994).

Appendix B

The Algorithm for Computing the Phase Speed

For a suitable quantity, such as the potential temperature or the vertical velocity field, $\phi\,(x, z, t)$ is used to denote the two dimensional flow field at instant t in the $x - z$ plane. Compared with a reference frame $\phi_0 = \phi\,(x, z, t_0)$, the wave structure moves a distance of $\triangle d$ in x-axis direction in the subsequent frame $\phi_1 = \phi\,(x, z, t_0 + \triangle t)$. Then the phase speed is given by

$$c = \frac{\triangle d}{\triangle t}. \tag{B.0.1}$$

The displacement $\triangle d$ can by estimated by finding the maximum of the spatial correlation between ϕ_0 and ϕ_1. The correlation is computed by an algorithm based on the Fast Fourier Transformation (FFT). The Fourier transformation pairs are denoted by

$$\phi \Leftrightarrow \Phi. \tag{B.0.2}$$

The correlation theorem states

$$\mathrm{Corr}\,(\phi_0,\phi_1) \Leftrightarrow \Phi_0 \Phi_1^*, \tag{B.0.3}$$

where the asterisk denotes the complex conjugate. In practice, we take two frames of data with a properly chosen time delay so that the primary flow structure does not change much. The correlation is calculated by the inverse FFT transformation according to the correlation theorem.

The estimate of $\triangle d$ can be further improved by an empirical method. Given that the discrete maximum of Corr (ϕ_0,ϕ_1) is found at $x_0 = n \triangle x$, a parabolic curve

$$C\left(x\right) = \alpha\left(x - x_0\right)^2 + \beta\left(x - x_0\right) + \gamma \qquad \text{(B.0.4)}$$

is fitted with a number of data points adjacent to the discrete maximum by a least square method. The maximum of this parabolic curve is presumably the best estimate of $\triangle d$. The better-than-the-grid-size estimate of the displacement is

$$\triangle d = x_0 + \frac{\beta}{2\alpha}. \qquad \text{(B.0.5)}$$

Bibliography

Almgren, A. S., J. B. Bell, and W. G. Szymczak, 1996: A numerical method for the incompressible Navier-Stokes equations based on an approximate projection. SIAM J. Sci. Comput., 17(2).

Almgren, A. S., J. B. Bell, P. Colella, L. H. Howell, and M. L. Welcome, 1998: A Conservative Adaptive Projection Method for the Variable Density Incompressible Navier-Stokes Equations, J. Comp. Phys., 142, 1-46.

Altas, D, J. I. Metcalf, J. H. Richater and E. E. Gossard, 1970: The birth of 'CAT' and microscale turbulence, J. Atmos. Sci., 27, 903-913

Alvo, P, R. L. Desjardins., P. H. Schueoo and J. I. MacPherson, 1984: Aircraft measurement of CO2 exchange over various ecosystems, Boundary-Layer Meteorol., 29, 167-183

Antonia, R. A., A. J. Chambers, C. A. Frieche, and C. W. van Atta, 1979: Temperature ramps in the atmospheric surface layer, J. Atmos. Sci., 36, 99-108

Bakwin, P. S., S. C. Wofsy, S. M. Fan, M. Keller, S Trumbore, and J. M. Da Casta: Emission of nitric oxide (NO) from tropical forest soils and exchange of NO between the forest canopy and atmospheric boundary layer, J. Geophys. Res., 95, D10

Baldocchi, D. D., B. B. Hicks and T. O. Meyers, 1988: Measuring biosphere-atmosphere exchanges of biologically related gases with micrometeorological methods, Ecology, 69(5), 1131-1340

Baldocchi, D. D. and T. P. Meyers, 1988: Turbulence structure in a deciduous forest, Boundary-layer Meteorol., 43, 345-364

Bayly, B. J. and S. A. Orszag, 1988: instability mechanisms in shear-flow transition, Ann. Rev. Fluid. Mech. 1988, 20, 359-91

Bergström, H. and U. Högström, 1989: Turbulent exchange above a pine forest II. Organized structures, Boundary-Layer Meteorol., 231-263

Black, T. A., *et al.*, 1996: Annual cycles of water vapor and carbon dioxide fluxes in and above a boreal aspen forest, Global Change Biology, 2, 219-229

Budagovsky, A. I., Ross, J. K. and Tooming, H. G., 1968: In "Aktinometriya I optika atmosfery" (Actinometry and Atmospheric Optics), pp299-307, Valgus, Tallinn (Russian)

Bussinger, J. A., 1986: Evaluation of the accuracy with which dry deposition can be measured with current micrometeorological techniques, J. Climate and Appl. Meteorol., 25, 1100-1124

Campbell, G. S. and J. M. Norman, 1998: An introduction to environmental biophysics, 2nd Ed., Springer, New York, 70

Caufield, C. P., S. Yoshida and W. R. Peltier, 1996: Secondary instability and three-dimensionalization in a laboratory accelerating layer with varying density differences, Dynamics of Atmospheres and Oceans, 23, 125-138

Chorin, A. J., 1969: Numerical solutions for the Naview-Stokes equations, J. Math. Compt., 22, 745-762

Dabbert, W. F., D. H. Lenschow, T. W. Hosrdt, P. R. Zimmerman, S. P. Oncley, A. C. Delany, 1993: Atmosphere-surface exchange measurements, Science, 260, 1472-1481

Davis, P. A. and W. R. Peltier, 1976: Resonant parallel shear instability in the stably stratified planetary boundary layer, J. Atmos. Sci., 33, 1287-1300

Davis, P. A. and W. R. Peltier, 1979: Some characteristics of the Kelvin-Helmholtz and resonant overreflection mode of shear flow instability and of their interaction through vortex pairing, J. Atmos. Sci, 36, 2394-2412

Delisi, D. P., and G. Corcos, 1973: A study of internal waves in a wind tunnel, Boundary-Layer Meteorol., 5, 121-137

Denmead, O. T., E. F. Bradley, 1985: Flux-gradient relationships in a forest canopy. In. The forest-atmosphere interaction, B. A. Huntchinson and B. B. Hicks (eds.), Reidel, Dordecht, 421-444

Desjardins, R. L., E. J. Brack, P. Alvo and P. H. Schueoo, 1982: Aircraft monitoring of surface carbon dioxide exchange, Science, 216, 733-735

Desjardins, R. L., E. J. Brack, P. Alvo and P. H. Schueoo, 1985: Measurements of turbulent heat and CO2 exchange over forests from aircraft, in The Forest-Atmosphere Interaction, edited by B. A. Hutchinson and B. B. Hicks, D. Reidel, Hingham, Mass

Drazin, P. G. and Reid, W. H., 1981: Hydrodynamic Stability, Cambridge University Press, London

Finnigan, J. J., 1979a: Turbulence in waving wheat. I. Mean Statistics and Honami, Boundary-layer Meteorol., 16, 181-211

Finnigan, J. J., 1979b: Turbulence in waving wheat. II. Structure of Momentum Transfer, Boundary-layer Meteorol., 16, 213-236

Finnigan, J. J. and Mulhearn, P. J., 1978a: Modeling waving crops in a wind tunnel, Boundary-layer Meteorol., 14, 253-277

Finnigan, J. J. and Mulhearn, P. J., 1978b: A simple mathematical model of airflow in waving plant canopies, Boundary-layer Meteorol., 14, 415-431

Fitzjarrald, D. R. and K. E. Moore, 1990: Mechanisms of nocturnal exchange between the rain forest and the atmosphere, J. Geophy. Res., 95(D10), 16,839-16,850

Fowler, D. and J. H. Duyzer, 1989: Micrometeorological techniques for the measurement of trace gas exchange. In: Exchange of trace gases between terrestrial ecosystem and the atmosphere, 189-207, M. O. Andreae and D. S. Schimel (eds), John Wiley & Sons, New York

Fritschen L. J., 1985: Characterization of boundary conditions affecting forest environmental phenomena. In. The forest-atmosphere interaction, B. A. Huntchinson and B. B. Hicks (eds.), Reidel, Dordecht, 3-23

Fritts, D. C. and P. K. Rastogi, 1985: Convective and dynamical instabilities due to gravity wave motions in the lower and middle atmosphere: Theory and observations, Radio Sci., 20, 1247-1277

Fritts, D. C., 1984: Shear excitation of atmospheric gravity waves, II, Nonlinear radiation from a free shear layer, J. Atmos. Sci, 41, 524-537

Galoux, A., P Benecke, G. Gietl, H. Hager, C. Kayser, O. Kiese, K. R. Knoerr, C. E. Murphy, G. Schnock and T. R. Sinclair, 1981: Radiation, heat, water, and carbon dioxide balances, in Dynamic properties of forest ecosystems, ed by D.E. Reichle, Cambridge Unviversity Press, Cambridge, 87-204

Gao, W., R. H. Shaw, and K. T. Paw U, 1989: Observation of organized structure in turbulent flow within and above a forest canopy, Boundary-Layer Meteorol., 47, 349-377

Goldstein, S., 1931: On the stability of superposed streams of fluid of different densities, Proc. R. Soc. Lond., A132, 524-548

Gossard, E. E. and Hooke, W. H., 1975: Wave in the atmosphere, Elsevier, Amsterdam.

Goulden, M. L., J. W. Munger, S-M Fan, B. C. Daube, S. C. Wofsy,1996a: Exchange of carbon dioxide by a deciduous forest: response to interannual climate variability, Science, 271, 1576-1578

Goulden, M. L., J. W. Munger, S-M Fan, B. C. Daube, S. C. Wofsy, 1996b: Measurements of carbon sequestration by long-term eddy covariance: methods and a critical evaluation of accuracy, Global Change Biology, 2, 168-182

Grass, A. J., 1971: Structural features turbulent flow over smooth and rough boundaries, J. Fluid Mech., 50, 233-255

Hazel, P, 1972: Numerical studies of the stability of inviscid stratified shear flows, J. Fluid Mech., 51, 39-61

Ho, C. and P. Huerre, 1984: Perturbed free shear layer, Ann. Rev. Fluid Mech. 16, 365-424

Hollinger, D. Y., F. M. Kelliher, J. N. Byers, J. N. Hunt, T. M. McSeveny, and P. L. Weir, 1994: Carbon dioxide exchange between an undisturbed old-growth temperate forest and the atmosphere. Ecology, 75, 134-150

Hu, X. and X. Lee, 1998: Kelvin-Helmholtz billows over forest canopy, Proceedings of 23rd Conference on Agricultural and Forest Meteorology, American Meteorological Society, Albuquerque, 429-430

Hu, X., X. Lee and D. E. Stevens: A numerical simulation of nocturnal wave-like air motions over forests, preprints, 14th Symposium on Boundary Layer and Turbulence, American Meteorological Society, 7-11 August 2000, Aspen, CO, 553-554

Inoue, E., 1955: Studies of the phenomenon of waving plants ("HONAMI") caused by wind. Part 1., Mechanism and Characteristics of waving plants phenomena, J. Agric. Meteorol. (Janpan) , 11, 18-22

Kaimal, J. C. and J. J. Finnigan, 1994: Atmospheric boundary layer flows, Oxford University Press, New York, Oxford

Kaplan, W. A., S. C. Wofsy, M. Keller, and J. Maria da Costa: Emission of NO and deposition of O3 in a tropical forest system, J. Geophys. Res., 93, 1389-1395

Klaassen, G. P., and W. R. Peltier, 1985: The onset of turbulence in finite-amplitude Kelvin-Helmholtz billows, J. Fluid Mech. , 155, 1-35

Klaassen, G. P., and W. R. Peltier, 1991: The influence of stratification on secondary instability in free shear layers, J. Fluid Mech. , 227, 74-106

Kristensen, L., and D. Fitzjarrald, 1984: The effect of line averaging on scalar flux measurement, J. Atm. Oc. Tech., 1 , 138-146

Laufer, J., 1975: New trend in experimental turbulence research, Annual reviews in Fluid Mechenics, Vol. 7, 307

Lee, X. and A. G. Barr, 1998: Climatology of gravity waves in a forest, Q. J. R. Meterol. Soc., 124, 1403-1419

Lee, X. and T. A. Black, 1994: Relating eddy correlation sensible heat flux to horizontal sensor separation in the unstable atmospheric surface layer. J. Geophy. Res., 99, 18545-18553

Lee, X., 1997: Gravity Waves in a Forest: A Linear Analysis, J. Atmos. Sci., 54, 2574-2585

Lee, X., R. H. Shaw and T. A. Black, 1994: Modeling the effect of mean pressure gradient on the mean flow within forests, Agric. For. Meteorol., 68, 201-212

Lee, X., T. A. Black, G. D. Hartog, H. H. Neumann, Z. Nesic, J. Olenjbik, 1996: Carbon dioxide exchange and nocturnal processes over a mixed deciduous forest, Agric. For. Meteorol., 81, 13-29

Lee, X., H. H. Neumann, G. Den, Hartog, J. D. Fuentes, T. A. Blackm R. E. Mickle, P. C. Yang and P. D. Blanken, 1997: Observation of gravity waves in a boreal forest. Boundary-Layer Meteorol., 84, 383-398

Lenschow, D. H., 1995: Micrometeorological techniques for measuring biosphere-atmosphere trace gases exchange, in Biogenic trace gases: measuring emissions from soil and water, ed. P. A. Matson and R. C. Harris, Blackwell Science, 127-163

Lu, C-H, D. R. Fitzjarrald, 1994: Seasonal and diurnal variations of coherent structures over a deciduous forest, Boundary-layer Meteorol., 69, 43-69

Maitani, T., Y. Hiramatsu and T. Seo, 1984: Wave-like wind fluctuations observed in the stable surface layer over a plant canopy, Boundary-layer Meteorol., 29, 273-283

Maitani, T., 1989: Wave-like wind fluctuations observed in the stable surface layer over a plant canopy, Boundary-layer Meteorol., 48, 19-31

Marht, L. 1999: Stratified atmospheric boundary layers, Boundary-Layer Meteorol., 90, 375-396

Miles, J. W. and L. N. Howard, 1964: Note on heterogeneous shear flow, J. Fluid Mech., 20, 331-336

Nakagawa, H. and I. Nezu, 1977: Prediction of the contributions to the Reynolds stress from bursting events in open channel flows, J. Fluid Mech., 80, 99-128

Patnaik, P. C., F. S. Sherman and G. M. Corcos, 1976: A numerical simulation of Kelvin-Helmholtz waves of finite amplitude, J. Fluid Mech., 73, 215-240

Paw U, K. T., R. H. Shaw, and T. Maitani, 1990: Gravity waves, coherent structures and plant canopies. Preprints, 9th AMS Symposium on Turbulence and Diffusion, 29 April-3 May, Roskilde, Denmark, American Meteorological Society, Boston, MA, 244-246

Paw U, K. T., R. H. Shaw, T. Maitani, and R. M. Cionco, 1989: Gravity waves in an almind orchard. Preprints, 19th AMS Conference on Agricultural and Forest Meteorology, 7-10 March, Charleston, SC, American Meteorological Society, Boston, MA, 184-185

Paw U, K. T., Y. Brunet, S. Collineau, R. H. Shaw, T. Maitani, J. Qiu and L. Hipps, 1992: On coherent structures in turbulence above and within agricultural plant canopies, Agric. For. Meteorol., 61, 55-68

Peltier, W. R., J. Halle, and T. L. Clark, 1978: The evolution of finite amplitude Kelvin-Helmholtz billows, Geophys. Astrophys. Fluid Dyn., 10, 53-87

Phong-Anant, D., R. A. Antonia, A. J. Chambers, S. Rajagopalan, 1980: Features of the organized motion in the atmospheric surface layer, J. Geophys. Res., 85:424-432

Raupach, M. R, 1988: Canopy transport processes, in W. L. Steffen and O. T. Denmead (eds.), Flow and transport in the natural environment: Advances and applications, Springer, Berlin, 95-127

Raupach, M. R., 1979: Anomalies in flux-gradient relationships over forest. Boundary-Layer Meteorol., 16, 467-486

Raupach, M. R., J. J. Finnigan, and Y. Brunet, 1989: Coherent eddies in vegetation canopies. Proc. Fourth Australian Conference on Heat and Mass Transfer, Christchurch, New Zealand, 9-12, May, University of Canterbury, Christchurchm New Zealand, 75-90

Raupach, M. R., R. A. Antonia, and S. Rajagopalan, 1991: Rough-wall turbulent boundary layers, Appl. Mechs. Revs. 44, 1-25

Raupach, M. R., J. J. Finnigan, and Y. Brunet, 1996: Coherent eddies and turbulence in vegetation canopies: the mixing-layer analogy, Boundary-Layer Meteorol., 78, 351-382

Ross, J, 1975: Radiative transfer in plant communities, in Vegetation and the atmosphere, Vol. 2, ed. By J. L Monteith, Academic Press, London

Schilling, V. K. and U. Janssen, 1992: Particle dispersion due to dynamical instabilities in the lower stratosphere, Contrib. Atmos. Phys., 65, 259-273

Schmid, H. P., H.-B. Su, C. S. Vogel and P. S. Curtis, 2000: Nighttime turbulence statistics and trace gas exchange in a mixed deciduous forest, preprints, 14th Symposium on Boundary Layer and Turbulence, American Meteorological Society, 7-11 August 2000, Aspen, CO, 555-558

Schimidt, R. A., and F. A. Wood, 1972: Interpretation of microclimate data in relation to basidiospore release by Fomes annosus, Phytopathology, 62, 319-321

Sellers, P. J., F. Hall, H. Margolis, B. Kelly, D. Baldocchi, G. den Hartog, J. Cihlar, M. G. Ryan, B. Goodison, P. Crill, K. J. Ranson, D. Lettermaiser, and D. E. Wickland, 1995: The boreal ecosystem-atmosphere study (BOREAS): an overview and early results from 1994 field year. Bull. Amer. Meteorol. Soc. 76, 1549-1577

Sellers, P. J., R. E. Dickinson, D. A. Randall, A. K. Betts, F. G. Hall, J. A. Berry, G. J. Collatz, A. S. Denning, H. A. Mooney, C. A. Nobre, N. Sato, C. B. Field, and A. Henderson-Sellers, 1997: Modeling the exchanges of energy, water, and carbon between continents and the atmosphere, Science, 275, 502-509

Shaw, R. H. and A. R. Pereira, 1982: Aerodynamic roughness of a plant canopy: a numerical study, Agric. Meteorol., 26, 51-65

Shaw, R. H., G. den Hartog, and H. H. Neumann: 1988, Influence of Foliar Density and Thermal Stability on Profiles of Reynolds Stress and Turbulence Intensity in a Deciduous Forest, Boundary-Layer Meteorology, 45, 391-409

Shaw, R. H. and U. Schmann: 1992, Large-Eddy Simulation of Turbulent Flow above and within a Forest, Boundary-Layer Meteorology, 61, 47-64

Smith, R. B., 1979: The influence of mountains on the atmosphere. Advances in Geophysics, 21, 87-230, (B. Saltzman Ed.)

Stevens, D. E., A. S. Almgren, and J. B. Bell, 2000: A numerical comparison of different anelastic models in a coupled atmosphere-fire model, in preparation

Stevens, D. E., A. S. Almgren, J. B. Bell, V. E. Beckner, and C. A. Rendleman, 2000: Small Scale Processes and Entrainment in a Stratocumulus Marine Boundary Layer, J. Atmos. Sci., 57(4), 567-581

Susanna, G. And D. B. Baldocci, 1996: Seasonal variation of CO2 and water vapor exchange rates over a temperate deciduous forest, Global Change Biology, 2, 183-197

Sykes, R. I. and W. S. Lewellen, 1982: A numerical study of breaking Kelvin-Helmholtz billows using a Reynolds-stress turbulence closure model, J. Atmos. Sci, 39, 1506-1520

Thom, A. S., 1975: Momentum, mass and heat exchange of plant communities. In Monteith J. L. (ed) Vegetation and the atmosphere 1. Academic Press, New York, 57-110

Thorpe, S. A., 1969: Experiments on the stability of stratified shear flows, Radio Science, 4, 1327-1331

Thorpe, S. A., 1985: Laboratory observations of secondary structures in Kelvin-Helmholtz billows and consequences for ocean mixing. Geophys. Astrophys. Fluid Dyn., 34m 175-199

Thorpe, S. A., 1987: Transitional phenomena and the development of turbulence in stratified fluids: A review. J. Geophys. Res., 92, 5231-5248

Werne, J. and D. C. Fritts, 1999: Stratified shear turbulence: Evolution and statistics, Geophysical research letters, Vol. 26, No. 4, 439-442

Whittaker, R. H., 1975: Communities and Ecosystems, 2nd ed., 385 pp., Macmillan, New York.

Wilczak, J. M. and J. A. Businger, 1983: Thermally indirect motions in the convective atmospheric boundary layer, J. Atmos. Sci., 40, 343-358

Wilczak, J. M. and J. E. Tillman, 1980: The three-dimensional structure of convection in the atmospheric surface layer, J. Atmos. Sci., 37, 2424-2443

Wilson, N. R. and R. H. Shaw, 1977: A higher order closure model for canopy flow, J. Appl. Meteorol., 16, 1197-1205

Wofsy, S. C., M. L. Goulden, W. Munger, S-M Fan, P. S. Bakwin, B. C. Bassow, F. A. Bazzaz, 1993. Net exchange of CO2 in a mid-latitude forest. Science, 260, 1314-1317

Wofsy, S. T., R. C. Harris and W. A. Kaplab, 1988: Carbon dioxide in the atmosphere over the Amazon basin, J. Geophy. Res., 93(D2) 1377-1387

Woods, J. D., 1969: On Richardson's number as a criterion for laminar-turbulent-laminar transition in the ocean and atmosphere, Radio Science, 4, 1289-1298

Woodwell, G. M., and Dykeman, W. R., 1966: Respiration of a forest measured by CO2 accumulation during temperature inversions, Sciences, 154, 1031-1034.

Wyngaard, J. C., 1988: Convective processes in the lower atmosphere, in W. L. Steffen and O. T. Demead (eds.), Flow and transport in the natural environment: Advances and applications, Springer, Berlin, 240-260

Yang, P. C., T. A. Black, W. J. Chen, P. D. Blanken, H. H Neumann, M. D. Novak, Z. Nesic and X. Lee, 1997: Effect of turbulence on nocturnal CO2 flues above a boreal aspen forest. Preprint, 12th Symposium on Boundary layers and Turbulence, 395-396, AMS, Vancouver, BC, Canada